

AD-A100 808

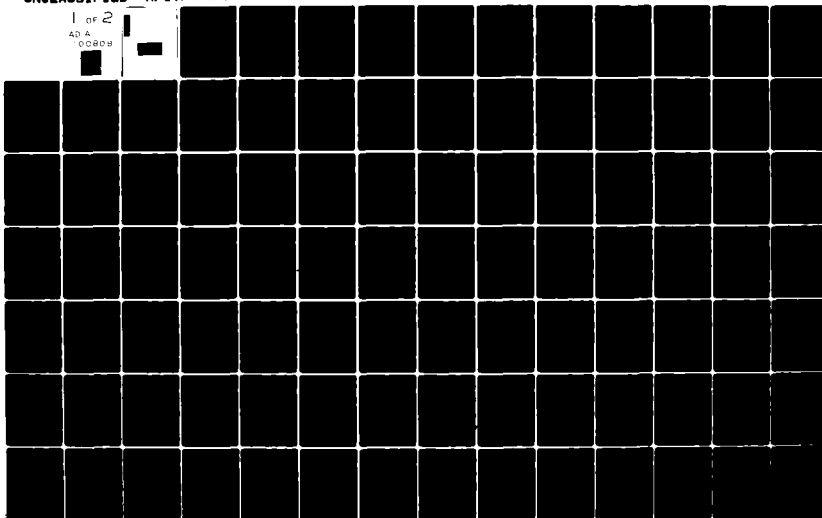
AIR FORCE INST OF TECH WRIGHT-PATTERSON AFB OH SCHOO--ETC F/G 1/4
FLIGHT CONTROL SYSTEM ANALYSIS AND DESIGN FOR A REMOTELY PILOTE--ETC(U)
DEC 80 B L JONES
AFIT/GAE/AA/80D-12

UNCLASSIFIED

NL

1 of 2

AD A
00808



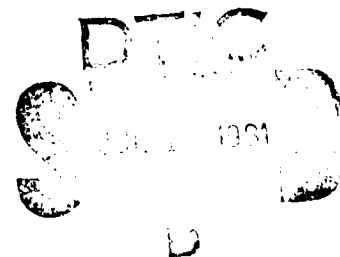
AFIT/GAE/AA/80D-12

Accession For	
NTIS GRA&I	<input checked="checked" type="checkbox"/>
DTIC TAB	<input type="checkbox"/>
Unannounced	<input type="checkbox"/>
Justification	
By	
Distribution/	
Availability Codes	
Avail and/or	
Dist	Special
A	

FLIGHT CONTROL SYSTEM ANALYSIS
AND DESIGN FOR A REMOTELY PILOTED
VEHICLE WITH THRUST VECTORING UNIT

THESIS

AFIT/GAE/AA/80D-12 Brian L. Jones, B.S.A.E.
2Lt USAF



Approved for public release; distribution unlimited.

FLIGHT CONTROL SYSTEM ANALYSIS AND DESIGN FOR A
REMOTELY PILOTED VEHICLE WITH THRUST VECTORING UNIT

THESIS

Presented to the Faculty of the School of Engineering
of the Air Force Institute of Technology
Air University
in Partial Fulfillment of the
Requirements for the Degree of
Master of Science

by

Brian L. Jones, B.S.A.E.

2d Lt

USAF

Graduate Aeronautical Engineering

December 1980

Approved for public release; distribution unlimited.

Preface

The study of aircraft flight control is a very broad field. In selecting a thesis topic, I was interested in choosing a project that would permit me to experience as many aspects of this field as possible. This necessitated that the project be small enough in scope that it afforded me the opportunity to engage in analysis as well as design. The NEXTRPV program was well suited to meet this goal. Whereas this project is not necessarily glamorous, it gave me the chance to experience "basic" engineering which I believe is an important part of any education.

This thesis originally began as strictly a flight control system analysis and design for an existing remotely piloted vehicle (RPV). As the project progressed, it became evident that the RPV was fairly stable and would not need as much flight control augmentation as initially anticipated. Therefore, this thesis was extended to include an investigation of a practical application of this RPV.

Many people contributed to this thesis. To each of them, I say thank you. Special thanks goes to my thesis advisor, Captain James T. Silverthorn, for his numerous suggestions and neverending attention. My gratitude is extended to Professors Robert A. Calico and John J. D'Azzo whose assistance was invaluable. My appreciation is also expressed to Mrs Anna Lloyd for preparing this manuscript. Lastly, I would like to thank my wife, Susan, whose constant support, encouragement, and understanding made the completion of this project possible.

Brian L. Jones

Contents

	<u>Page</u>
Preface	ii
List of Figures	v
List of Tables	viii
Notation	ix
Abstract	xv
I. Introduction	1
Background	1
Problem Statement, Scope, and Assumptions	2
Approach and Presentation	3
II. RPV Model Generation	5
Method	5
Input Data for Digital Datcom	5
Formulation of the RPV Representations	9
Data Reduction	10
Hand Calculations of the Remaining Terms	16
Summary	16
III. Analysis of the RPV	20
Handling Qualities	20
Equations of Motion	21
Modal Analysis	23
Transfer Functions and Time Responses	30
Conclusions	33
IV. Design and Evaluation	35
Longitudinal Design	35
Lateral-Directional Design	36
Sensitivity Studies and Redesign	41
Handling Qualities Check	45
Transfer Functions and Time Responses	49
Nonlinear Simulation	53
V. Practical Application	56
Analysis of the F-15	56
Guillemin-Truxal Design	59
Entire Eigenstructure Assignment	61
Extension of Observer Theory	65

	<u>Page</u>
VI. Concluding Remarks	78
Conclusions	78
Recommendations	79
Bibliography	80
Appendix A: Hand Calculations	82
Appendix B: Aircraft Equations of Motion	95
Appendix C: Time Responses	111
Vita	136

List of Figures

<u>Figure</u>		<u>Page</u>
1	Circular Cross-Section Approximation for the Fuselage and Boom	6
2	Deck Structure for Digital Datcom	11
3	Comparison of the Actual RPV and its Digital Datcom Representation with the TVU Attached	12
4	Comparison of the Actual RPV and its Digital Datcom Representation with the TVU Unattached	13
5	Short Period Natural Frequency Handling Quality . . .	23
6	Basic RPV Bank Angle due to a 15 deg Step Aileron Command	28
7	Basic RPV Bank Angle due to a 5 deg Impulse Aileron Command	29
8	Open-Loop State Equations for the RPV, Case 2	31
9	Root Locus for Pitch Rate Feedback to the Elevator .	37
10	Root Locus for Integral of Pitch Rate Feedback to the Elevator	37
11	Root Locus for the Yaw Damper Including the Washout Circuit	39
12	Root Locus for the Yaw Damper Excluding the Washout Circuit	39
13	Root Locus for Integral of Roll Rate Feedback to the Ailerons	40
14	Root Locus for Yaw Rate Feedback to the Ailerons . .	40
15	Pole Movement due to Variations in Airspeed	43
16	Pole Movement due to Variations in Vertical Tail Area	45
17	Augmented RPV Bank Angle due to a 15 deg Step Aileron Command	48
18	Augmented RPV Bank Angle due to a 5 deg Impulse Aileron Command	48
19	Closed-Loop State Equations for the RPV	50

<u>Figure</u>		<u>Page</u>
20	Digital Simulation Algorithm for a 1 sec Pulse Elevator Command of -5 deg	54
21	F-15 Longitudinal State Equation	58
22	Reduced Order Servo Approximations for the RPV . . .	64
23	Generalized Block Diagram for Model Matching	67
24	Closed-Loop State Equation for Model Matching . . .	74
25	Comparison of the F-15 and the Model Matching RPV Velocity due to a 1 sec Pulse Elevator Command of -5 deg	75
26	Comparison of the F-15 and the Model Matching RPV Angle of Attack due to a 1 sec Pulse Elevator Command of -5 deg	75
27	Comparison of the F-15 and the Model Matching RPV Pitch Angle due to a 1 sec Pulse Elevator Command of -5 deg	76
28	Comparison of the F-15 and the Model Matching RPV Pitch Rate due to a 1 sec Pulse Elevator Command of -5 deg	76
29	Comparison of the F-15 and the Model Matching RPV Elevator Deflection Angle due to a 1 sec Pulse Elevator Command of -5 deg	77
30	RPV Forward Velocity due to a 1 sec Pulse Elevator Command of -5 deg	112
31	RPV Angle of Attack due to a 1 sec Pulse Elevator Command of -5 deg	113
32	RPV Pitch Angle due to a 1 sec Pulse Elevator Command of -5 deg	114
33	RPV Pitch Rate due to a 1 sec Pulse Elevator Command of -5 deg	115
34	RPV Elevator Deflection Angle due to a 1 sec Pulse Elevator Command of -5 deg	116
35	RPV Elevator Deflection Rate due to a 1 sec Pulse Elevator Command of -5 deg	117
36	RPV Sideslip Angle due to a 1 sec Pulse Aileron Command of 5 deg	118

<u>Figure</u>		<u>Page</u>
37	RPV Yaw Angle due to a 1 sec Pulse Aileron Command of 5 deg	119
38	RPV Yaw Rate due to a 1 sec Pulse Aileron Command of 5 deg	120
39	RPV Bank Angle due to a 1 sec Pulse Aileron Command of 5 deg	121
40	RPV Roll Rate due to a 1 sec Pulse Aileron Command of 5 deg	122
41	RPV Aileron Deflection Angle due to a 1 sec Pulse Aileron Command of 5 deg	123
42	RPV Aileron Deflection Rate due to a 1 sec Pulse Aileron Command of 5 deg	124
43	RPV Rudder Deflection Angle due to a 1 sec Pulse Aileron Command of 5 deg	125
44	RPV Rudder Deflection Rate due to a 1 sec Pulse Aileron Command of 5 deg	126
45	RPV Sideslip Angle due to a 1 sec Pulse Rudder Command of 5 deg	127
46	RPV Yaw Angle due to a 1 sec Pulse Rudder Command of 5 deg	128
47	RPV Yaw Rate due to a 1 sec Pulse Rudder Command of 5 deg	129
48	RPV Bank Angle due to a 1 sec Pulse Rudder Command of 5 deg	130
49	RPV Roll Rate due to a 1 sec Pulse Rudder Command of 5 deg	131
50	RPV Aileron Deflection Angle due to a 1 sec Pulse Rudder Command of 5 deg	132
51	RPV Aileron Deflection Rate due to a 1 sec Pulse Rudder Command of 5 deg	133
52	RPV Rudder Deflection Angle due to a 1 sec Pulse Rudder Command of 5 deg	134
53	RPV Rudder Deflection Rate due to a 1 sec Pulse Rudder Command of 5 deg	135

List of Tables

<u>Table</u>		<u>Page</u>
I	Physical Dimensions of the RPV	7
II	Required Lift Coefficient for Straight and Level Flight	15
III	RPV Mathematical Models	17
IV	Handling Qualities	22
V	Characteristic Equations of the Basic RPV.	25
VI	Modal Characteristics of the Basic RPV	26
VII	Transfer Functions for the Basic RPV, Case 2	32
VIII	Extremum of the Parameter Sensitivity Study	44
IX	Comparison of the Augmented RPV, Basic RPV, and the Handling Qualities	46
X	Transfer Functions for the Augmented RPV	51
XI	F-15 Mathematical Model	57
XII	F-15 Longitudinal Transfer Functions	60
XIII	Guillemin-Truxal Cascade Compensators for Model Matching	62
XIV	Guillemin-Truxal Feedback Compensators for Model Matching	63
XV	Comparison of the F-15 Eigenvectors and the Closed Loop RPV Eigenvectors produced by Entire Eigenstructure Assignment	66
XVI	Weight and Center of Gravity Locations of the Major RPV Components	86
XVII	Moments of Inertia of the RPV's Major Components	93
XVIII	RPV Moments of Inertia	94
XIX	Definitions of the Longitudinal Stability Derivatives.	100
XX	Definitions of the Lateral-Directional Stability Derivatives	106

Notation

A	Plant coefficient matrix
\underline{A}	Inertial acceleration (ft/sec ²)
A_{in}	Aileron input (rad)
B	Control matrix
B	Feedback state from yaw damper
b	Wing span (ft)
C	Coefficient matrix for model matching
C	Output matrix
c	Speed of sound (ft/sec)
\bar{c}	Mean aerodynamic chord (ft)
C_D	Drag coefficient
C_L	Lift coefficient
C_{Lq}	Nondimensional variation of lift with pitch rate
$C_{L\alpha}$	Nondimensional variation of lift with angle of attack
$C_{L\dot{\alpha}}$	Nondimensional variation of lift with angle of attack rate
$C_{\ell p}$	Nondimensional variation of rolling moment with roll rate
$C_{\ell r}$	Nondimensional variation of rolling moment with yaw rate
$C_{\ell \beta}$	Nondimensional variation of rolling moment with sideslip angle
$C_{\ell \delta a}$	Nondimensional variation of rolling moment with aileron deflection
$C_{\ell \delta r}$	Nondimensional variation of rolling moment with rudder deflection
C_{in}	Pitching moment coefficient
C_{m0}	Pitching moment coefficient at zero angle of attack
C_{mq}	Nondimensional variation of pitching moment with pitch rate
C_{m_u}	Nondimensional variation of pitching moment with velocity

$C_{m_{\dot{\alpha}}}$	Nondimensional variation of pitching moment with angle of attack
$C_{m_{\dot{\alpha}}}$	Nondimensional variation of pitching moment with angle of attack rate
$C_{m_{\delta e}}$	Nondimensional variation of pitching moment with elevator deflection
C_{n_p}	Nondimensional variation of yawing moment with roll rate
C_{n_r}	Nondimensional variation of yawing moment with yaw rate
$C_{n_{\beta}}$	Nondimensional variation of yawing moment with sideslip angle
$C_{n_{\delta a}}$	Nondimensional variation of yawing moment with aileron deflection
$C_{n_{\delta r}}$	Nondimensional variation of yawing moment with rudder deflection
C_{x_q}	Nondimensional variation of X-force with pitch rate
C_{x_u}	Nondimensional variation of X-force with velocity
$C_{x_{\alpha}}$	Nondimensional variation of X-force with angle of attack
$C_{x_{\dot{\alpha}}}$	Nondimensional variation of X-force with angle of attack rate
$C_{x_{\delta e}}$	Nondimensional variation of X-force with elevator deflection
C_{y_p}	Nondimensional variation of Y-force with roll rate
C_{y_r}	Nondimensional variation of Y-force with yaw rate
$C_{y_{\beta}}$	Nondimensional variation of Y-force with sideslip angle
$C_{y_{\delta a}}$	Nondimensional variation of Y-force with aileron deflection
$C_{y_{\delta r}}$	Nondimensional variation of Y-force with rudder deflection
C_{z_u}	Nondimensional variation of Z-force with velocity
$C_{z_{\delta e}}$	Nondimensional variation of Z-force with elevator deflection
C_1	Constant (sec)
C_2	Constant
D	Solution matrix for model matching
$D(s)$	Denominator polynomial in the Laplace domain

E_{in}	Elevator input (rad)
F	Force (lb)
FCS	Flight control system
$G(s)$	Forward transfer function in the Laplace domain
$G_c(s)$	Compensator in the Laplace domain
g	Acceleration due to gravity (ft/sec ²)
H	Angular momentum (ft-lb-sec)
\underline{IN}	Closed-loop control inputs (rad)
I_x	Moment of inertia about the X-axis (slug-ft ²)
I_{xz}	Product of inertia (slug-ft ²)
I_y	Moment of inertia about Y-axis (slug-ft ²)
I_z	Moment of inertia about Z-axis (slug-ft ²)
J	Cost function
j	$(-1)^{1/2}$
K	Feedback matrix
L	Lift (lb)
L	Rolling moment (ft-lb)
L	Feedback matrix for model matching
M	Mach number
M	Pitching moment (ft-lb)
\underline{M}	Moment vector (ft-lb)
m	Mass (slug)
mac	Mean aerodynamic chord (ft)
N	Yawing moment (ft-lb)
$N(s)$	Numerator polynomial in the Laplace domain
n	Load factor (g's)
P	Roll rate (rad/sec)

p	Perturbation roll rate (rad/sec)
Q	Pitch rate (rad/sec)
q	Perturbation pitch rate (rad/sec)
\bar{q}	Dynamic pressure (lb/ft ²)
R	Weighting matrix for model matching
R	Yaw rate (rad/sec)
R_{in}	Rudder input (rad)
RPV	Remotely piloted vehicle
r	Perturbation yaw rate (rad/sec)
\underline{r}	Reciprocal basis vector
S	Wing area (ft ²)
T	Thrust (lb)
T	Time constant (sec)
TF	Transfer function
TVU	Thrust vectoring unit
U	Forward velocity (ft/sec)
u	Perturbation forward velocity (ft/sec)
\underline{u}	Open-loop control inputs (rad)
$'u$	Nondimensional velocity (u/U_0)
V	Side velocity (ft/sec)
\underline{V}	Velocity (ft/sec)
\underline{v}	Eigenvector
v	Perturbation side velocity (ft/sec)
W	Vertical velocity (ft/sec)
W	Weight (lb)
w	Perturbation vertical velocity (ft/sec)
\underline{w}	Reciprocal basis vector

\underline{x}	State vector
x_{cg}	X-axis center of gravity location (% mac)
∇	Characteristic equation
α	Error matrix for model matching
α	Angle of attack (rad)
β	Coupling matrix for model matching
β	Sideslip angle (rad)
γ	Constant matrix for model matching
δ	Control surface deflection (rad)
δ_T	Throttle setting
ϵ	Error
ζ	Damping ratio
θ	Pitch angle (rad)
λ	Eigenvalue
$\underline{\xi}$	Eigenvector
π	3.141592654
ρ	Density of air (slug/ft ³)
Σ	Summation
σ	Real part of an imaginary number
Φ	Constant matrix for model matching
ϕ	Bank angle (rad)
ϕ	Elements of Φ
$ \phi/\beta _{dr}$	Phi to beta ratio
ϕ_{osc}/ϕ_{ave}	Phi oscillatory to phi average ratio
Ψ	Constant matrix for model matching
ψ	Elements of Ψ
ψ	Yaw angle (rad)

ω_d	Damped frequency (rad/sec)
ω_n	Natural frequency (rad/sec)
$\underline{\omega}^{bi}$	Inertial angular velocity (rad/sec)

Subscripts

a	Aileron
cmd	Command
DR	Dutch roll mode
e	Elevator
0	Equilibrium condition
P	Phugoid mode
R	Roll mode
r	Rudder
S	Spiral mode
sp	Short period mode
x	X-axis direction
y	Y-axis direction
z	Z-axis direction
—	Vector

Superscripts

.	Time derivative
'	F-15 model

Abstract

— This study investigated the stability and control of a remotely piloted vehicle (RPV) with a thrust vectoring unit attached. All geometric and aerodynamic data was generated and used to analyze the RPV. Specific handling qualities were developed and compared with the RPV characteristics. This comparison indicated that the RPV was too oscillatory in both the phugoid and dutch roll modes. Also, the RPV displayed a dominant spiral mode. A flight control system was synthesized to eliminate these traits. Evaluation of this flight control system was conducted through the use of three different sensitivity studies and a nonlinear simulation. In addition, a model matching application was examined for this RPV. Model matching entails using design procedures to synthesize an expanded flight control system so that the RPV has dynamic characteristics similar to the F-15.

FLIGHT CONTROL SYSTEM ANALYSIS AND DESIGN FOR
A REMOTELY PILOTED VEHICLE WITH THRUST VECTORING UNIT

I. Introduction

Background

In aircraft design, the aeronautical engineer is faced with many design objectives. For military aircraft, these objectives would include such traits as: low observability, high lethality and survivability, STOL capability, and lastly, air-to-air and air-to-ground capability. Several schools of thought exist on how to satisfy these objectives. One alternative is the use of a thrust vectoring unit (TVU). With such a unit employed, the tail section could be removed without any reduction in aircraft control. This would reduce the infrared signature and hence lower an aircraft's observability. Also, thrust vectoring increases an aircraft's maneuverability, which, in turn, increases its lethality and survivability while enhancing its air-to-air and air-to-ground capability. In addition, thrust vectoring has been shown to improve an aircraft's STOL capability.

With a continual reduction in funding, the Air Force needs to find inexpensive ways in which to develop and test such theories as thrust vectoring. One answer to this problem is using remotely piloted vehicles (RPVs) as flight test vehicles. RPVs can be operated at a small fraction of the cost of a test aircraft, resulting in substantial savings in research dollars.

The two above mentioned concepts were combined to form the NEXTRPV program under the direction of the Control Systems Development Branch

(AFWAL/FICL), Flight Dynamics Laboratory, Air Force Wright Aeronautical Laboratories. Their stated objective was to

demonstrate the use of practical thrust vectoring and digital flight control systems in a low cost flight research vehicle oriented toward a more stealthy design with an expanded maneuvering envelope.

The approach the laboratory intended to pursue was to first integrate the TVU into the RPV through an analog control system. Flight control authority would gradually be transferred to the TVU over a series of test flights. Following the successful completion of the TVU full authority test flight, the entire procedure would be repeated using a digital control system. At the conclusion of this phase, the tail section would be removed for a final performance evaluation.

The RPV chosen for this program suited it well for several reasons. Since this RPV was obtained from a previous program, it had already been flight proven. Thus, all considerations other than flight control system (FCS) design were eliminated from this project. Also, the twin boom/vertical tail assembly required little modification for the TVU addition (see Fig 3). Lastly, since the RPV was already constructed, the associated development costs were saved.

Problem Statement, Scope, and Assumptions

The purpose of this study was to determine the stability and control characteristics, develop specific handling qualities, synthesize a FCS to satisfy these handling qualities, and investigate a practical application of this RPV.

This study was restricted to the TVU zero authority case. In other words, the TVU was attached to the RPV, but was given no control

authority. The only exception appeared in the basic analysis. In this phase, center of gravity location and TVU attachment were used as parameters. X-axis center of gravity (x_{cg}) assumed three locations: 10, 25, and 40 percent mean aerodynamic chord (mac). The TVU attached and unattached cases were examined for each x_{cg} location. The practical application was restricted to the longitudinal case. As shown in Chapter V, the lateral-directional case would simply be a repetition of the same theory.

Initially, several simplifying assumptions were imposed. Perturbations about straight and level flight were assumed. This allowed the linearized aircraft equations of motion to be decoupled into longitudinal and lateral-directional sets. For the FCS design, only pitch, roll, and yaw rates were acceptable feedbacks. It was further assumed that a processing unit would be accessible should compensation be required. Lastly, full state feedback was assumed available for the practical application.

Approach and Presentation

This study was separated into four major phases. Phase one consisted of obtaining all necessary geometric and aerodynamic data for this RPV, followed by the generation of six sets of stability derivatives (TVU attached and unattached cases for three x_{cg} locations). These sets made up the mathematical models used in this study. Chapter II of this report presents the results of phase one.

The basic analysis of the RPV constituted phase two. This analysis began with the development of specific RPV handling qualities. The aircraft equations of motion were derived and a modal analysis of the six models generated in phase one was conducted. Phase two concluded

with a comparison of the modal analysis with the RPV handling qualities.

The report on phase two is contained in Chapter III.

Phase three involved the design and evaluation of a FCS to satisfy all the handling qualities. Sensitivity studies and a nonlinear simulation were used to evaluate the FCS. Phase three is documented in Chapter IV.

Lastly, phase four entailed an investigation into a practical application (model matching) for this RPV. An expanded FCS was synthesized to make this RPV have dynamic characteristics similar to an F-15. Three different design procedures were examined and are described in Chapter V.

The final chapter of this report, Chapter VI, presents conclusions and recommendations.

II. RPV Model Generation

Aircraft stability and control characteristics are usually examined based upon a linearized set of differential equations of motion. The development of these equations (see Chapter III) contains numerous parameters which fall into three categories: physical quantities, flight condition defining quantities, and stability derivatives. The purpose of this chapter is to generate these parameters for this particular RPV.

Method

The physical quantities (mass, moment of inertia, etc.) and flight condition defining terms (airspeed, dynamic pressure, etc.) were easily determined from the size of the RPV and its expected flight regime. Thus, the major crux of the model generation became calculating the stability derivatives. Applicable publications were consulted in order to determine the most appropriate method of calculating these derivatives. Most publications reviewed listed The USAF Stability and Control DATCOM (Ref 8) as a reference. These manuals contain empirical formulas and methods for determining stability and control derivatives, aircraft moments of inertia, etc. A computerized version of these methods appears as The USAF Stability and Control Digital Datcom (Ref 18). Due to the widespread acceptance of Datcom methods and the versatility of a computer program, it was decided that Digital Datcom would be the best source of stability derivatives.

Input Data for Digital Datcom

Digital Datcom requires three types of input data: aircraft geometry, airfoil section characteristics, and flight condition.

Aircraft geometry was obtained by directly measuring the RPV's physical dimensions. A circular cross-section approximation was employed for the fuselage and booms (see Fig 1). Table I is a summary of all

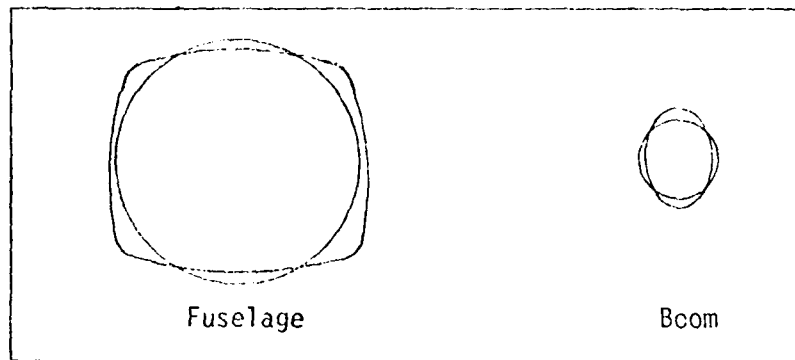


Figure 1. Circular Cross-Section Approximation for the Fuselage and Boom

measurements.

Two major modifications were planned for the RPV and were incorporated into the mathematical model. The first was a two foot nose extension and the second was the addition of the TVU. Both modifications were modelled as part of the fuselage.

Next, airfoil section characteristics were required for each airfoil. The wing was found to have a varying airfoil section, a NACA 23012 at the root and a NACA 4412 at the tip. The horizontal tail was a NACA 0009 while the vertical tails were NACA 0010 airfoil sections. Since NACA airfoil sections were found (Ref 1), Digital Datcom's internal aerodynamics package was utilized for the generation of section characteristics. An approximation of the wing's varying airfoil section was formulated by computing two sets of stability derivatives, one set for each of the root and tip airfoil sections, and linearly averaging the results. This approximation should be accurate since the difference between the individual stability derivatives was small.

Table I. Physical Dimensions of the RPV

a. Wing, Horizontal Tail, and Vertical Tail Dimensions*			
	W.	H.T.	V.T.
Apex, ft:			
x-axis	4.25	11.39	9.49
z-axis	0.60	2.10	0
Chord, ft:			
root	2.52	1.29	2.15
tip	2.00	1.29	1.30
Incidence Angle, deg:	0.95	0	0
Span, ft:			
exposed	13.00	4.88	2.17
theoretical	13.71	5.00	2.33
Sweptback Angle, deg:			
leading edge:			
inboard panel	3.50	0	35.00
outboard panel	3.50	0	35.00
trailing edge:			
inboard panel	0	0	18.00
outboard panel	-1.40	0	18.00

* See Ref 18 for definitions of terms.

Table I. (continued)

b. Fuselage Dimensions			
x-station, ft	perimeter, ft	area, ft ²	radius, ft
2.00	3.33	0.88	0.53
2.42	3.42	0.93	0.54
2.83	3.58	1.02	0.57
3.25	3.71	1.09	0.59
3.67	3.79	1.14	0.60
3.83	3.83	1.17	0.61
4.25	3.75	1.12	0.60
4.75	3.75	1.12	0.60
5.25	3.75	1.12	0.60
5.75	3.75	1.12	0.60
6.25	3.75	1.12	0.60
6.75	3.75	1.12	0.60

c. Boom Dimensions			
x-station, ft	perimeter, ft	area, ft ²	radius, ft
5.00	0.67	0.035	0.11
5.42	1.58	0.20	0.25
5.83	1.83	0.27	0.29
6.33	1.92	0.29	0.30
6.75	1.67	0.22	0.26
7.17	1.62	0.21	0.26
7.58	1.58	0.20	0.25
8.00	1.50	0.18	0.24
8.42	1.42	0.16	0.22
8.83	1.35	0.15	0.22
9.25	1.29	0.13	0.21
9.67	1.21	0.12	0.19
10.08	1.12	0.10	0.18
10.50	1.00	0.080	0.16
10.92	0.92	0.067	0.15
11.25	0.83	0.055	0.13

Flight condition defining parameters was the last set of input data needed. After consideration of the engine capabilities and the flight profiles expected, the airspeed regime was determined to range from Mach 0.05 to Mach 0.20. Similarly, the angle of attack range was formulated as -4 deg to 15 deg. Sea level conditions were assumed for all quantities requiring atmospheric conditions.

Formulation of the RPV Representations

The choice of Digital Datcom specified the basic RPV representation as a straight tapered wing and one vertical tail of increased area. It was decided to employ a scale factor of 1.75 in increasing the vertical tail area. This choice was somewhat arbitrary since no documentation could be found on this type of approximation. Geometric relationships (sweepback angles) and aspect ratio were preserved in the scaling up of the vertical tail.

In addition, the cross-sectional areas (in the body namelist) were increased to include the effects of the booms. Because of the blanking effect of the TVU, only the area of one boom was added to the fuselage. When the TVU was absent from the RPV configuration, the areas of both booms were added to the fuselage. All other data utilized in the representations was taken from Table I.

Two parameters were chosen for investigation: xcg location and TVU attachment. The xcg location assumed three values (10, 25, and 40 percent mac). Both the TVU attached and unattached cases were examined for each xcg location. Thus, a total of six cases were investigated:

- Case 1 - TVU attached, xcg = 10% mac
- Case 2 - TVU attached, xcg = 25% mac
- Case 3 - TVU attached, xcg = 40% mac
- Case 4 - TVU unattached, xcg = 10% mac
- Case 5 - TVU unattached, xcg = 25% mac
- Case 6 - TVU unattached, xcg = 40% mac

Hence, the effect of the TVU and the xcg location on the RPV characteristics could be determined.

With the input data finalized, the RPV representations were complete. Figure 2 contains the input data cards for Digital Datcom. The four underlined statements had to be changed with each case. A visual interpretation of the RPV with the TVU attached and unattached can be found in Figs 3 and 4, respectively.

Data Reduction

Since the entire flight regime specified 16 Mach numbers and 20 angles of attack per Mach number, Digital Datcom generated 320 sets of stability derivatives for each case (i.e., a data bank). Unfortunately, the aircraft equations of motion could accept only one set of stability derivatives at a time. Thus, a nominal flight condition was needed. Three techniques were examined in the selection of this flight condition: lift averaging, best endurance, and best range.

The lift averaging technique assumed straight and level flight. Thus,

$$\begin{aligned}
 W &= L \\
 &= \frac{1}{2} \rho V^2 S C_L
 \end{aligned}$$

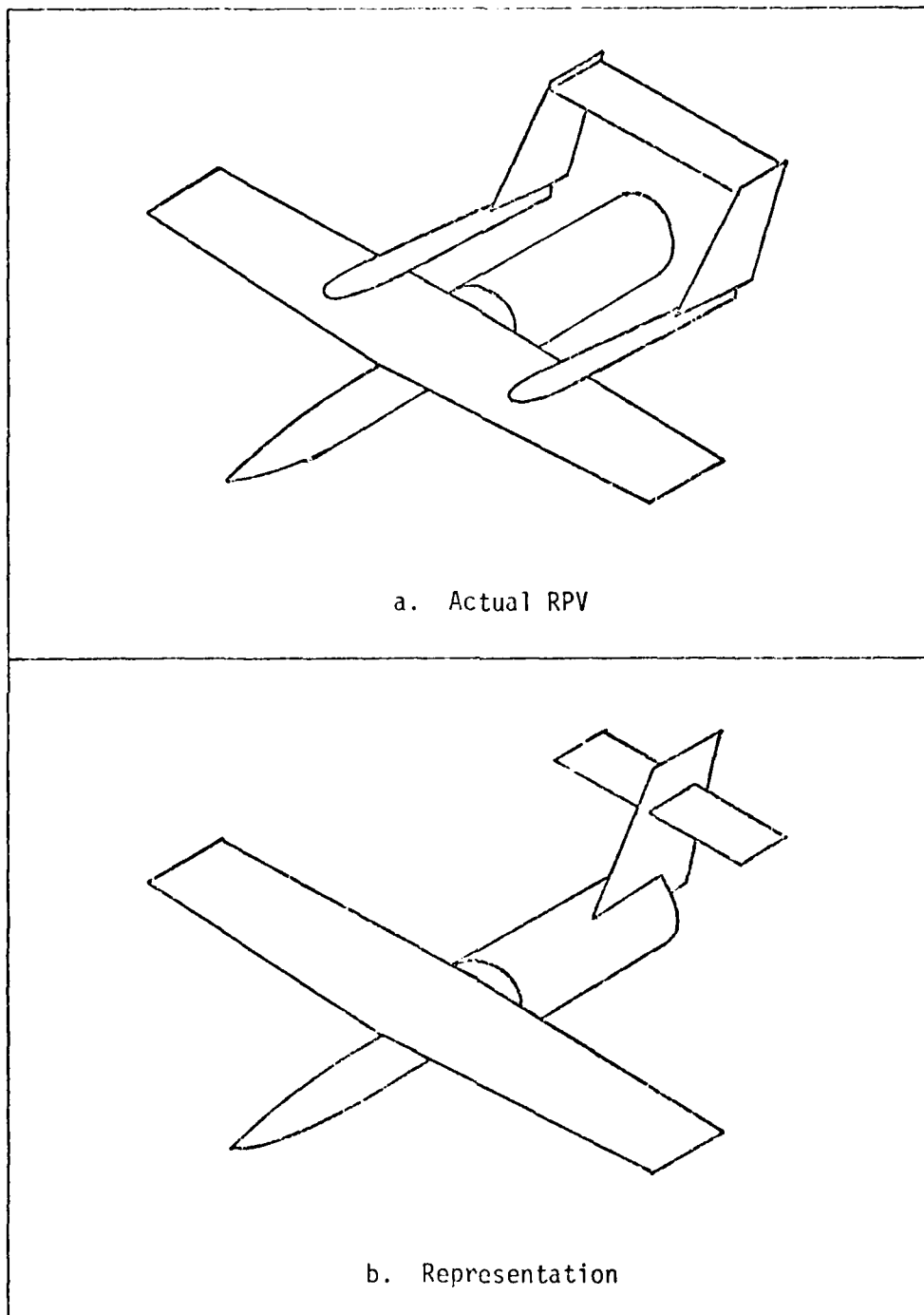
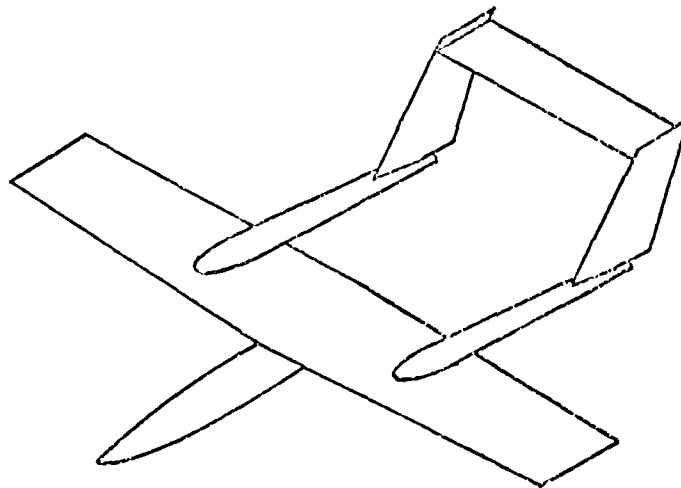
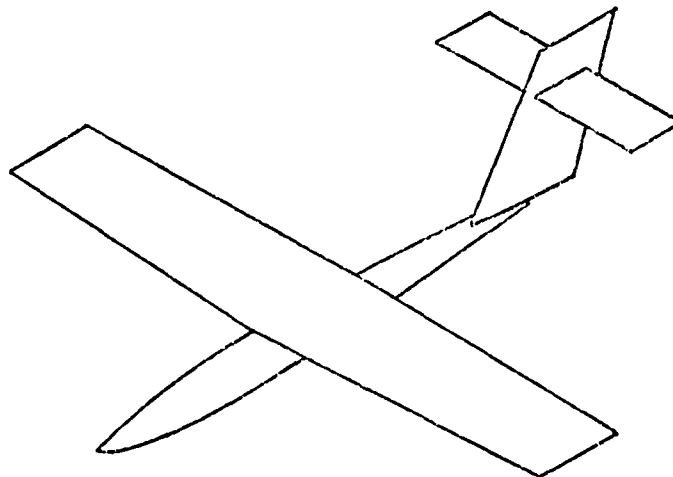


Figure 3. Comparison of the Actual RPV and Its Digital Datcom Representation with the TVU Attached



a. Actual RPV



b. Representation

Figure 4. Comparison of the Actual RPV and Its Digital Datcom Representation with the TVU Unattached

Substituting $V^2 = M^2 c^2$ and solving for C_L yields

$$C_L = \frac{2 W}{S \rho c^2 M^2}$$

Assuming the maximum weight (250 lb) and substituting the appropriate values gives

$$C_L = \frac{5.45 \times 10^{-3}}{M^2} \quad (1)$$

or

$$M = \frac{7.38 \times 10^{-2}}{C_L^{1/2}} \quad (2)$$

From Eq (1), C_L can be calculated over the range of reasonable Mach numbers (Table II). A linear average of lift coefficient was determined as $C_L = 0.59$ which represented the average amount of lift required over the entire flight regime. Substituting this value into Eq (2) produced an associated Mach number of Mach 0.10. Digital Datcom specifies its flight condition in terms of angle of attack rather than the lift coefficient. Therefore, the data bank was interpolated (using Mach 0.10 and $C_L = 0.59$) to produce an associated angle of attack of $\alpha = 2$ deg.

As alternate methods for selecting a nominal flight condition, best endurance and best range flight profiles were considered (Ref 7: Sec III, 33, 37). After considering that the RPV would be flown by sight, it became apparent that neither of these two flight profiles could be maintained. Therefore, the results of the lift averaging technique (Mach 0.10, $\alpha = 2$ deg) were used as the nominal flight condition.

Table II. Required Lift Coefficient for Straight and Level Flight

M	C_L
0.20	0.14
0.19	0.15
0.18	0.17
0.17	0.19
0.16	0.21
0.15	0.24
0.14	0.28
0.13	0.32
0.12	0.38
0.11	0.45
0.10	0.54
0.09	0.67
0.08	0.85
0.07	1.11
0.06	1.51
0.05	2.18
Linear Average	0.59

Finally, the trim condition needed to be verified to insure that this was an appropriate choice of flight condition. During straight and level flight, the pitching moment equation becomes

$$C_m = C_{m0} + C_{m\alpha} \alpha + C_{m\delta e} \delta e$$

In a trimmed aircraft, $C_m = 0$. Using this value and solving for δe_{trim} produces

$$\delta e_{trim} = \frac{-C_{m0} - C_{m\alpha} \alpha}{C_{m\delta e}}$$

Substituting the Case 2 values

$$\begin{aligned} \delta e_{trim} &= \frac{-0.06 + (0.023)(2.0)}{-0.034} \\ &= 0.33 \text{ deg} \end{aligned}$$

Thus, it was decided that the RPV was in a trimmed flight condition. Table III contains a complete summary of the stability derivatives at the nominal flight condition.

Hand Calculations of the Remaining Terms

Three types of parameters were still needed to complete the model of the RPV: the remaining stability derivatives (e.g. $C_{x\alpha}$), the control derivatives (e.g. $C_{m\delta e}$), and the physical quantities (e.g. I_y). The complete derivation of these parameters is given in Appendix A. In addition, these parameters are summarized in Table III.

Summary

Table III contains a summary of the mathematical models used in this study. Five approximations were included in the generation of

Table III. RPY Mathematical Models

	TVU Attached			TVU Unattached		
	xcg = 10% mac (Case 1)	xcg = 25% mac (Case 2)	xcg = 40% mac (Case 3)	xcg = 10% mac (Case 4)	xcg = 25% mac (Case 5)	xcg = 40% mac (Case 6)
m, slugs	7.63	7.33	6.68	6.28	6.03	5.50
S, ft ²	30.99	30.99	30.99	30.99	30.99	30.99
c, ft	2.27	2.27	2.27	2.27	2.27	2.27
b, ft	13.71	13.71	13.71	13.71	13.71	13.71
Ix, slug-ft ²	19.26	19.26	19.26	19.26	19.26	19.26
Iy, slug-ft ²	65.24	65.24	65.24	65.24	65.24	65.24
Iz, slug-ft ²	79.52	79.52	79.52	79.52	79.52	79.52
Ixz, slug-ft ²	4.38	4.38	4.38	4.38	4.38	4.38
U0, ft/sec	111.54	111.64	111.64	111.64	111.64	111.64
q, lb/ft ²	14.81	14.81	14.81	14.81	14.81	14.81
Cxu	-0.10	-0.10	-0.10	-0.08	-0.08	-0.08
Cxi	0	0	0	0	0	0
Cxi	0.22	0.22	0.22	0.24	0.24	0.24
Cxi	0	0	0	0	0	0
Cxq	-1.18	-1.18	-1.18	-1.18	-1.18	-1.18
Czu	2.13	2.02	1.92	2.13	2.02	1.92
CLi	5.52	5.52	5.52	5.52	5.52	5.52
CLi	9.08	7.54	6.02	8.11	6.63	5.15
CLq	0	0	0	0	0	0
Cmu	-6.59	-5.97	-5.38	-6.59	-5.97	-5.38
Cmi	-2.16	-1.32	-0.49	-1.96	-1.12	-0.29
Cmq	-14.64	-13.40	-12.29	-15.55	-13.87	-12.52

All stability and control derivatives have units of per rad.

Table III. (Continued)

	TVU Attached			TVU Unattached		
	xcg = 10% mac (Case 1)	xcg = 25% mac (Case 2)	xcg = 40% mac (Case 3)	xcg = 10% mac (Case 4)	xcg = 25% mac (Case 5)	xcg = 40% mac (Case 6)
Cy ₁	-0.26	-0.26	-0.26	-0.43	-0.43	-0.43
Cyr	0	0	0	0	0	0
Cyp	-0.0092	-0.010	-0.011	-0.0079	-0.0086	-0.0092
C ₁₁	-0.034	-0.034	-0.034	-0.082	-0.082	-0.0082
Cir	0.13	0.13	0.18	0.13	0.18	0.18
Cip	-0.56	-0.55	-0.53	-0.56	-0.54	-0.52
Cn ₁	0.16	0.15	0.14	0.16	0.14	0.13
Cnr	-0.18	-0.17	-0.15	-0.17	-0.16	-0.14
Crp	-0.055	-0.054	-0.053	-0.054	-0.053	-0.052
Cx ₁ e	0	0	0	0	0	0
Cz ₁ e	-0.66	-0.66	-0.66	-0.66	-0.66	-0.66
C ₁ e	-2.04	-1.94	-1.84	-2.04	-1.94	-1.24
Cy ₁ a	0	0	0	0	0	0
C ₁ a	0.13	0.13	0.13	0.13	0.13	0.13
Cn ₁ a	-0.015	-0.015	-0.015	-0.015	-0.015	-0.015
Cyr	0.90	0.90	0.90	0.90	0.90	0.90
C ₁ r	0.067	0.067	0.067	0.067	0.067	0.067
Cn ₁ r	-0.42	-0.40	-0.38	-0.42	-0.40	-0.38

All stability and control derivatives have units of per rad.

these models:

1. Circular cross-sections were used for the fuselage.
2. A straight tapered wing was substituted for the cranked wing.
3. One vertical tail of increased area (75% greater) was substituted for the twin vertical tails.
4. The effects of the booms were incorporated into the fuselage representation.
5. Average stability derivatives were computed using the root wing section and tip wing section cases.

III. Analysis of the RPV

Before any reasonable FCS synthesis could be undertaken, flight specifications had to be developed and the unaugmented system analyzed. Thus, the purpose of this chapter is to present specific RPV handling qualities, followed by the above mentioned analysis. This analysis was divided into four parts: derivation of the aircraft equations of motion, examination of the modal characteristics, generation of transfer functions and time responses, and development of conclusions.

Handling Qualities

A literature review resulted in only one publication (Ref 14) which specifically addressed RPV handling qualities; unfortunately, sections of this publication are incomplete. However, since all publications reviewed relied heavily upon the criteria set forth in various Military Specifications, it was decided that a comparison study of the following four specifications would provide the most appropriate source of handling qualities:

1. RPV Flying Qualities Design Criteria, AFFDL-TR-76-125 (Ref 14).
2. Flying Qualities of Piloted Aircraft, MIL-F-8785B (Ref 4).
3. Flying Qualities of Piloted V/STOL Aircraft, MIL-F-83300 (Ref 5).
4. Flight Control Systems - Design, Installation, and Test of Piloted Vehicles, MIL-F-9490D (Ref 17).

When present, the specifications from AFFDL-TR-76-125 were used since this report specifically addressed RPVs. The handling qualities in the Military Specifications were used to complement those areas

which AFFDL-TR-76-125 did not cover. Table IV contains the results of this comparison study. It consists primarily of eigenvalue specifications which establish the allowable range of values for the roots of the characteristic equation.

Several restrictions in determining these handling qualities were imposed from the onset:

- The general specifications, such as "Each mode will have sufficient damping", are not repeated in Table IV.

- Since the aircraft in this study was a RPV, all stick force, pedal force, and control force specifications were omitted. It was assumed that the servo would generate sufficient power to deflect all control surfaces.

- Since this RPV was designated as a research vehicle, it was assumed that it would be flown on a "good" day. Therefore, atmospheric disturbance specifications were deleted.

- This RPV will be flown by sight; thus, display specifications were omitted.

- It was assumed that the data link was sufficiently reliable and capable of transmitting all necessary information.

- Redundancy and failure rates were not considered.

Equations of Motion

The aircraft equations of motion are a set of nonlinear, coupled force and moment equations which completely describe the motion of an aircraft in inertial space. By assuming perturbations about straight and level flight, these equations can be decoupled into a longitudinal set and a lateral-directional set. Linearizing these equations about

Table IV. Handling Qualities

Classification: Class III - medium maneuverability	
Flight Phase: Category A - rapid maneuvering	
Level: Level 1 - normal operation	
Longitudinal Case:	
ζ_{sp}	- $0.35 < \zeta_{sp} < 1.30$
ω_{nsp}	- See Fig 5
ζ_p	- $\zeta_p \geq 0.04$
Residual Oscillation	- $< \pm 0.60$ deg
Dynamic Oscillation	- A short term dynamic oscillation produced by a pulse elevator shall not diverge faster than a time to double of 15 sec.
Lateral-Directional Case:	
ζ_{DR}	- $\zeta_{DR} > 0.19$
ω_{nDR}	- $\omega_{nDR} > 0.40$ rad/sec
Dutch Roll Time Parameter	- $\zeta_{DR} \omega_{nDR} > 0.35 + \Delta \zeta_{DR} \omega_{nDR}$ where $\Delta \zeta_{DR} \omega_{nDR} = 0.014$ $[\omega_{nDR}^2 (\phi/P)_{DR} - 20]$
T_R	- $T_R < 1.4$ sec
Spiral Mode	- For a steady state disturbance in ϕ of 20 deg, the time to double must be greater than 20 sec.
Roll Effectiveness	- > 30 deg ϕ in 1.5 sec
Roll-Spiral Coupling	- None

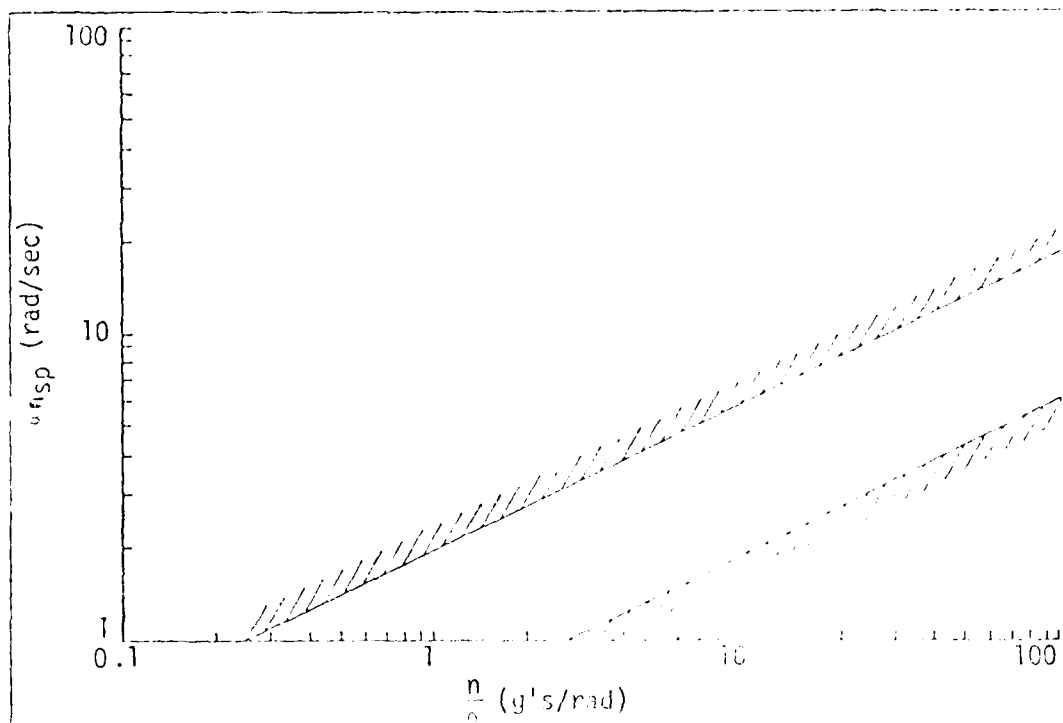


Figure 5. Short Period Natural Frequency Handling Quality

an arbitrary equilibrium condition permitted the perturbation equations of motion to be formed. These equations were written in state equation form so that individual transfer functions and modal characteristics could be determined. The complete derivation of the perturbation state equations is found in Appendix B.

Modal Analysis

The models of Chapter II were used in the perturbation equations of motion, resulting in twelve sets of state equations, six for each of the longitudinal and lateral-directional cases. Recall that a state equation is of the form

$$\dot{\underline{x}} = \underline{A} \underline{x} + \underline{B} \underline{u}$$

where the \underline{A} matrix determines the characteristic equation of the system. Each \underline{A} matrix was used in a computer program (Ref 16) which determined

the characteristic equation, and hence, the modal characteristics of each system. Table V summarizes the characteristic equations while Table VI summarizes the modal characteristics.

A comparison of Table VI with Table IV indicated that:

- ξ_{sp} , ω_{DR} , T_R satisfied their respective handling qualities by a wide margin.
- ξ_p satisfied its specification, but only by a small margin.
- ω_{sp} did not satisfy its handling quality in cases 4 and 5, and was at its upper limit in the other cases.
- ξ_{DR} and T_S did not satisfy their respective specifications.
- Since all the longitudinal roots were stable, no dynamic oscillations exceeded a time to double of 15 sec.
- No roll-spiral coupling existed since each mode had a real root.
- Frequently, residual oscillations are the result of nonlinearities in the control system (e.g. dead zone). Hence, no simple way to evaluate these effects existed within the scope of this study.

Two handling qualities required more investigation than the above comparison: dutch roll time parameter ($\tau_{DR} = 1/\omega_{DR}$) and roll effectiveness. The dutch roll time parameter handling quality is given in terms of the phi to beta ratio ($|\phi/\beta|_{DR}$). This ratio may be found by determining the magnitude of the phi and beta envelopes at an instant of time from the rudder pulse time responses (Ref 4:673). Utilizing this procedure and the time responses from Appendix C, the dutch roll time parameter specifications were determined using the average $|\phi/\beta|_{DR}$ with the following results:

Table V. Characteristic Equations of the Basic RPV

Longitudinal Case:	
<u>Case</u>	<u>Characteristic Equation</u>
1	$(s^2 + 6.34s + 39.35)(s^2 + 0.040s + 0.16) = 0$
2	$(s^2 + 7.38s + 37.01)(s^2 + 0.042s + 0.15) = 0$
3	$(s^2 + 8.20s + 24.16)(s^2 + 0.052s + 0.11) = 0$
4	$(s^2 + 9.64s + 65.72)(s^2 + 0.040s + 0.18) = 0$
5	$(s^2 + 12.73s + 31.49)(s^2 + 0.046s + 0.16) = 0$
6	$(s + 11.27)(s + 4.68)(s^2 + 0.074s + 0.093) = 0$
Lateral-Directional Case:	
<u>Case</u>	<u>Characteristic Equation</u>
1	$(s + 11.50)(s - 0.042)(s^2 + 1.49s + 19.03) = 0$
2	$(s + 11.18)(s - 0.042)(s^2 + 1.42s + 17.76) = 0$
3	$(s + 10.88)(s - 0.042)(s^2 + 1.34s + 16.50) = 0$
4	$(s + 11.30)(s - 0.044)(s^2 + 1.23s + 17.85) = 0$
5	$(s + 10.99)(s - 0.043)(s^2 + 1.17s + 16.63) = 0$
6	$(s + 10.71)(s - 0.044)(s^2 + 1.08s + 15.41) = 0$

Table VI. Modal Characteristics of the Basic RPV

Case Characteristic	1	2	3	4	5	6
ζ_{sp} ω_{sp} , $\frac{\text{rad}}{\text{sec}}$ *	0.50 6.27 (10.31)	0.61 6.08 (10.74)	0.83 4.92 (11.78)	0.60 8.11 (12.54)	0.75 8.48 (13.06)	1.10 7.26 (14.32)
ζ_p ω_p , $\frac{\text{rad}}{\text{sec}}$	0.051 0.40	0.055 0.39	0.077 0.34	0.047 0.42	0.057 0.40	0.12 0.30
T_R , sec	0.087	0.089	0.092	0.086	0.088	0.090
T_S , sec **	-24.04 (16.66)	-24.04 (16.66)	-23.36 (16.19)	-22.68 (15.72)	-22.78 (15.79)	-21.88 (15.17)
ζ_{DR} ω_{DR} , $\frac{\text{rad}}{\text{sec}}$	0.16 3.85	0.17 4.21	0.17 4.84	0.15 4.57	0.17 5.21	0.17 5.58
ζ_{DR} ω_{DR} , sec^{-1}	0.62	0.71	0.82	0.70	0.88	0.96

* $n/\%$ is given in parentheses.

** Negative sign indicates instability. Time to double (sec) is given in parentheses.

<u>Case</u>	<u>ζ/ξ_{DR}</u>	<u>Handling Quality</u>
2	1.63	$\zeta_{DR}/\xi_{DR} > 0.48$
5	1.87	$\zeta_{DR}/\xi_{DR} > 0.78$

Comparing these values with Table VI showed that the dutch roll time parameter specification was satisfied.

Likewise, the roll effectiveness of the RPV needed to be determined. With maximum deflection of the ailerons (15 deg), the RPV produced 62 deg and 64 deg of bank in 1.5 sec for cases 2 and 5, respectively (Fig 6). Hence, the RPV had over twice the required roll effectiveness.

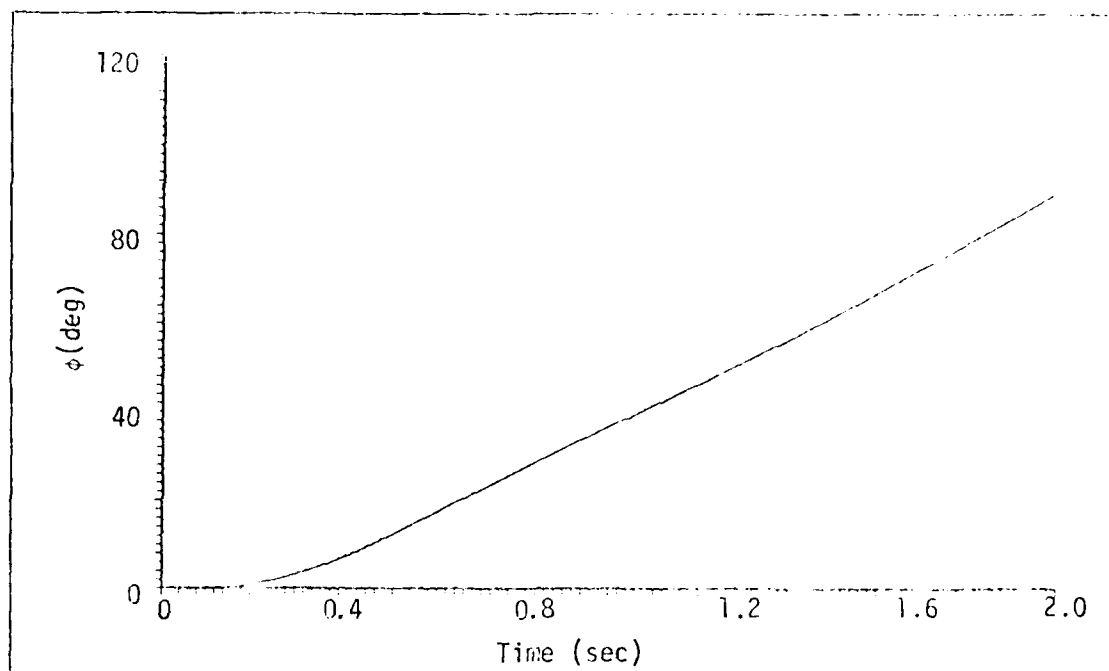
Although not specifically mentioned in the handling qualities, one other characteristic needed attention, the ratio of the oscillatory component to the average component of bank angle (ϕ_{osc}/ϕ_{ave}). This ratio is determined by analyzing the peaks of a bank angle time response due to an impulse aileron command. Since $\zeta_{DR} < 0.20$, the following empirical formula could be used:

$$\frac{\phi_{osc}}{\phi_{ave}} = \frac{\phi_1 + \phi_3 - 2\phi_2}{\phi_1 + \phi_3 + 2\phi_2} \quad (3)$$

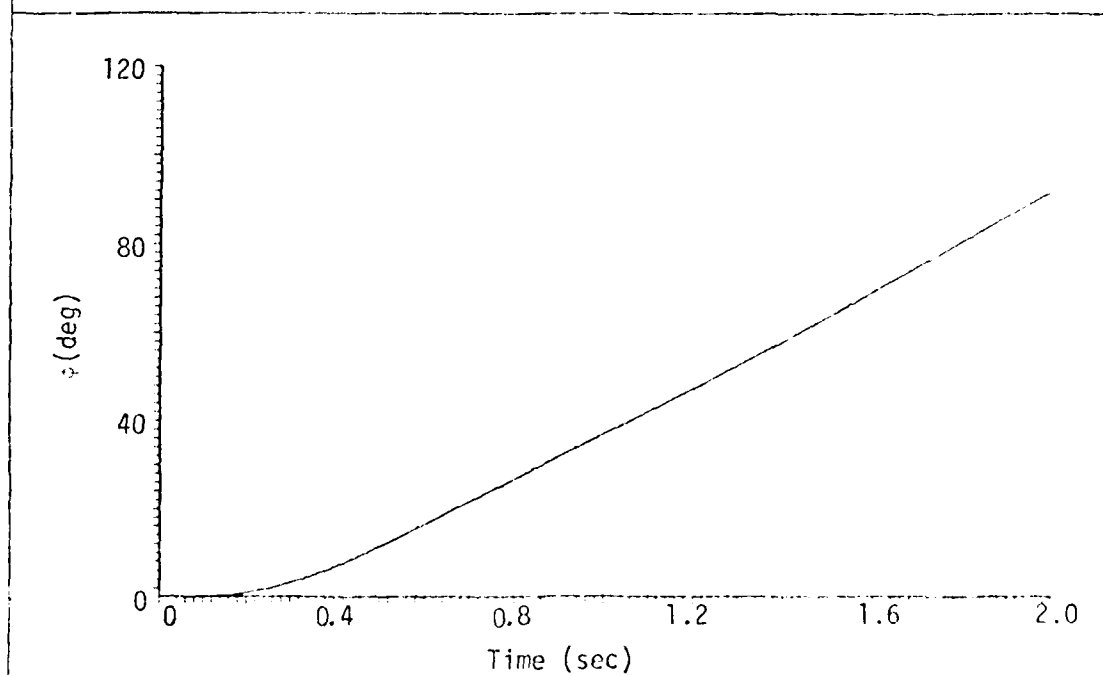
where ϕ_1 , ϕ_2 , and ϕ_3 corresponded to the first second, and third peaks (Ref 4: xxii). Hence, the impulse time responses (Fig 7) were used in Eq (3) and produced

<u>Case</u>	<u>ϕ_{osc}/ϕ_{ave}</u>
2	-0.0081
5	-0.0108

Thus, the RPV was not very oscillatory.



a. Case 2



b. Case 5

Figure 6. Basic RPV Bank Angle due to a 15 deg Step Aileron Command

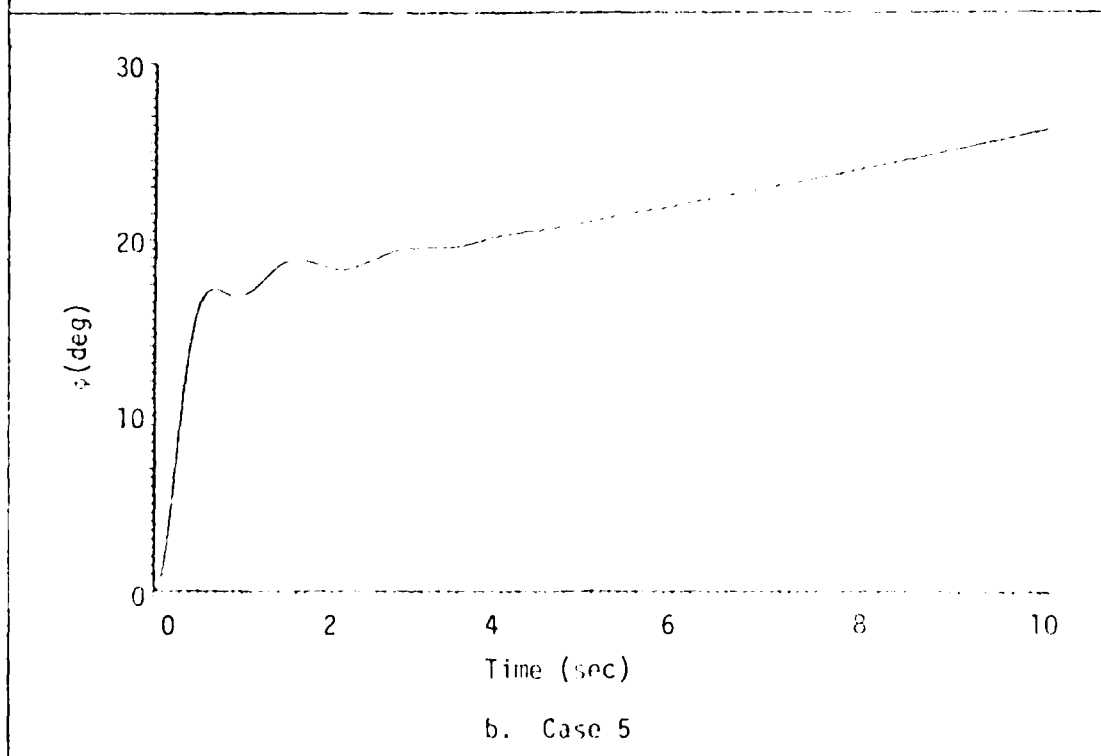
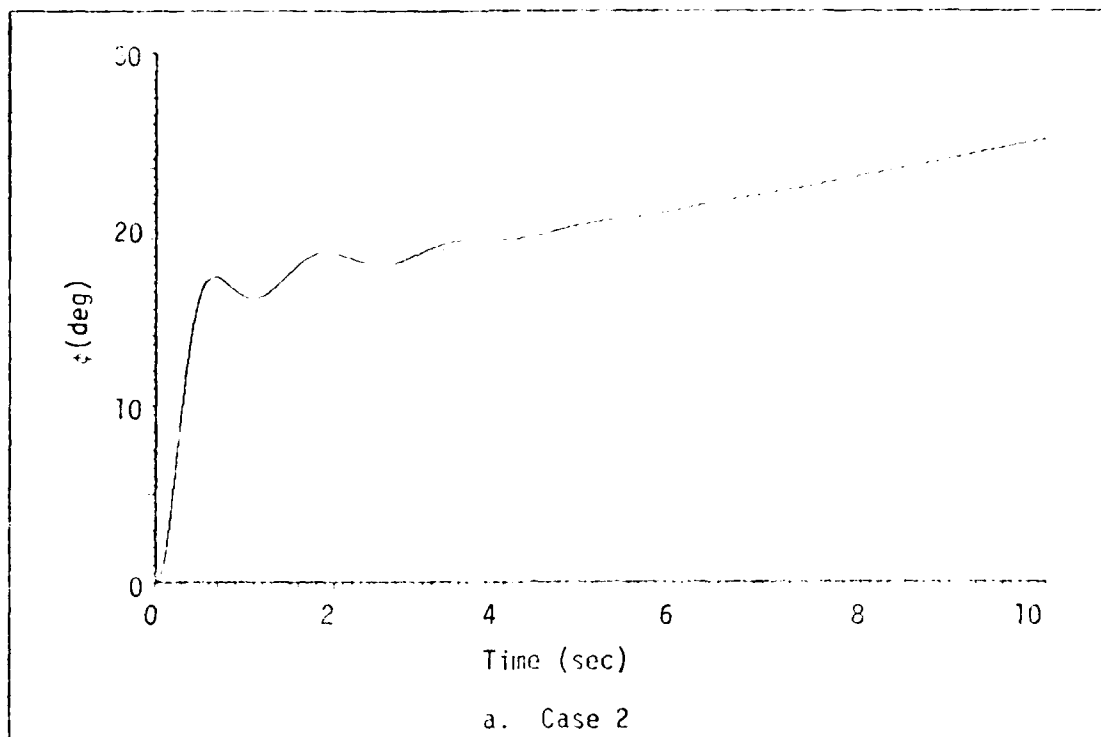


Figure 7. Basic RPV Bank Angle due to a 5 deg
Impulse Aileron Command

Transfer Functions and Time Responses

Before transfer functions and time responses could be generated, the actuator dynamics must be included in the equations of motion. Modified Futaba FPS-14 servos were used for the RPV's actuators. Test of these servos produced two different representations:

$$TF_{\text{servo}} = \frac{(15.7)^2}{s^2 + (2)(.8)(15.7)s + (15.7)^2} \quad (4)$$

$$TF_{\text{servo}} = \frac{(14.45)^2}{s^2 + (2)(.8)(14.45)s + (14.45)^2} \quad (5)$$

Equation (4) corresponded to a 5.5 in.-lb. load and 5.0 volt input. Equation (5) corresponded to a 11.8 in.-lb. load and 10.0 volt input. Since the RPV would have a peak input of 22 volts, some type of extrapolation of Eqs (4) and (5) was needed. It was decided that a 50 percent reduction in break frequency in Eq (5) would adequately compensate for the larger input and whatever slippage that occurred due to the linkage. Hence, the following representation was utilized for the RPV actuators:

$$\begin{aligned} TF_{\text{servo}} &= \frac{(7.22)^2}{s^2 + (2)(.8)(7.22)s + (7.22)^2} \\ &= \frac{52.20}{s^2 + 11.56s + 52.20} \end{aligned} \quad (6)$$

The corresponding differential equation is

$$\ddot{\delta} = -52.20\delta - 11.56\dot{\delta} + 52.20\delta_{\text{cmd}} \quad (7)$$

The equations of motion were augmented with Eq (7) resulting in the open-loop state equations given in Fig 8. From these equations, the transfer functions for the basic RPV were generated (Ref 16). Only Case 2 is presented in this report (Table VII) since the FCS design will be based on this case.

a. Longitudinal Case

$$\begin{bmatrix} \dot{u} \\ \dot{x} \\ \dot{\theta} \\ \dot{q} \\ \dot{\delta e} \\ \ddot{\delta e} \end{bmatrix} = \begin{bmatrix} -0.059 & 0.33 & -0.29 & 0 & 0 & 0 \\ -0.66 & -3.06 & 0 & 0.95 & -0.36 & 0 \\ 0 & 0 & 0 & 1.00 & 0 & 0 \\ 0.88 & -25.15 & 0 & -4.30 & -43.50 & 0 \\ 0 & 0 & 0 & 0 & 0 & 1.00 \\ 0 & 0 & 0 & 0 & -52.20 & -11.56 \end{bmatrix} \begin{bmatrix} u \\ \alpha \\ \theta \\ q \\ \delta e \\ \dot{\delta e} \end{bmatrix} + \begin{bmatrix} 0 \\ 0 \\ 0 \\ 0 \\ 0 \\ 52.20 \end{bmatrix} \delta e_{cmd}$$

b. Lateral-Directional Case

$$\begin{bmatrix} \dot{y} \\ \dot{r} \\ \dot{p} \\ \dot{q} \\ \dot{\delta a} \\ \ddot{\delta a} \\ \dot{\delta r} \\ \ddot{\delta r} \end{bmatrix} = \begin{bmatrix} -0.48 & -1.00 & -0.29 & -0.0003 & 0 & 0 & 0.51 & 0 \\ 14.04 & -0.85 & 0 & -1.06 & 1.23 & 0 & -41.04 & 0 \\ 0 & 0 & 0 & 1.00 & 0 & 0 & 0 & 0 \\ -24.56 & 3.52 & 0 & -11.22 & 43.83 & 0 & 13.67 & 0 \\ 0 & 0 & 0 & 0 & 0 & 1.00 & 0 & 0 \\ 0 & 0 & 0 & 0 & -52.20 & -11.56 & 0 & 0 \\ 0 & 0 & 0 & 0 & 0 & 0 & 1.00 & 0 \\ 0 & 0 & 0 & 0 & 0 & -52.20 & -11.56 & 0 \end{bmatrix} \begin{bmatrix} \beta \\ r \\ q \\ p \\ \delta a \\ \dot{\delta a} \\ \delta r \\ \dot{\delta r} \end{bmatrix} + \begin{bmatrix} 0 \\ 0 \\ 0 \\ 0 \\ 0 \\ 52.20 \\ 0 \\ 0 \end{bmatrix} \begin{bmatrix} \delta a_{cmd} \\ \delta r_{cmd} \end{bmatrix}$$

Figure 8. Open-Loop State Equations for the RPV, Case 2

Table VII. Transfer Functions for the Basic RPV, Case 2

Longitudinal Case:	
\dot{v}	$= (s^2 + 7.38 s + 37.01)(s^2 + 0.042 s + 0.15)(s^2 + 11.56 s + 52.20)$
$N_{\delta_{e\text{cmd}}}^u$	$= -2.34 (s + 4.76)(s - 163.08)$
$N_{\delta_{e\text{cmd}}}^{\alpha}$	$= -19.04 (s + 114.58)(s^2 + 0.57 s + 0.28)$
$N_{\delta_{e\text{cmd}}}^{\theta}$	$= -2219.32 (s + 0.089)(s + 2.82)$
$N_{\delta_{e\text{cmd}}}^{\dot{\theta}}$	$= -2219.32 s(s + 0.089)(s + 2.82)$
$N_{\delta_{e\text{cmd}}}^{\ddot{\theta}}$	$= 52.20 (s^2 + 7.38 s + 37.01)(s^2 + 0.042 s + 0.15)$
$N_{\delta_{e\text{cmd}}}^{\ddot{\theta}}$	$= 52.20 s(s^2 + 7.38 s + 37.01)(s^2 + 0.042 s + 0.15)$
Lateral-Directional Case:	
\dot{v}	$= (s + 11.18)(s - 0.042)(s^2 + 1.42 s + 17.76)(s^2 + 11.56 s + 52.20)^2$
$N_{\delta_{a\text{cmd}}}^{\beta}$	$= -1.24 (s + 0.26)(s - 36.70)$
$N_{\delta_{a\text{cmd}}}^r$	$= 1.23 (s - 2.27)(s + 2.54)(s - 26.33)$
$N_{\delta_{a\text{cmd}}}^{\dot{\beta}}$	$= 43.83 (s^2 + 1.43 s + 15.19)$
$N_{\delta_{a\text{cmd}}}^p$	$= 43.83 s (s^2 + 1.43 s + 15.19)$
$N_{\delta_{a\text{cmd}}}^{\dot{\beta}}$	$= 52.20 (s + 11.18)(s - 0.042)(s^2 + 1.42 s + 17.76)(s^2 + 11.56 s + 52.20)$
$N_{\delta_{a\text{cmd}}}^{\ddot{\beta}}$	$= 52.20 s(s + 11.18)(s - 0.042)(s^2 + 1.42 s + 17.76)(s^2 + 11.56 s + 52.20)$
$N_{\delta_{a\text{cmd}}}^{\dot{r}}$	$= 0$
$N_{\delta_{a\text{cmd}}}^{\ddot{r}}$	$= 0$
$N_{\delta_{r\text{cmd}}}^{\beta}$	$= 0.51 (s - 0.078)(s + 11.91)(s + 79.23)$
$N_{\delta_{r\text{cmd}}}^r$	$= -40.04 (s + 11.65)(s^2 + 0.24 s + 0.49)$
$N_{\delta_{r\text{cmd}}}^{\dot{\beta}}$	$= 13.67 (s + 4.32)(s - 14.21)$
$N_{\delta_{r\text{cmd}}}^p$	$= 13.67 s(s + 4.32)(s - 14.21)$
$N_{\delta_{r\text{cmd}}}^{\dot{\beta}}$	$= 0$
$N_{\delta_{r\text{cmd}}}^{\ddot{\beta}}$	$= 0$
$N_{\delta_{r\text{cmd}}}^{\dot{r}}$	$= 52.20 (s + 11.18)(s - 0.042)(s^2 + 1.42 s + 17.76)(s^2 + 11.56 s + 52.20)$
$N_{\delta_{r\text{cmd}}}^{\ddot{r}}$	$= 52.20 s(s + 11.18)(s - 0.042)(s^2 + 1.42 s + 17.76)(s^2 + 11.56 s + 52.20)$

Typically, a pilot's command consists of an input and, a short time later, removal of that input. With this in mind, a 1 sec pulse was selected as the input for all time responses. The magnitude of this pulse was -5 deg for the elevator command and +5 deg for the aileron and rudder commands. A set of time responses, for case 2, were generated (Ref 16) using these inputs and are contained in Appendix C.

Even though only one input was used, several general observations were made.

- All the time responses had the shape that would be expected for this input (Refs 2:47, 129-130 and 12:306, 668).

- The peak values were high. This stemmed from the slow airspeed and large control surface effectiveness.

- The phugoid natural frequency was much higher than most aircraft.

- The dutch roll mode was very oscillatory.

- The spiral mode had a dominant effect that could not be ignored.

Conclusions

Several conclusions were drawn from the modal analysis and time responses. These conclusions define the design objectives for Chapter IV. In the longitudinal case, phugoid natural frequency needed to be decreased since oscillations of this magnitude and frequency were undesirable. In the lateral-directional case, the effect of dutch roll oscillation needed to be reduced and the spiral mode needed to be stabilized.

The effect of the TVU on the RPV was minimal. All natural frequencies were slightly reduced as was the short period damping ratio. The other characteristics remained essentially unchanged.

As the xcg location moved further aft, the following characteristics were increased: \dot{m}_{sp} , \dot{q}_p , and \dot{m}_{DGR} . Also, \dot{m}_{sp} was decreased. All other characteristics remained essentially unchanged.

IV. Design and Evaluation

All design processes consist of the same procedure: synthesize, evaluate, and resynthesize. The purpose of this chapter is to complete this design process for a FCS to correct the deficiencies found in Chapter III. The synthesis phase consisted of a longitudinal design and a lateral-directional design. The evaluation phase consisted of three sensitivity studies, a final handling qualities check, the generation of transfer functions and time responses, and a nonlinear simulation.

Longitudinal Design

Even though the longitudinal case satisfied all its handling qualities, the phugoid mode was quite oscillatory. Thus, it was desirable to reduce this oscillatory response either by increasing ζ_p or decreasing ω_{np} . Because of the constraint of only rates for acceptable feedbacks, the choices of feedbacks for augmentation were pitch rate and pitch rate with compensation.

It required only a brief glance at the root locus of the pitch rate feedback system (Fig 9) to realize that it would not provide appropriate augmentation. This was due to the zero that was very close to the phugoid poles which translated into a very large gain for a small increase in damping ratio. In itself, the large gain was not a problem; rather, it was its effect on the other roots that presented the difficulty. A large gain would cause the short period root to become less stable and its handling quality to become unsatisfied. In addition, the actuator dynamics would change greatly which was undesirable. Therefore, the conclusion was that the addition of compensation would be advantageous.

The desire to keep the compensation simple and to eliminate the effect of the zero at the origin dictated the choice of a pure integrator as the feedback compensator. The root locus (Fig 10) revealed that the zero at the origin was effectively removed and that the short period root became unstable faster than without compensation. The short period handling qualities restricted the amount of feedback gain to less than 5.14. A feedback gain of 0.050 produced the best compromise between maximum augmentation and minimum effect on the other roots. Thus, the control law was

$$\delta_{cmd}(s) = E_{in}(s) + \frac{0.050}{s} q(s) \quad (8)$$

An examination of the phugoid characteristics showed that the damping ratio increased from $\zeta_p = 0.055$ to $\zeta_p = 0.25$ while the natural frequency remained essentially constant. Hence, the oscillatory phugoid mode was reduced substantially.

Lateral-Directional Design

The analysis of Chapter III suggested that the dutch roll damping ratio should be increased and the spiral mode should be stabilized. A standard yaw damper, consisting of yaw rate feedback to the rudder (passing through a washout circuit), was used to augment the dutch roll mode. The main difficulty in this design was selecting the washout pole location. A large time constant for this pole indicates a large increase in both damping ratio and uncoordinating effect (Ref 12:600). A washout pole location of $s = -1.75$ ($T = 0.57$ sec) produced the best compromise to the trade-off described above. A feedback gain of 0.032 was selected because it corresponded to the maximum dutch roll damping

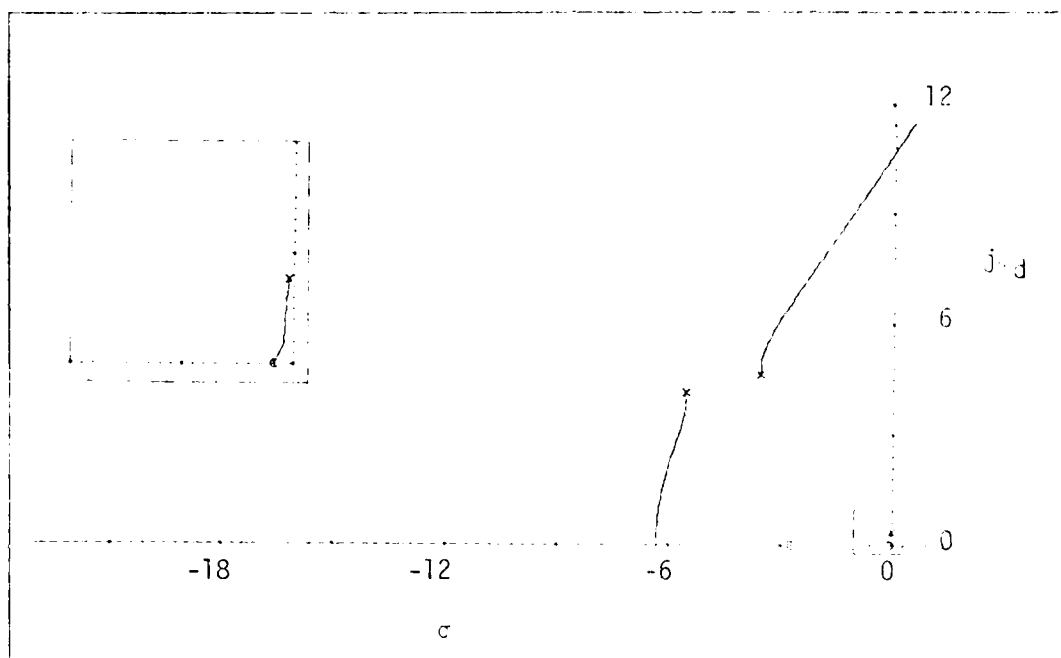


Figure 9. Root Locus for Pitch Rate Feedback to the Elevator

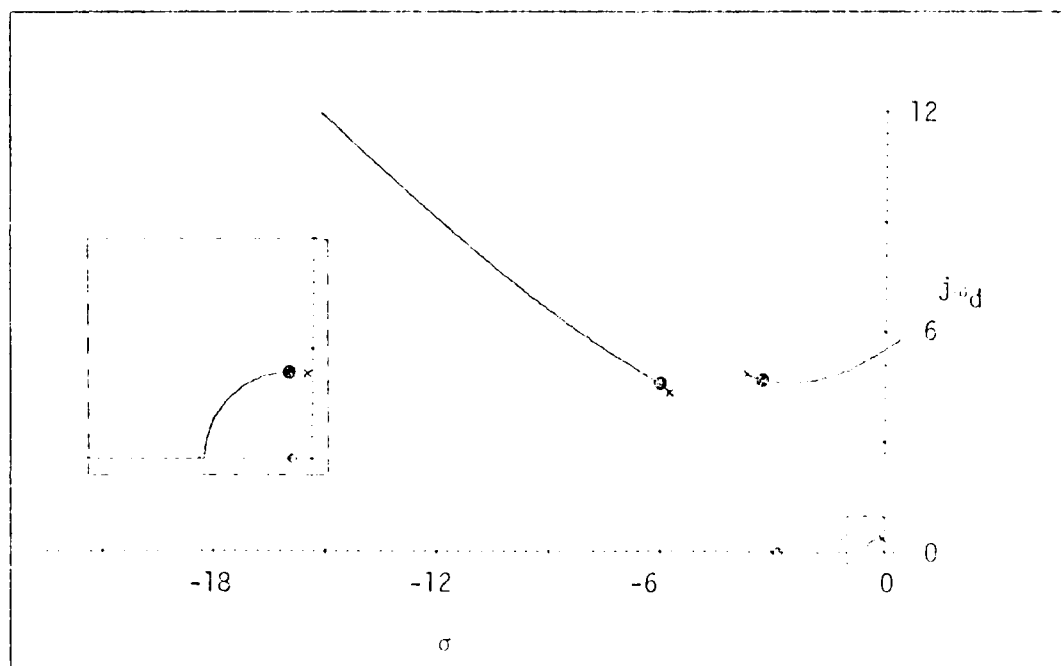


Figure 10. Root Locus for Integral of Pitch Rate Feedback to the Elevator

ratio (see Fig 11). Thus, the control law was

$$\delta_{cmd}(s) = R_{in}(s) + \frac{0.038s}{s + 1.75} r(s) \quad (9)$$

An examination of the dutch roll characteristics revealed that the damping ratio increased from $\zeta_{DR} = 0.17$ to $\zeta_{DR} = 0.29$ while the natural frequency increased from $\omega_{nDR} = 4.21$ rad/sec to $\omega_{nDR} = 5.12$ rad/sec.

To simplify the system, the washout circuit was removed from Eq (9). With this control law, a feedback gain of 0.032 produced the maximum dutch roll damping ratio (see Fig 12). The dutch roll characteristics revealed that the damping ratio increased to $\zeta_{DR} = 0.21$. Unfortunately, this increase was not enough to satisfy the handling qualities by an adequate margin. Thus, the washout circuit was reinserted into Eq (9).

The spiral mode was most dominant in the lateral time responses. Thus, either integral of roll rate or yaw rate feedback to the ailerons would be the most effective means of stabilizing the spiral mode. For the integral of roll rate feedback system (Fig 13), a feedback gain of 0.012 brought the spiral root just inside the left hand plane resulting in a control law

$$\delta_{cmd}(s) = A_{in}(s) + \frac{0.012}{s} p(s) \quad (10)$$

Implementation of Eq (10) had no effect on any lateral-directional characteristic except the spiral root which moved to $s = -0.0003$ from $s = 0.041$.

For the yaw rate feedback system (Fig 14), a feedback gain of 0.044 established a stable spiral mode. The control law for this system was

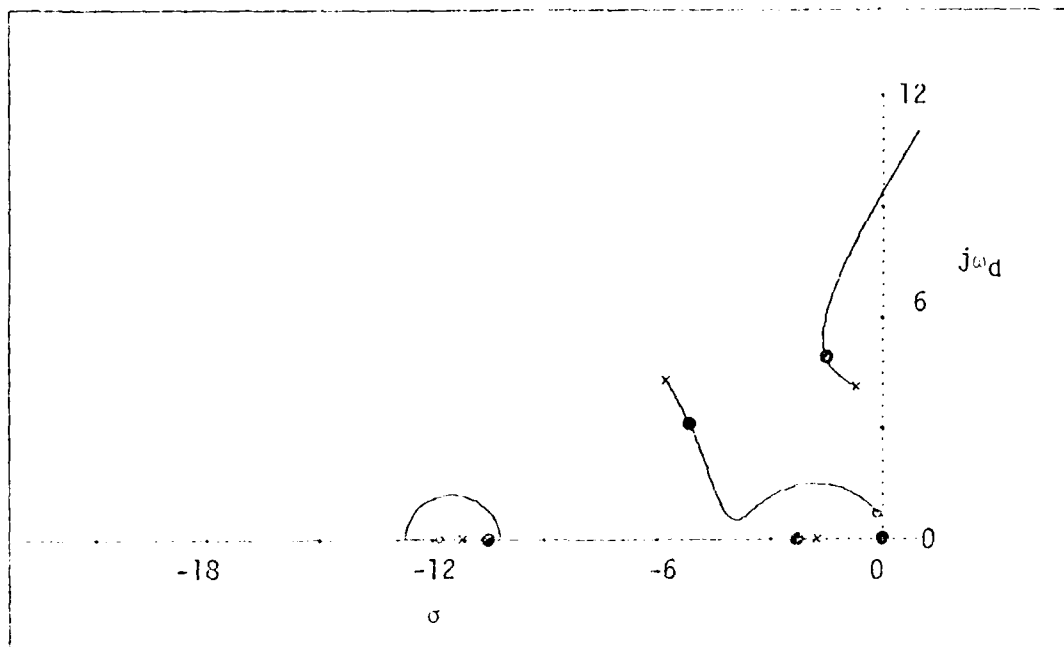


Figure 11. Root Locus for the Yaw Damper Including the Washout Circuit

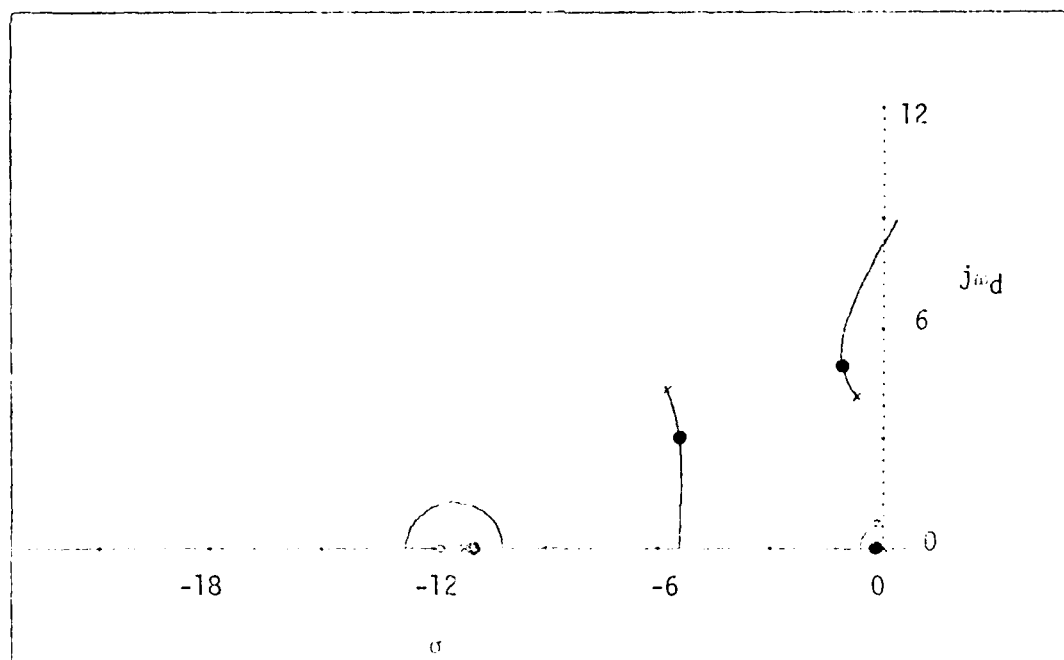


Figure 12. Root Locus for the Yaw Damper Excluding the Washout Circuit

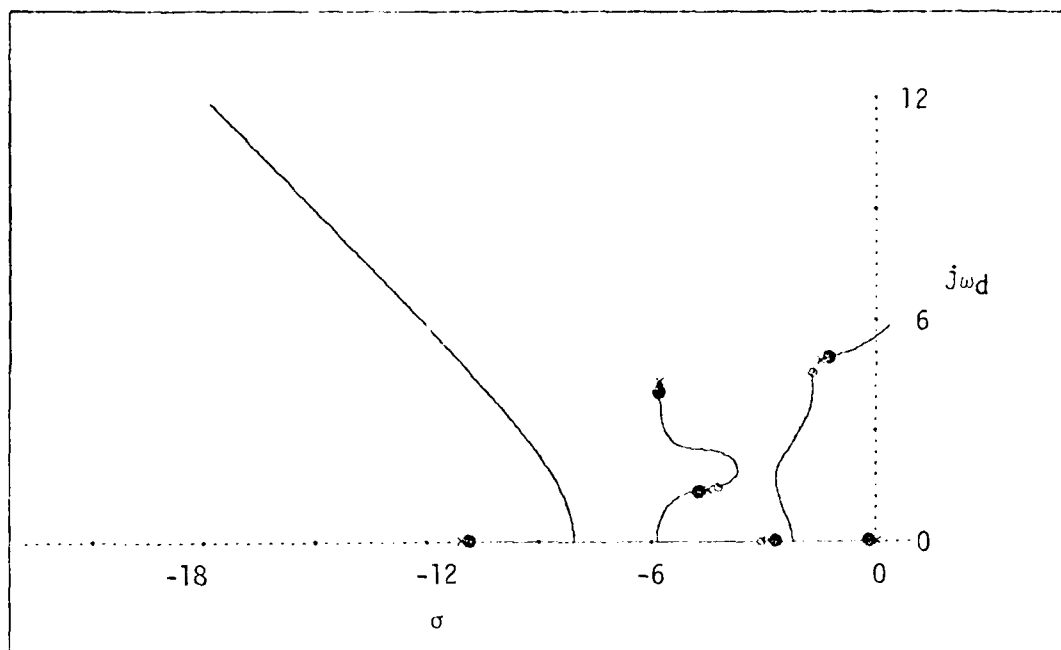


Figure 13. Root Locus for Integral of Roll Rate Feedback to the Ailerons

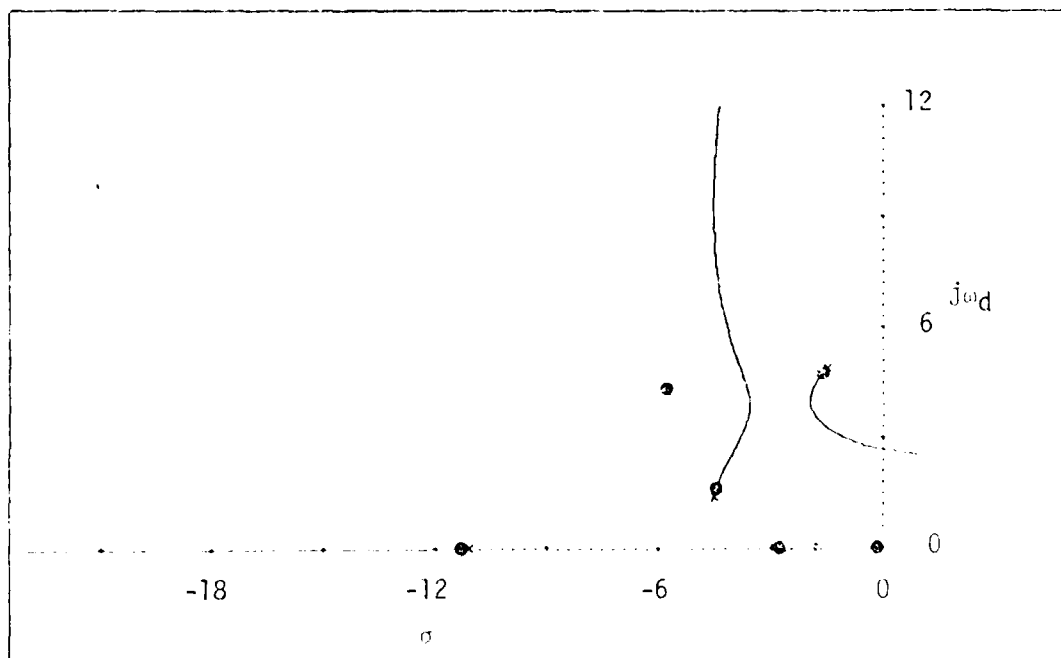


Figure 14. Root Locus for Yaw Rate Feedback to the Ailerons

$$s_{a_{cmd}}(s) = A_{in}(s) - 0.044 r(s) \quad (11)$$

Implementation of Eq (11) also had no effect on any lateral-directional characteristic other than moving the spiral root to $s = -0.0001$ from $s = 0.041$.

Thus, both Eqs (10) and (11) accomplished the desired goal of stabilizing the spiral mode. Equation (11) was selected as the more desirable control law because it did not require any compensation or any additional instrumentation, such as a roll rate gyro.

Sensitivity Studies and Redesign

Three types of sensitivity studies were used to evaluate the FCS: a flight condition study, a parameter study, and a physical quantity study. Each study based its results on a modal analysis. The flight condition study varied the airspeed throughout the entire speed regime. The parameter study varied each parameter in the equations of motion (except U_0 , \bar{q} , S , and \bar{c}) by ± 25 percent. Lastly, the physical quantity study varied the vertical tail area.

The modal analysis from the flight condition study showed that three handling qualities were not satisfied over the entire airspeed regime. First, the short period natural frequency handling quality became unsatisfied at the higher airspeeds ($M \geq 0.12$). Feedback gain adjustment had no effect on increasing the range of airspeeds that satisfied this handling quality. Thus, a restriction was imposed stipulating that this handling quality would not be satisfied at the higher airspeeds. This restriction was acceptable when considering that the higher airspeeds were clearly in the upper limits of the RPV's capabilities. Secondly, this study revealed that the spiral

mode was too unstable at low airspeeds. Increasing the feedback gain in Eq (11) to 0.09 stabilized this mode throughout the entire airspeed regime. Lastly, this study found that the dutch roll damping ratio did not satisfy its specification at the higher airspeeds ($M \geq 0.15$). A feedback gain of 0.03 maximized this damping ratio throughout the airspeed regime. Unfortunately, as in short period natural frequency, the entire airspeed regime could not be satisfied and the higher airspeeds restriction was imposed. Again, this was acceptable when considering the RPV's capabilities.

Hence, the control laws (Eqs (3), (9), and (11)) were refined to

$$\delta e_{cmd}(s) = E_{in}(s) + \frac{0.050}{s} q(s) \quad (12)$$

$$\delta a_{cmd}(s) = A_{in}(s) - 0.090 r(s) \quad (13)$$

$$\delta r_{cmd}(s) = R_{in}(s) + \frac{0.030 s}{s + 1.75} r(s) \quad (14)$$

Plots of the pole locations due to a varying airspeed, with the above control laws implemented, may be found in Fig 15. These plots show pole locations for airspeeds from Mach 0.05 to Mach 0.15 at Mach 0.01 intervals. The arrows indicate increasing airspeed.

The second study entailed tabulating the modes of the RPV as each parameter in the equations of motion (except U_0 , \bar{q} , S , and τ) was varied ± 25 percent. Comparing the extremum (Table VIII) with the handling qualities (Table IV) showed that all handling qualities were satisfied. Thus, an error in any one parameter of less than 25 percent will not cause any handling quality to be exceeded. Of course, no assurance can be made if more than one parameter changes.

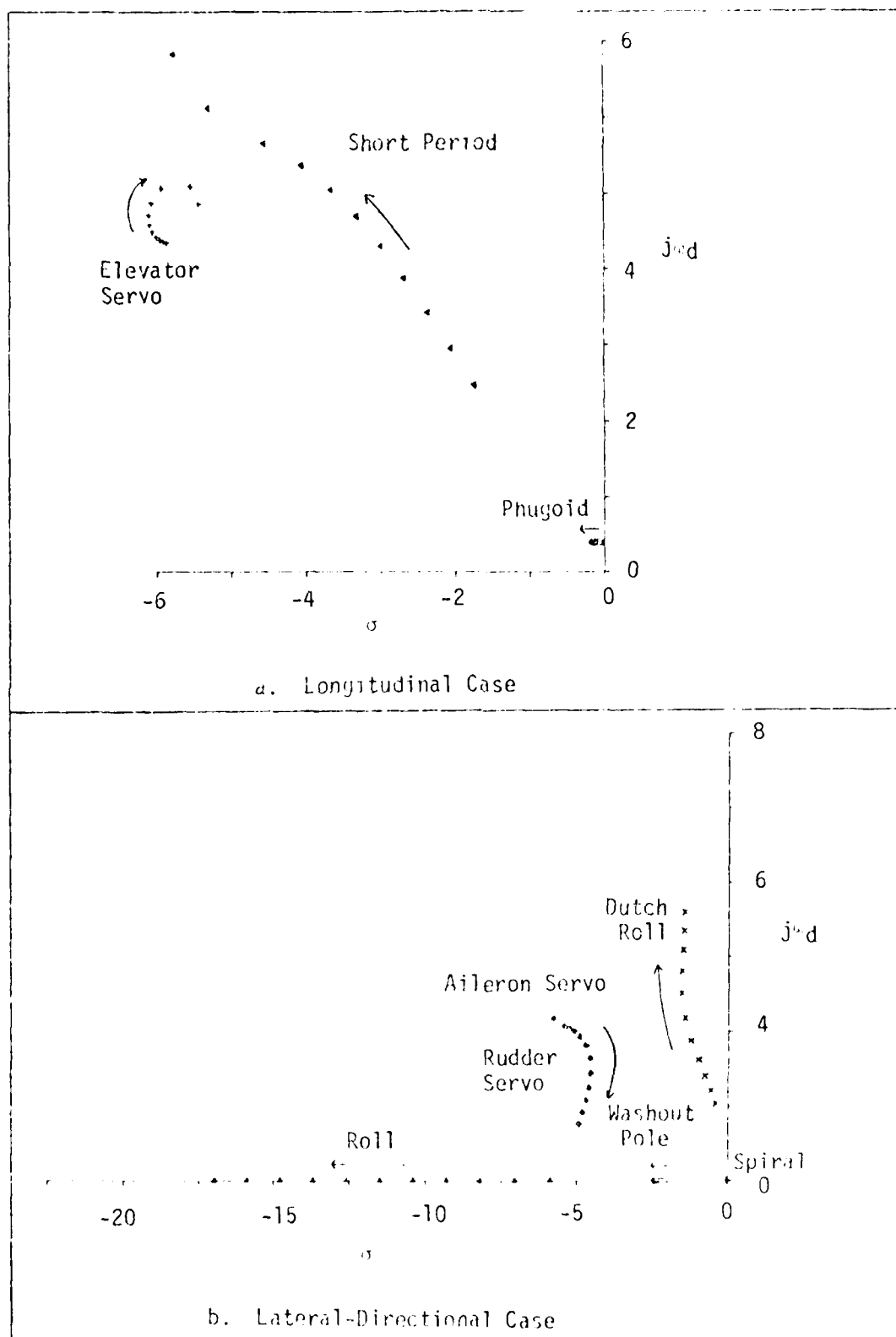


Figure 15. Pole Movement due to Variations in Airspeed

Table VIII. Extremum of the Parameter Sensitivity Study *

	Nominal Value	Largest Value	Smallest Value
ω_{np} , rad/sec	0.41	0.46 (-m)	0.36 (-C _{zu})
ζ_p	0.25	0.31 (-C _{mα})	0.20 (-C _{mξ_e})
ω_{sp} , rad/sec	5.74	6.46 (-I _y)	5.14 (-C _{mα})
ζ_{sp}	0.58	0.64 (-m)	0.52 (-C _{Lα})
ω_{DR} , rad/sec	4.60	5.63 (-I _z)	3.92 (+I _z)
ζ_{DR}	0.31	0.40 (-C _{nβ})	0.26 (+C _{nβ})
T _R , sec	0.087	0.11 (-C _{ξ_p})	0.066 (-I _x)
T _S , sec	22.91	48.86 (-C _{$\zeta_{\delta a}$})	14.86 (+C _{$\zeta_{\delta a}$})

* Source of the extremum is given in parentheses. The sign indicates whether the parameter was increased or decreased.

The last study was completed because of the single vertical tail approximation. Three scale factors (1.50, 1.75, and 2.00) were examined to determine the effect of the vertical tail area on the system modes. As expected, the vertical tail area had no effect on the longitudinal case. Little effect was found on the lateral-directional case. A plot of pole locations due to varying vertical tail area is shown in Fig 16. The arrows indicate increasing vertical tail area. Comparing

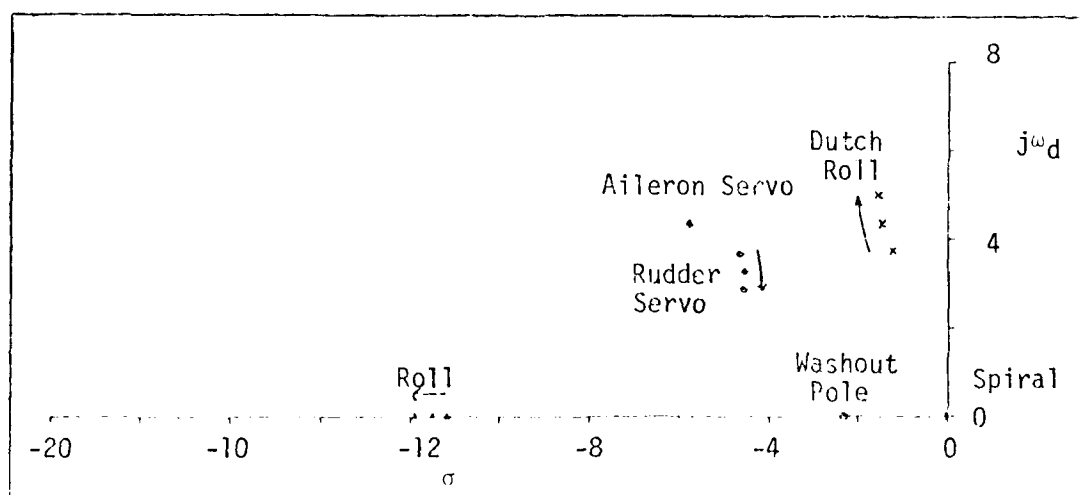


Figure 16. Pole Movement due to Variations in Vertical Tail Area

Fig 16 and Table IV revealed that all handling qualities were satisfied. Thus, a substantial variation in vertical tail area did not cause any handling quality to become unsatisfied.

Handling Qualities Check

A final check of the handling qualities was made with the control laws (Eqs (12) - (14)). A comparison of the augmented RPV, the basic RPV, and the handling qualities (Table IX) revealed that all characteristics satisfied their respective handling qualities.

Table IX. Comparison of the Augmented RPV,
Basic RPV, and the Handling Qualities

	Augmented RPV	Basic RPV	Handling Qualities
ζ_{sp}	0.58	0.61	$0.35 \leq \zeta_{sp} \leq 1.30$
$\omega_{n_{sp}}$, rad/sec	5.74	6.08	Fig 5
ζ_p	0.25	0.055	$\zeta_p \geq 0.04$
ω_{np} , rad/sec	0.41	0.39	*
T_R , sec	0.087	0.089	$T_R < 1.40$
T_S , sec **	22.91 (ω)	-24.04 (16.66)	$T_S \geq 0$ or $T_S \leq -23.85$ (>20.00)
ζ_{DR}	0.31	0.17	$\zeta_{DR} > 0.19$
$\omega_{n_{DR}}$, rad/sec	4.60	4.21	$\omega_{n_{DR}} > 0.40$
Dutch Roll Time Parameter, sec^{-1}	1.44	0.71	$\zeta_{DR} \omega_{n_{DR}} > 0.35$

* No handling quality exists.

** Negative sign indicates instability. Time to double (sec) is given in parentheses.

As before, the dutch roll time parameter ($\tau_{DR} \text{ sec}$) specification was dependent on the phi to beta ratio ($|\dot{\phi}/\dot{\beta}|_{DR}$). The time responses of Appendix C revealed that the graphical method of determining $|\dot{\phi}/\dot{\beta}|_{DR}$ used in Chapter III could not be utilized. Therefore, an analytical method was used. The $|\dot{\phi}/\dot{\beta}|_{DR}$ is the ratio of the magnitude of the $\dot{\phi}$ component to the magnitude of the $\dot{\beta}$ component of the dutch roll eigenvector. Thus,

$$\left| \frac{\dot{\phi}}{\dot{\beta}} \right|_{DR} = \left| \frac{-0.0075 + j0.0017}{0.0084 + j0.0567} \right|$$

$$= 0.13$$

Since

$$\omega_{DR}^2 \left| \frac{\dot{\phi}}{\dot{\beta}} \right|_{DR} = 2.84$$

$$\dagger 20.00$$

the dutch roll time parameter specification became $\tau_{DR} \text{ sec} \leq 0.35$, which was satisfied by the augmented RPV.

In addition, the roll effectiveness of the augmented RPV needed to be computed. With maximum deflection of the ailerons (15 deg), the augmented RPV produced 62 deg of bank in 1.5 sec (Fig 17). Hence, no change in roll effectiveness was experienced due to the FCS.

Lastly, since $\tau_{DR} = 0.20$, Eq (3) could not be utilized to determine τ_{osc}/ϕ_{ave} . Rather

$$\frac{\tau_{osc}}{\phi_{ave}} = \frac{\tau_1 + \tau_2}{1 + \tau_2} \quad (15)$$

should be used (Ref 4: xxii). Thus, the impulse time response (Fig 18) was used in Eq (15) and produced

$$\frac{\tau_{osc}}{\phi_{ave}} = 0.044$$

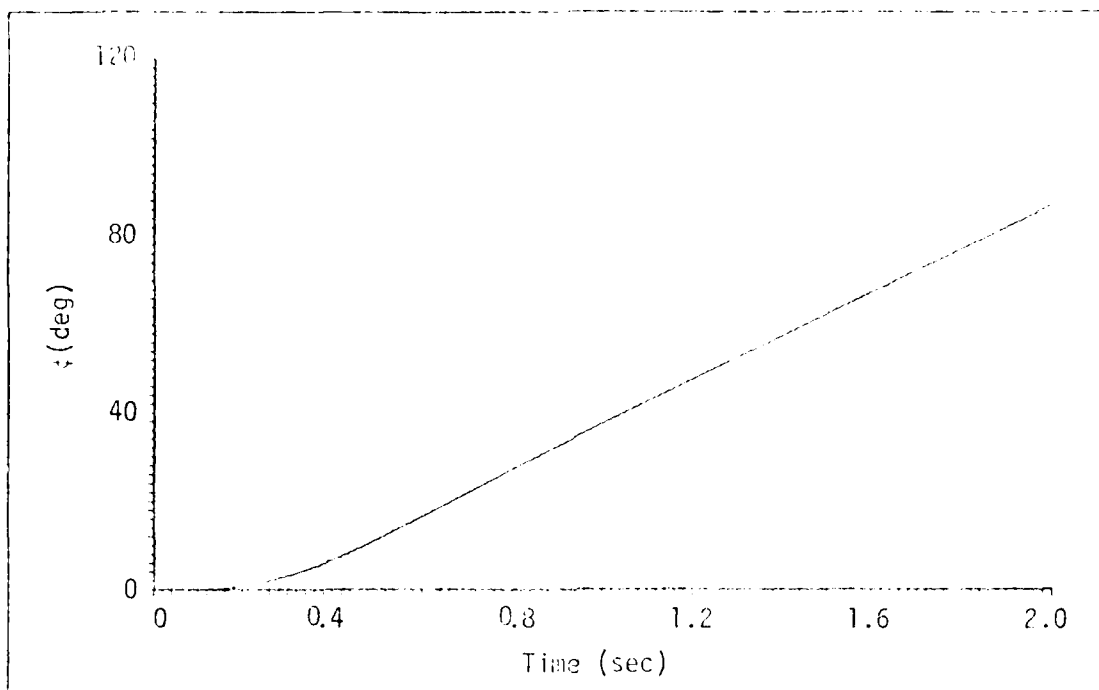


Figure 17. Augmented RV Bank Angle due to a 15 deg Step Aileron Command

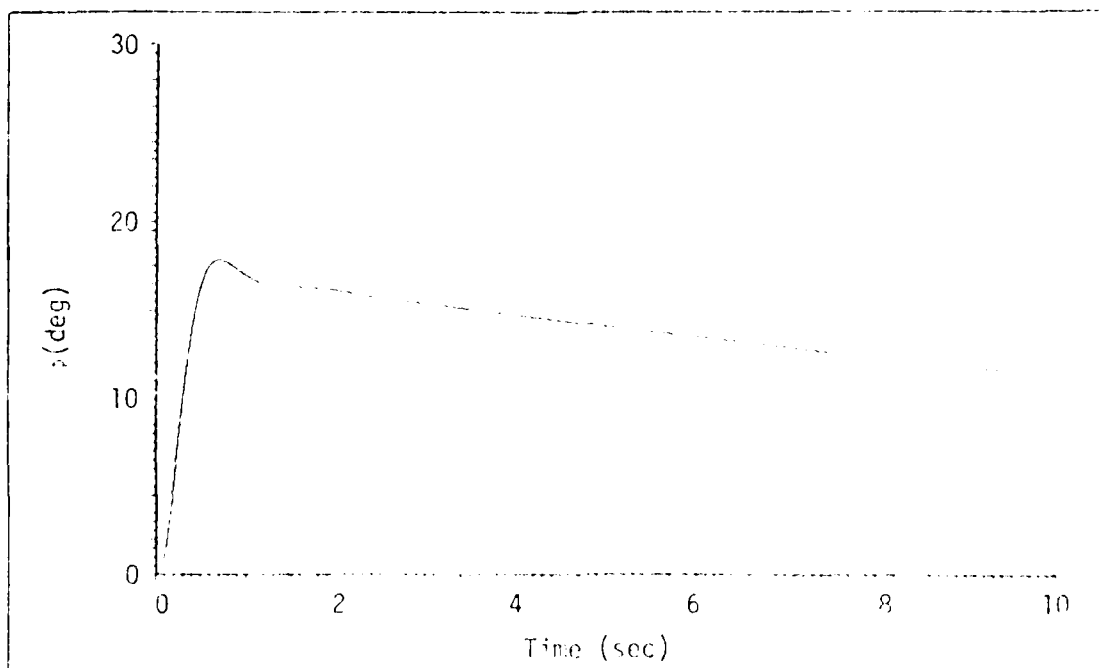


Figure 18. Augmented RV Bank Angle due to a 5 deg 10 pulse Aileron Command

Hence, the augmented RPV was not very oscillatory.

Transfer Functions and Time Responses

Before transfer functions and time responses could be determined, the closed-loop state equation must be derived. Recall the form of the open-loop state equation

$$\dot{\underline{x}} = \underline{A} \underline{x} + \underline{B} \underline{u} \quad (16)$$

where

$$\underline{u} = \underline{K} \underline{x} + \underline{IN} \quad (17)$$

Substituting Eq (17) into Eq (16) and simplifying

$$\begin{aligned} \dot{\underline{x}} &= \underline{A} \underline{x} + \underline{B}(\underline{K} \underline{x} + \underline{IN}) \\ &= (\underline{A} + \underline{BK}) \underline{x} + \underline{B} \underline{IN} \end{aligned} \quad (18)$$

Substituting the control laws (Eqs (12) - (14) into Eq (18) provided the closed-loop state equation given in Fig 19. Notice that a new state variable had to be added to the lateral-directional state equation due to the washout circuit in the yaw damper. The new state was chosen to be the yaw damper feedback B and defined as

$$B(s) = \frac{0.030 s}{s + 1.75} r(s)$$

Using the closed-loop state equation (Fig 19), transfer functions and time responses of the augmented RPV were generated (Ref 16). Table X contains the resultant transfer functions while the time responses are in Appendix C. Comparing these time responses with the basic RPV time responses verified that the design objectives had been achieved.

Table X. Transfer Functions for the Augmented RPV

Longitudinal Case:	
v	$= (s^2 + 0.21 s + 0.17)(s^2 + 6.62 s + 32.98)(s^2 + 12.16 s + 57.99)$
N_{Ein}^u	$= -2.34 (s + 4.76)(s - 163.08)$
N_{Ein}^y	$= -19.04 (s + 114.58)(s^2 + 0.57 s + 0.28)$
N_{Ein}^θ	$= -2219.32 (s + 0.089)(s + 2.82)$
N_{Ein}^q	$= -2219.32 s(s + 0.089)(s + 2.82)$
N_{Ein}^{se}	$= 52.20 (s^2 + 7.38 s + 37.01)(s^2 + 0.042 s + 0.15)$
$N_{Ein}^{\dot{se}}$	$= 52.20 s(s^2 + 7.38 s + 37.01)(s^2 + 0.042 s + 0.15)$
Lateral-Directional Case:	
φ	$= (s + 11.50)(s + 0.044)(s + 2.32)(s^2 + 2.89 s + 21.12)$ $(s^2 + 11.56 s + 52.20)(s^2 + 9.11 s + 31.49)$
N_{Ain}^p	$= -64.78(s + 0.21)(s + 2.42)(s - 36.72)(s^2 + 10.95 s + 46.42)$
N_{Ain}^r	$= 64.09(s + 1.75)(s - 2.27)(s + 2.54)(s - 26.44)$ $(s^2 + 11.55 s + 52.18)$
N_{Ain}^δ	$= 2288.02(s + 2.30)(s^2 + 2.96 s + 20.39)(s^2 + 9.49 s + 29.63)$
N_{Ain}^p	$= 2288.02 s(s + 2.30)(s^2 + 2.96 s + 20.39)(s^2 + 9.49 s + 29.63)$
N_{Ain}^{sa}	$= 52.20(s - 0.041)(s + 2.31)(s + 11.10)(s^2 + 9.82 s + 30.75)$ $(s^2 + 2.68 s + 23.44)$
$N_{Ain}^{\dot{sa}}$	$= 52.20 s(s - 0.041)(s + 2.31)(s + 11.10)(s^2 + 9.82 s + 30.75)$ $(s^2 + 2.68 s + 23.44)$
$N_{Ain}^{\dot{r}}$	$= 100.27 (s - 0.0004)(s - 2.27)(s + 2.55)(s - 26.32)$

Table X. (Continued)

$$\begin{aligned}
 N_{Ain}^{sr} &= 100.27 s(s - 0.0004)(s - 2.27)(s + 2.55)(s - 25.32) \\
 N_{Ain}^B &= 1.92 (s - 0.0004)(s - 2.27)(s + 2.55)(s - 25.32) \\
 &\quad (s^2 + 11.56 s + 52.20) \\
 N_{Rin}^3 &= 26.45 (s + 0.019)(s + 1.75)(s + 11.74)(s + 79.24) \\
 &\quad (s^2 + 11.63 s + 51.16) \\
 N_{Rin}^r &= -2090.00 (s + 1.75)(s + 11.65)(s^2 + 0.24 s + 0.49) \\
 &\quad (s^2 + 11.56 s + 52.20) \\
 N_{Rin}^i &= 713.53 (s + 1.75)(s + 10.47)(s - 12.95)(s^2 + 4.15 s + 22.30) \\
 N_{Rin}^p &= 713.53 s(s + 1.75)(s + 10.47)(s - 12.95)(s^2 + 4.15 s + 22.30) \\
 N_{Rin}^{sa} &= 9813.84 (s + 1.75)(s + 11.65)(s^2 + 0.24 s + 0.49) \\
 N_{Rin}^{ia} &= 9813.84 s(s + 1.75)(s + 11.65)(s^2 + 0.24 s + 0.49) \\
 N_{Rin}^{sr} &= 52.20 (s + 0.045)(s + 1.75)(s + 11.52)(s^2 + 1.37 s + 16.24) \\
 &\quad (s^2 + 11.19 s + 53.26) \\
 N_{Rin}^{ir} &= 52.2 s(s + 0.045)(s + 1.75)(s + 11.52)(s^2 + 1.37 s + 16.24) \\
 &\quad (s^2 + 11.19 s + 53.26) \\
 N_{Rin}^B &= -62.70 (s - 0.0003)(s + 11.65)(s^2 + 0.24 s + 0.49) \\
 &\quad (s^2 + 11.56 s + 52.20)
 \end{aligned}$$

Nonlinear Simulation

The last form of evaluation was a complete nonlinear simulation which examined the effect of coupling on the FCS. Initially, an analog simulation was completed with the results being of low quality. Therefore, a digital simulation was accomplished using the numerical integration subroutine ODE (Ref 13) (see Fig 20). The equations of motion, in their most basic form (Eqs (35) and (33)), were used as was the same control inputs. Recall the nonlinear states (except U) have the same value as the perturbation states since the equilibrium conditions were chosen zero. Appendix C contains the results of this nonlinear simulation. A comparison with the other time responses indicated that the coupling effect between modes was quite small. Thus, the decoupling assumption produced minimal error and was acceptable.

In the formulation of the simulation algorithm (Fig 20), one critical selection was made, the increment time. Shannon's sampling theorem dictated that $\Delta t \leq 0.68$ sec for complete reproduction of the response (Ref 9: Sec III, 21). In practice, a much faster increment time than $\Delta t = 0.68$ sec is desirable. Thus, $\Delta t = .02$ sec was chosen for the first 2.0 sec of the simulation and $\Delta t = 0.10$ sec for the remainder of the simulation.

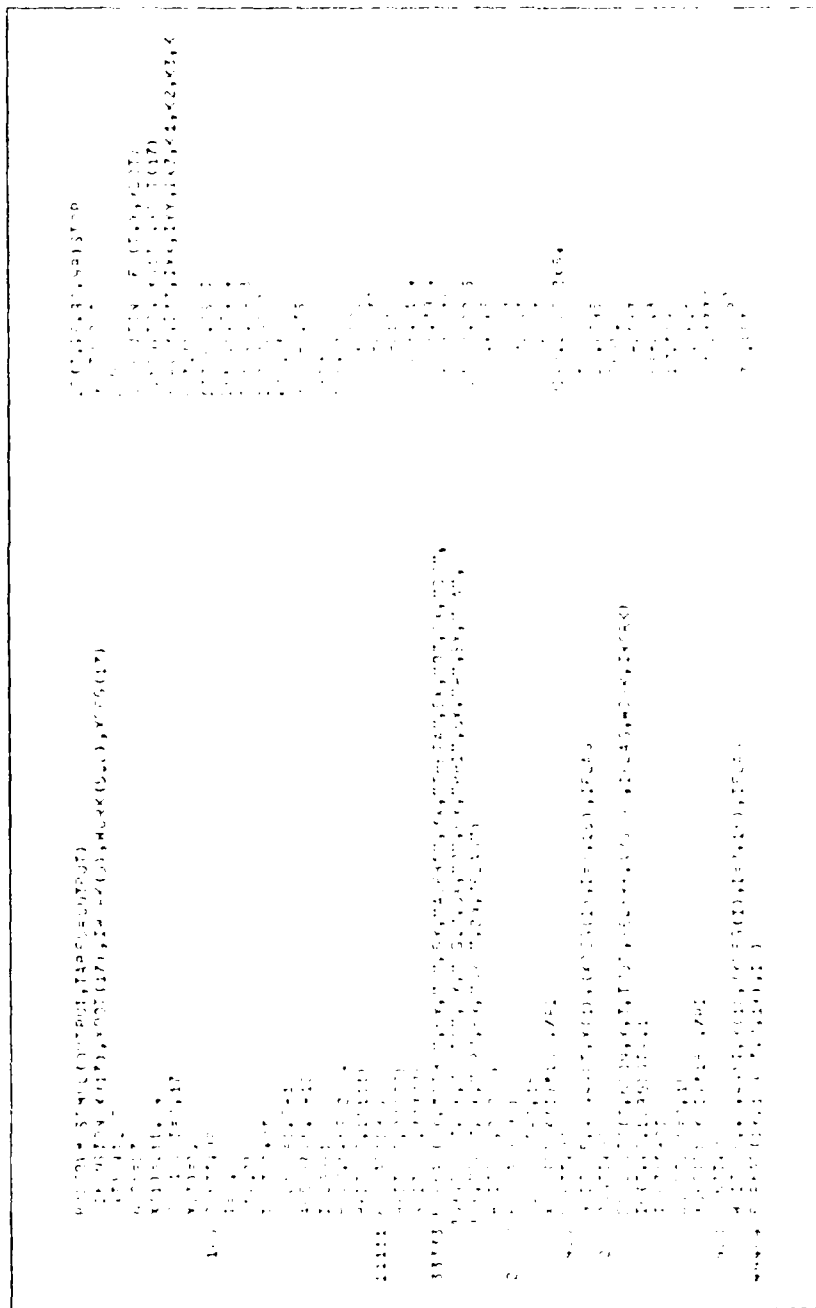


Figure 20. Digital Simulation Algorithm for a 1 sec
Pulse Elevator Command of -5 deg

V. A Practical Application

This study would not be complete without addressing an application of this RPV. It was hoped that by demonstrating its usefulness, motivation for continued research in this area would be generated. The chosen application was termed model matching, i.e., making the RPV have similar dynamic characteristics as another aircraft through the design of an expanded FCS. The aircraft chosen for duplication was the F-15. The first step of this procedure was to determine the F-15's dynamic characteristics. Then, three design procedures were investigated for accomplishing this duplication: Guillemin-Truxal design, Entire Eigenstructure Assignment, and an extension of Observer theory. Only the longitudinal case was examined since the lateral-directional case would be a repetition of the same theory.

Analysis of the F-15

The mathematical model for the F-15 was obtained from Ref 19 and is contained in Table XI. As with the RPV, the equations of motion were augmented with the actuator dynamics. The following representation was utilized for the F-15 servo (Ref 19):

$$TF_{\text{servo}} = \frac{20}{s + 20}$$

The corresponding differential equation was

$$\dot{\delta e} = -20 \delta e + 20 \delta e_{\text{cmd}} \quad (19)$$

The equations of motion were augmented with Eq (19) resulting in the longitudinal state equation given in Fig 21. Transfer functions

Table XI. F-15 Mathematical Model

m	$= 1085 \text{ slugs}$
U_0	$= 665 \text{ ft/sec}$
q	$= 388 \text{ lb/ft}^2$
S	$= 608 \text{ ft}^2$
\bar{c}	$= 16 \text{ ft}$
I_y	$= 155746 \text{ slug-ft}^2$
C_{x_u}	$= -.04$
$C_{x_{\dot{\alpha}}}$	$= 0$
$C_{x_{\alpha}}$	$= 0.24$
C_{x_q}	$= 0$
$C_{x_{\delta e}}$	$= 0$
C_{z_u}	$= -0.30$
$C_{L_{\dot{\alpha}}}$	$= 1.01$
$C_{L_{\alpha}}$	$= 3.78$
C_{L_q}	$= 3.12$
$C_{z_{\delta e}}$	$= 0$
C_{m_u}	$= 0$
$C_{m_{\dot{\alpha}}}$	$= -1.20$
C_{m_q}	$= -3.70$
$C_{m_{\delta e}}$	$= -0.69$

All stability and control derivatives have the units of per rad.

$$\begin{bmatrix} \dot{u} \\ \dot{\alpha} \\ \dot{\delta} \\ \dot{q} \\ \dot{e} \end{bmatrix} = \begin{bmatrix} -0.013 & 0.078 & -0.048 & 0 & 0 \\ -0.096 & -1.23 & 0 & 0.98 & 0 \\ 0 & 0 & 0 & 1.00 & 0 \\ 0.034 & -6.74 & 0 & -1.42 & -16.67 \\ 0 & 0 & 0 & 0 & -20.00 \end{bmatrix} \begin{bmatrix} u \\ \alpha \\ \delta \\ q \\ e \end{bmatrix} + \begin{bmatrix} 0 \\ 0 \\ 0 \\ 0 \\ 20.00 \end{bmatrix} \delta e_{cmd}$$

Figure 21. F-15 Longitudinal State Equation

(Table XII) and time responses (Figs 25 - 29) were generated from this state equation (Ref 16). Also, the longitudinal characteristics were determined as

$$\zeta_{sp} = 0.46$$

$$\omega_{sp} = 2.90 \text{ rad/sec}$$

$$\zeta_p = 0.10$$

$$\omega_p = 0.063 \text{ rad/sec}$$

Guillemin-Truxal Design

The Guillemin-Truxal design procedure is basically a pole/zero placement technique. From a desired closed-loop transfer function, the appropriate cascade or feedback compensator is mathematically calculated (Ref 6:408). This procedure guarantees duplication of the desired closed-loop transfer function for single input-single output systems. However, in this application, the RPV was a single input ($\delta\epsilon_{cmd}$)-multiple output ('u, α , θ , q, $\dot{\epsilon}$) system; therefore, the validity of this technique was questionable. However, it was decided that the duplication of one state might prove valuable. Of course, the duplication of one state would alter the other three states which might provide a closer match to all of the F-15 states.

For a cascade compensator $G_c(s)$, the closed-loop unity feedback transfer function is

$$\frac{N(s)}{D(s)} = \frac{G_c(s) G(s)}{1 + G_c(s) G(s)}$$

Solving for $G_c(s)$

$$G_c(s) = \frac{N(s)}{[D(s) - N(s)]G(s)}$$

Table XII. F-15 Longitudinal Transfer Functions

Δ	$= (s + 20)(s^2 + 0.013 s + 0.0040)(s^2 + 2.65 s + 8.39)$
N_{ecmd}^u	$= -9.45 (s - 2.10)$
N_{ecmd}^a	$= -328.07 (s^2 + 0.013 s + 0.0047)$
N_{ecmd}^r	$= -333.47 (s + 0.019)(s + 1.22)$
N_{ecmd}^q	$= -333.47 s (s + 0.019)(s + 1.22)$
N_{ecmd}^e	$= 20.00 (s^2 + 0.013 s + 0.0040)(s^2 + 2.65 s + 8.39)$

Applying this equation to the RPV and F-15 states (Ref 16) resulted in four cascade compensators (Table XIII), all of which were very complicated. From a hardware point of view, these compensators would be extremely difficult to implement, if not impossible. Thus, cascade compensators were rejected.

This same procedure was repeated for feedback compensators. The closed-loop transfer function is

$$\frac{N(s)}{D(s)} = \frac{G(s)}{1 + G_c(s)G(s)}$$

Solving for $G_c(s)$

$$G_c(s) = \frac{D(s)G(s) - N(s)}{N(s)G(s)}$$

This equation resulted in four feedback compensators (Table XIV) which were simpler than the cascade compensators, but still impractical to implement. Since both compensators were not feasible, the Guillemin-Truxal design procedure was dismissed as inappropriate for this application.

Entire Eigenstructure Assignment

Entire Eigenstructure Assignment is a design technique whereby the engineer may assign both the eigenvalues and eigenvectors to a system. This technique is based on full state feedback and uses the desired eigenvalues and eigenvectors to calculate the state feedback matrix (Ref 10). With only one input as in this application, the selection of the closed-loop eigenvalues completely determines the eigenvectors. Because of this, the effectiveness of this technique was also questionable.

Table XIII. Null-Invariant Cascade Compensators
for Model Matching

1) $G_c(s) = \frac{7.22(s + 1.12)(s^2 + 0.01s^2 + 7.38s + 07.07)(s^2 + 11.56s + 52.2)}{(s + 0.23)(s + 4.72)(s + 3.13)(s^2 + 20.80)s + 0.23)(s^2 + 2.55s + 0.23)}$
2) $G_c(s) = \frac{17.63(s^2 + 0.01s^2 + 7.38s + 07.07)(s^2 + 7.38s + 37.07)(s^2 + 11.56s + 52.2)}{(s + 0.23)(s + 4.72)(s + 3.13)(s^2 + 20.80)s + 0.23)(s^2 + 0.01s^2 + 7.38s + 37.07)(s^2 + 11.56s + 52.2)}$
3) $G_c(s) = \frac{0.15(s + 1.22)(s + 0.01s^2 + 7.38s + 07.07)(s^2 + 7.38s + 37.07)(s^2 + 11.56s + 52.2)}{(s + 2.82)(s + 0.23)(s + 4.72)(s + 3.13)(s^2 + 20.80)s + 0.23)(s^2 + 0.96s + 22.29)}$
4) $G_c(s) = \frac{0.15(s + 1.22)(s + 0.01s^2 + 7.38s + 07.07)(s^2 + 7.38s + 37.07)(s^2 + 11.56s + 52.2)}{(s + 1.60)(s + 0.23)(s + 4.72)(s + 3.13)(s^2 + 20.80)s + 0.23)(s^2 + 21.05s + 381.23)}$

Table XIV. Guillemin-fruxal Feedback Compensators
for Model Matching

$$u: G_c(s) = \frac{0.02(s + 0.14)(s - 0.12)(s + 5.46)(s^2 + 2.82s + 7.39)(s^2 + 59.93s + 1143.25)}{(s - 163.66)(s - 2.10)(s + 4.76)}$$

$$v: G_c(s) = \frac{0.050(s + 2.06)(s + 12.21)(s^2 + 0.029s + 0.680)(s^2 - 2.63s + 33.84)}{(s + 114.38)(s^2 + 0.057s + 0.19)(s^2 + 0.013s + 0.0047)} \frac{(s^2 + 0.013s + 0.0071)}{(s^2 + 0.013s + 0.0071)}$$

$$w: G_c(s) = \frac{0.0004(s + 0.47)(s + 0.017)(s + 3.83)(s + 12.07)(s^2 - 1.36s + 0.86)}{(s + 0.009)(s + 0.019)(s + 1.22)(s + 2.82)} \frac{(s^2 - 1.46s + 18.31)}{(s^2 - 1.46s + 18.31)}$$

$$z: G_c(s) = \frac{0.0004(s + 0.47)(s + 0.017)(s + 3.83)(s + 12.07)(s^2 - 1.36s + 0.86)}{s(s + 0.009)(s + 0.019)(s + 1.22)(s + 2.82)} \frac{(s^2 - 1.46s + 18.31)}{(s^2 - 1.46s + 18.31)}$$

Presently, the RPV and the F-15 are different order systems due to the actuator representations of each. Thus, the use of this technique will be difficult. To simplify the process, it was decided to employ a reduced-order servo model for the RPV. The criteria used for the selection of the reduced order model was time response to a pulse input. The output of the three models listed below was plotted against the RPV's second-order model (Fig 22) (Eq (6)).

Model	Reduced-Order Representation
1	$\frac{7.53}{s + 7.53}$
2	$\frac{6}{s + 6}$
3	$\frac{5}{s + 5}$

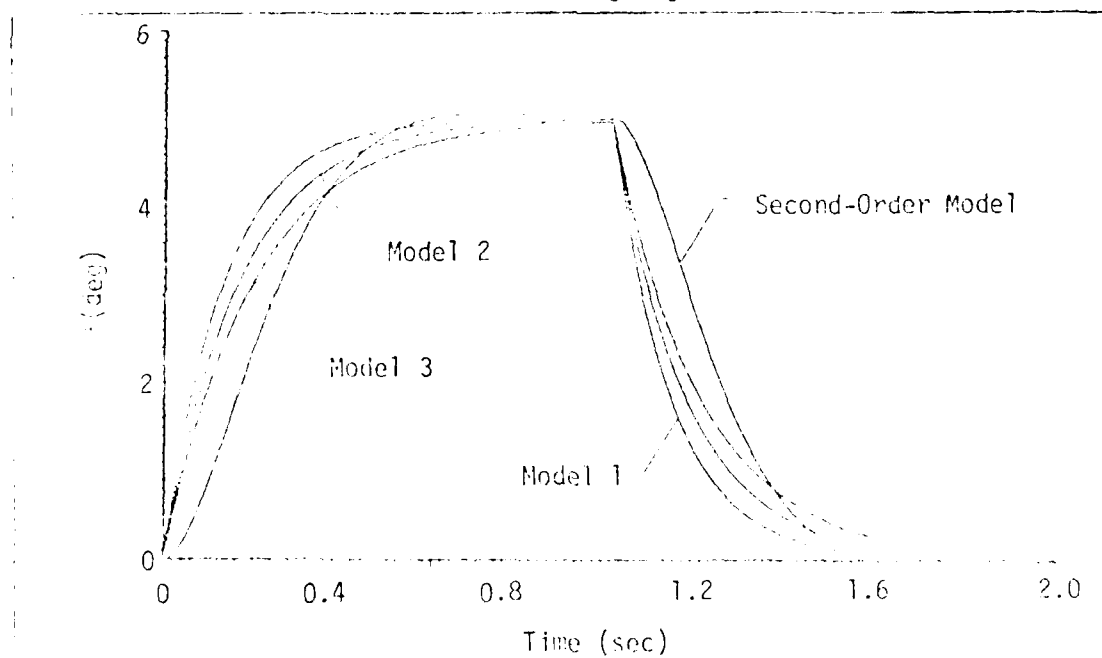


Figure 22. Reduced Order Servo Approximation for the RPV
Model 1 has the same 2 percent settling time as the second-order model.
The other models, both of which had slower responses, were examined

because they would be more likely to produce a better approximation to the second-order model. It was decided that model 2 provided the most accurate approximation to the second-order model, so it was used throughout the rest of this application.

The F-15 eigenvalues were assigned as the closed-loop eigenvalues of the RPV (Ref 3). As expected, the associated eigenvectors did not correspond to the F-15 eigenvectors (see Table XV). Thus the Entire Eigenstructure Assignment design technique was also dismissed as inappropriate for this application.

Extension of Observer Theory

With both the Guillemin-Truxal and the Entire Eigenstructure Assignment techniques yielding unacceptable results, something more basic to control system design was needed. Observer theory gave the necessary insight. The generalized block diagram (Fig 23) for this technique is in terms of an actual model, a desired model, and several feedback matrices (L , K , and K'). In an observer, K and K' would be identity matrices and the error feedback would go to the desired model instead of the actual model, i.e., the desired model would be made to track the actual model. In model matching the goal is for the actual model to track the desired model; hence, the error feedback goes to the actual model. K and K' were added to the system to increase flexibility. In this application, the RPV would be the actual model and the F-15 would be the desired model.

The closed-loop system was expressed in terms of several sets of state variables. It was found that the best choice of states were the five desired model (F-15) state variables (x') and the five error state

Table XV. Comparison of the F-15 Eigenvectors and the Closed-Loop RPV Eigenvectors produced by Entire Eigenstructure Assignment

Short Period Mode:	
RPV	F-15
$\begin{bmatrix} 0.030 \angle 233.04 \\ 0.32 \angle 303.03 \\ 0.34 \angle 242.73 \\ 1.00 \angle 0 \\ 0.20 \angle 150.30 \end{bmatrix}$	$\begin{bmatrix} 0.0056 \angle 176.65 \\ 0.38 \angle 267.87 \\ 0.34 \angle 242.73 \\ 1.00 \angle 0 \\ 0 \end{bmatrix}$
Phugoid Mode:	
RPV	F-15
$\begin{bmatrix} 46.36 \angle 46.11 \\ 10.57 \angle 226.24 \\ 16.43 \angle 264.10 \\ 1.00 \angle 0 \\ 7.14 \angle 46.82 \end{bmatrix}$	$\begin{bmatrix} 12.08 \angle 0.96 \\ 0.15 \angle 183.17 \\ 15.81 \angle 264.11 \\ 1.00 \angle 0 \\ 0 \end{bmatrix}$

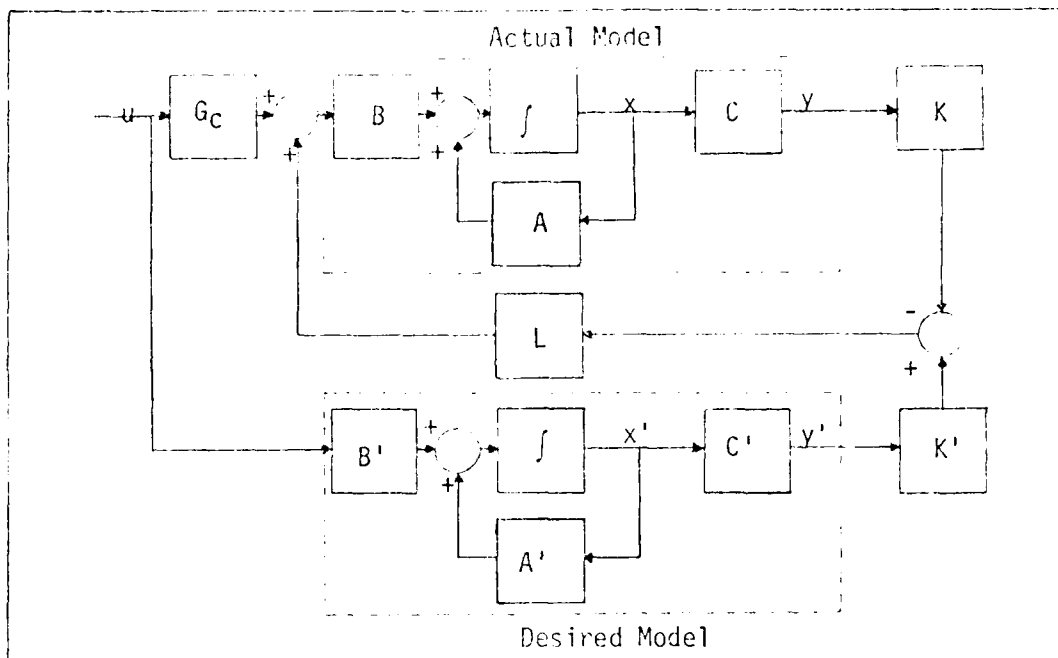


Figure 23. Generalized Block Diagram for Model Matching

variables ($\underline{\varepsilon}$), where

$$\underline{\varepsilon} = \underline{x} - \underline{x}' \quad (20)$$

Thus, the closed-loop state equation is

$$\begin{bmatrix} \dot{\underline{\varepsilon}} \\ \dot{\underline{x}'} \end{bmatrix} = \begin{bmatrix} A - BLKC & (A - BLKC) - (A' - BLK'C') \\ \underline{0} & A' \end{bmatrix} \begin{bmatrix} \underline{\varepsilon} \\ \underline{x}' \end{bmatrix} + \begin{bmatrix} BG_c + B' \\ B' \end{bmatrix} \underline{u} \quad (21)$$

The servo representations have been included in A and A' . Also, for single input systems, B and B' will always be zero vectors except for the last element. Hence, K' added no additional flexibility to the system and was assumed to be the identity matrix. For this application,

C and C' were also identity matrices. Finally, defining $R = LK$ provided insight into choosing the feedback matrices. Thus, Eq (21) became

$$\begin{bmatrix} \dot{\underline{\epsilon}} \\ \dot{\underline{x'}} \end{bmatrix} = \begin{bmatrix} A - BR & (A - BR) - (A' - BL) \\ 0 & A' \end{bmatrix} \begin{bmatrix} \underline{\epsilon} \\ \underline{x'} \end{bmatrix} + \begin{bmatrix} BG_C - B' \\ B' \end{bmatrix} \underline{u} \quad (22)$$

This form of the state equation yields insight into the proper choice of weighting matrices (R, L, and G_C). The solution of Eq (26) is in terms of the eigenfunctions ($\underline{y}_i e^{\lambda_i t}$). Thus, R should be chosen such that the dominant terms of the eigenfunctions of $(A - BR)$ die out rapidly. Even though all eigenvalues of $(A - BR)$ need to be negative, this does not indicate that all eigenvalues need to be far in the left hand plane. Only the ones associated with the dominant eigenfunctions need have large negative values. $[(A - BR) - (A' - BL)]$ is a coupling matrix. Ideally, the best choice for this matrix would be a zero matrix. Unfortunately, L does not have enough variables to accomplish this. Therefore, L should be chosen to minimize the coupling effect. Finally, it would be desirable if an input did not directly affect the error. Thus, G_C should be chosen to produce a zero vector for $(BG_C - B')$.

The techniques for choosing R and G_C are relatively simple. However, minimization of the coupling effect represents a greater challenge. To simplify the notation of this derivation, define

$$\alpha = A - BR$$

$$\beta = (A - BR) - (A' - BL)$$

Thus, Eq (22) becomes

$$\begin{bmatrix} \dot{\underline{e}} \\ \dot{\underline{x}}' \end{bmatrix} = \begin{bmatrix} \alpha & \beta \\ \underline{0} & A' \end{bmatrix} \begin{bmatrix} \underline{e} \\ \underline{x}' \end{bmatrix} + \begin{bmatrix} BG_C - B' \\ B' \end{bmatrix} \underline{u} \quad (23)$$

Examining the zero input response to Eq (23) produced valuable insight into the importance of β . The zero input response is

$$\begin{bmatrix} \underline{e}(t) \\ \underline{x}'(t) \end{bmatrix} = \begin{bmatrix} 10 \\ \Sigma_{i=1} \end{bmatrix} e^{\lambda_i t} \underline{v}_i \underline{r}_i^T \begin{bmatrix} \underline{e}(0) \\ \underline{x}'(0) \end{bmatrix} \quad (24)$$

where

$$\begin{aligned} \lambda_i &= i^{\text{th}} \text{ eigenvalue of } \begin{bmatrix} \alpha & \beta \\ \underline{0} & A' \end{bmatrix} \\ \underline{v}_i &= i^{\text{th}} \text{ eigenvector of } \begin{bmatrix} \alpha & \beta \\ \underline{0} & A' \end{bmatrix} \\ \underline{r}_i &= i^{\text{th}} \text{ reciprocal basis vector of } \begin{bmatrix} \alpha & \beta \\ \underline{0} & A' \end{bmatrix} \end{aligned}$$

Because of the upper block form of $\begin{bmatrix} \alpha & \beta \\ \underline{0} & A' \end{bmatrix}$, the system eigenvalues are simply the eigenvalues of α and A' . Also, $\underline{v}_i \underline{r}_i^T$ is a 10 x 10 matrix whose upper right 5 x 5 block (defined as γ) needs to be minimized for all i .

For the eigenvalues corresponding to α , the eigenvectors and reciprocal basis vectors are

$$\underline{v}_i = \begin{bmatrix} \underline{\xi}_i \\ \hline 0 \end{bmatrix} \quad \underline{r}_i = \begin{bmatrix} \underline{w}_i^T \\ \hline \underline{w}_i^T \beta [\lambda_{i\alpha} I - A']^{-1} \end{bmatrix} \quad (25)$$

where

$\underline{\xi}_i$ = i th eigenvector of α

\underline{w}_i = i th reciprocal basis vector of α

For the eigenvalues corresponding to A' , the eigenvectors and reciprocal basis vectors are

$$\underline{v}_i = \begin{bmatrix} [\lambda_{iA'} I - a]^{-1} \beta \underline{\xi}_i' \\ \hline \underline{\xi}_i' \end{bmatrix} \quad \underline{r}_i = \begin{bmatrix} 0 \\ \hline \underline{w}_i' \end{bmatrix} \quad (26)$$

where

$\underline{\xi}_i'$ = i th eigenvector of A'

\underline{w}_i' = i th reciprocal basis vector of A'

Now that the eigenvectors and reciprocal basis vectors have been determined, γ needs to be examined. Recall that L yields control over only the fifth row of \underline{e} . Therefore, the equations were simplified to isolate these terms. For the eigenvalues corresponding to α

$$\underline{v}_i \underline{r}_i^T = \begin{bmatrix} \underline{\xi}_i \\ \hline 0 \end{bmatrix} [\underline{w}_i^T \quad \underline{w}_i^T \beta [\lambda_{i\alpha} I - A']^{-1}]$$

or

$$\gamma = \sum_i \underline{\xi}_i \underline{w}_i^T \beta [\lambda_{i\alpha} I - A']^{-1} \quad (27)$$

Defining $\Phi = [\lambda_{i\alpha} I - A']^{-1}$ and expanding Eq (27) for the r -c component of γ

$$\gamma_{rc} = \sum_{k=1}^5 \epsilon_{ir} w_{ik} \left[\sum_{j=1}^5 \beta_{kj} \phi_{jc} \right]$$

$$= \sum_{k=1}^4 \epsilon_{ir} w_{ik} \left[\sum_{j=1}^5 \beta_{kj} \phi_{jc} \right] + \epsilon_{ir} w_{i5} \left[\sum_{j=1}^5 \beta_{5j} \phi_{jc} \right]$$

or, in matrix form

$$\gamma_{rc} = [\epsilon_{ir} w_{i5} \beta_{1c} \cdots \epsilon_{ir} w_{i5} \beta_{5c}] \begin{bmatrix} \beta_{51} \\ \vdots \\ \beta_{55} \end{bmatrix}$$

$$+ \sum_{k=1}^4 \epsilon_{ir} w_{ik} \left[\sum_{j=1}^5 \beta_{kj} \phi_{jc} \right] \quad (28)$$

For the eigenvalues corresponding to A'

$$\underline{v}_i \underline{r}_i^T = \left[\frac{[\lambda_i A' \ I - \alpha]^{-1} \beta \underline{\xi}_i'}{\underline{\xi}_i'} \right] [0^T \mid \underline{w}_i'^T]$$

or

$$\gamma = [\lambda_i A' \ I - \alpha]^{-1} \beta \underline{\xi}_i' \underline{w}_i'^T \quad (29)$$

Defining $\psi = [\lambda_i A' \ I - \alpha]^{-1}$ and expanding Eq (29) for the r-c component of γ

$$\gamma_{rc} = \sum_{k=1}^5 \left[\sum_{j=1}^5 \psi_{rj} \beta_{jk} \right] \epsilon_{ik}' w_{ic}'$$

$$= \sum_{k=1}^5 \left[\sum_{j=1}^4 \psi_{rj} \beta_{jk} \right] \epsilon_{ik}' w_{ic}' + \sum_{k=1}^5 \psi_{r5} \beta_{5k} \epsilon_{ik}' w_{ic}'$$

or, in matrix form

$$\gamma_{rc} = [\psi_{r5} \beta_{15} w_{i5}' \cdots \psi_{r5} \beta_{55} w_{i5}'] \begin{bmatrix} \beta_{51} \\ \vdots \\ \beta_{55} \end{bmatrix}$$

$$+ \sum_{k=1}^5 \left[\sum_{j=1}^4 \psi_{rj} \beta_{jk} \right] \epsilon_{ik}' w_{ic}' \quad (30)$$

Augmenting Eq (28) with Eq (30)

$$y_{rc} = \begin{bmatrix} \xi_{ir} w_{i5} \phi_{1c} & \cdots & \xi_{ir} w_{i5} \phi_{5c} \\ \vdots \\ \xi_{r5} w_{i1} w_{ic} & \cdots & \xi_{r5} w_{i5} w_{ic} \end{bmatrix} \begin{bmatrix} \beta_{51} \\ \vdots \\ \beta_{55} \end{bmatrix} + \begin{bmatrix} \sum_{k=1}^4 \xi_{ir} w_{ik} & \sum_{j=1}^5 \beta_{kj} \phi_{jc} \\ \vdots \\ \sum_{k=1}^5 \xi_{rj} \beta_{jk} & \xi_{ik} w_{ic} \end{bmatrix} \quad (31)$$

$$= C \underline{\beta}_5 + D \quad (32)$$

where

$$1 \leq c \leq 5$$

$$1 \leq i \leq 5$$

$$1 \leq r \leq 5$$

Thus, Eq (32) is a matrix equation consisting of 250 equations in terms of 5 variables.

Minimization of Eq (32) accomplishes the goal of minimizing the coupling effect. A cost function of one half the squared error was chosen for this minimization. Thus

$$J(\underline{\beta}_5) = \frac{1}{2} (C \underline{\beta}_5 + D)^T (C \underline{\beta}_5 + D)$$

Setting the first derivative of $J(\underline{\beta}_5)$ equal to zero and solving for $\underline{\beta}_5$ produced

$$\underline{\beta}_5 = -[C^T C]^{-1} C^T D \quad (33)$$

Thus, choosing the fifth row of β (hence, L) in accordance with Eq (33) will minimize the coupling effect.

For the model matching application, 22 sets of eigenfunctions were examined in choosing R (Ref 3) with the best one being

$$R = [162.1 \quad 25.54 \quad -49.12 \quad -3.17 \quad 7.26]$$

This R assigned the eigenvalues of α to $\lambda_1 = -2$, $\lambda_2 = -4$, $\lambda_3 = -15$, $\lambda_4 = -17$, and $\lambda_5 = -19$ with the eigenfunction corresponding to $\lambda_3 = -15$ being dominant over the other ones by one order of magnitude. Equation (33) was employed resulting in

$$\underline{p}_5^T = [7.89 \quad -13.24 \quad 13.98 \quad -4.62 \quad -15.38]$$

which in turn produced

$$L = [163.41 \quad 23.33 \quad -46.79 \quad -3.94 \quad 2.36]$$

and

$$K = \begin{bmatrix} 0.99 & 0 & 0 & 0 & 0 \\ 0 & 1.09 & 0 & 0 & 0 \\ 0 & 0 & 1.05 & 0 & 0 \\ 0 & 0 & 0 & 0.80 & 0 \\ 0 & 0 & 0 & 0 & 3.07 \end{bmatrix}$$

In this application, G_c was a scalar and determined to be 3.33. The above matrices were substituted into Eq (22) to produce the system state equation given in Fig 24. Time responses were produced with both the RPV and the F-15 responses on the same plot (Figs 25 - 29). These curves showed reasonable agreement, but not to the desired accuracy. However, with refinement, this method would produce exact duplication.

$$\begin{bmatrix} \dot{\epsilon}'_u \\ \dot{\epsilon}'_a \\ \dot{\epsilon}'_\theta \\ \dot{\epsilon}'_q \\ \dot{\epsilon}'_{\delta e} \\ \dot{\epsilon}'_u \\ \dot{\epsilon}'_a \\ \dot{\epsilon}'_\theta \\ \dot{\epsilon}'_q \\ \dot{\epsilon}'_{\delta e} \end{bmatrix} = \begin{bmatrix} -0.059 & 0.33 & -0.29 & 0 & 0 & -0.046 & 0.25 & -0.24 & 0 & 0 \\ -0.66 & -3.06 & 0 & 0.95 & -0.36 & -0.56 & -1.83 & 0 & -0.038 & -0.36 \\ 0 & 0 & 0 & 1.00 & 0 & 0 & 0 & 0 & 0 & 0 \\ 0.88 & -25.15 & 0 & -4.30 & -43.50 & 0.85 & -18.40 & 0 & -2.88 & -26.82 \\ -972.60 & -153.24 & 294.72 & 19.02 & -49.58 & 7.89 & -13.24 & 13.98 & -4.62 & -15.38 \end{bmatrix} \begin{bmatrix} \epsilon'_u \\ \epsilon'_a \\ \epsilon'_\theta \\ \epsilon'_q \\ \epsilon'_{\delta e} \\ \epsilon'_u \\ \epsilon'_a \\ \epsilon'_\theta \\ \epsilon'_q \\ \epsilon'_{\delta e} \end{bmatrix} + \begin{bmatrix} 0 \\ 0 \\ 0 \\ 0 \\ 0 \\ 0 \\ 0 \\ 0 \\ 0 \\ 0 \end{bmatrix} \dot{\epsilon}'_{cmd}$$

Figure 24. Closed-Loop State Equation for Model Matching

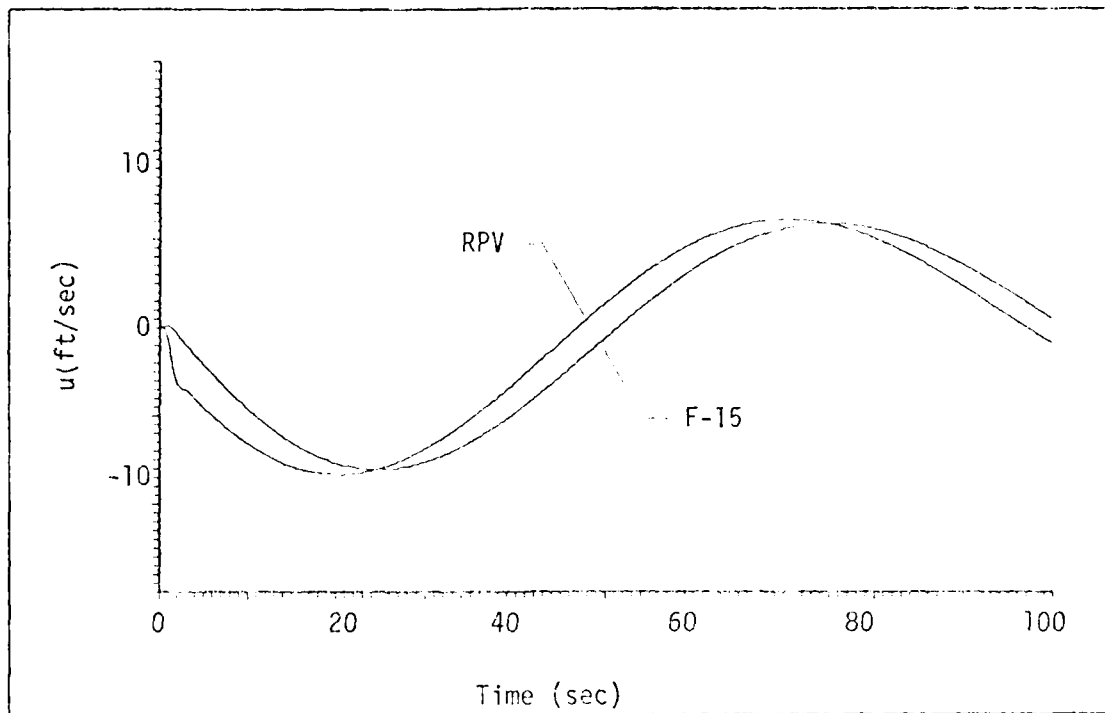


Figure 25. Comparison of the F-15 and the Model Matching RPV Velocity due to a 1 sec Pulse Elevator Command of -5 deg

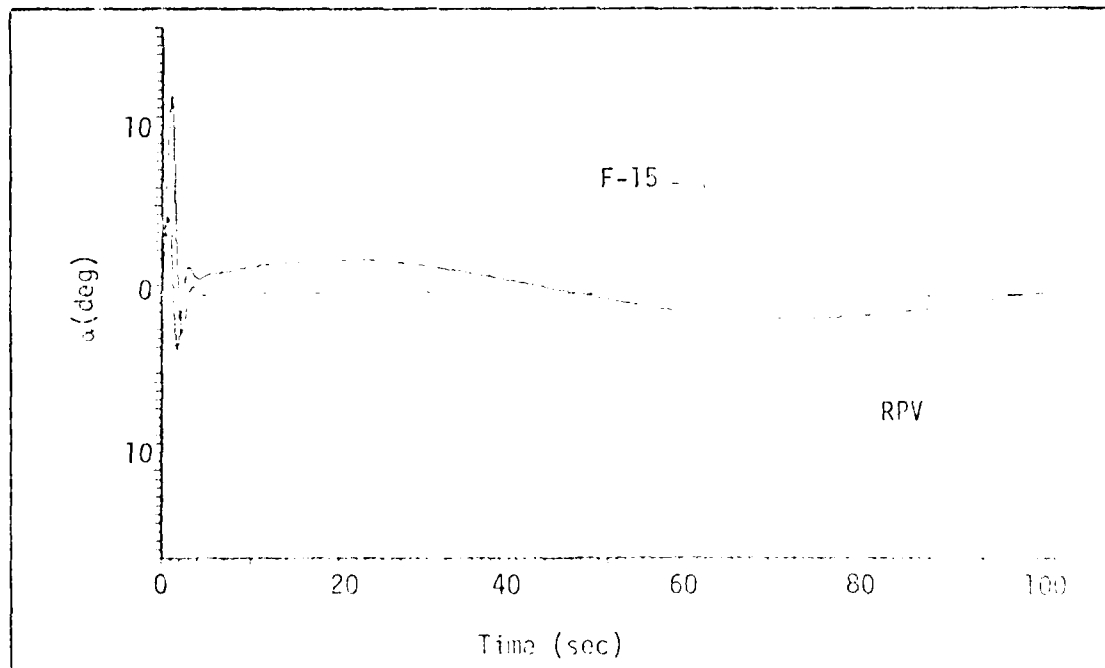


Figure 26. Comparison of the F-15 and the Model Matching RPV Angle of Attack due to a 1 sec Pulse Elevator Command of -5 deg

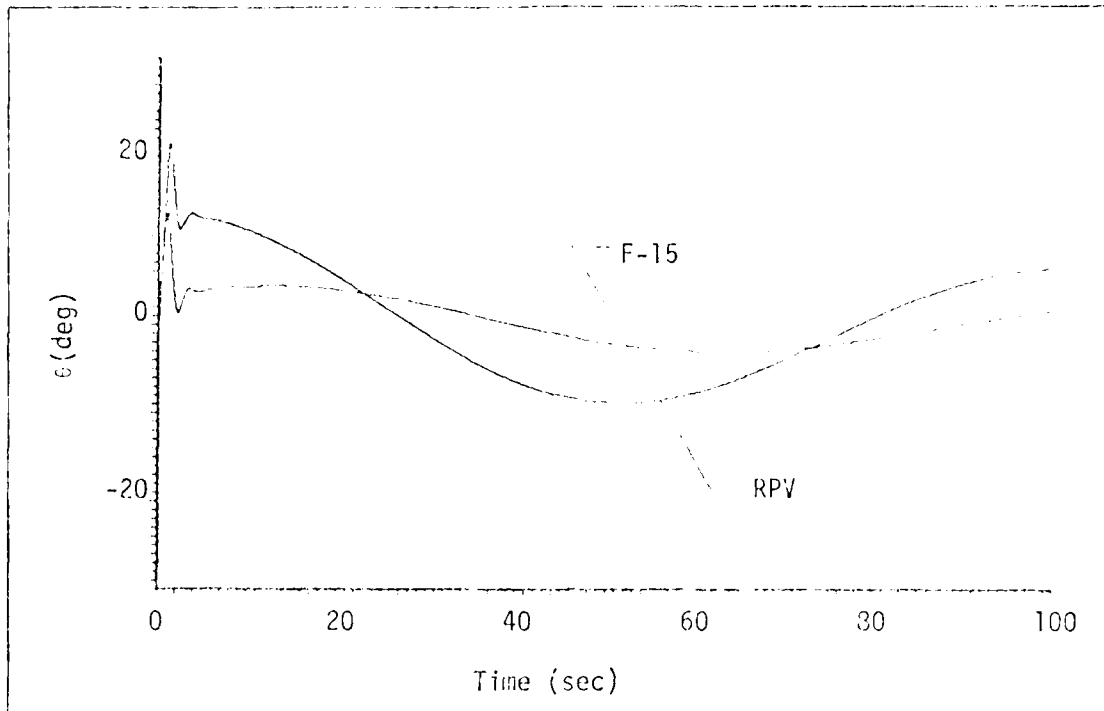


Figure 27. Comparison of the F-15 and the Model Matching RPV Pitch Angle due to a 1 sec Pulse Elevator Command of -5 deg

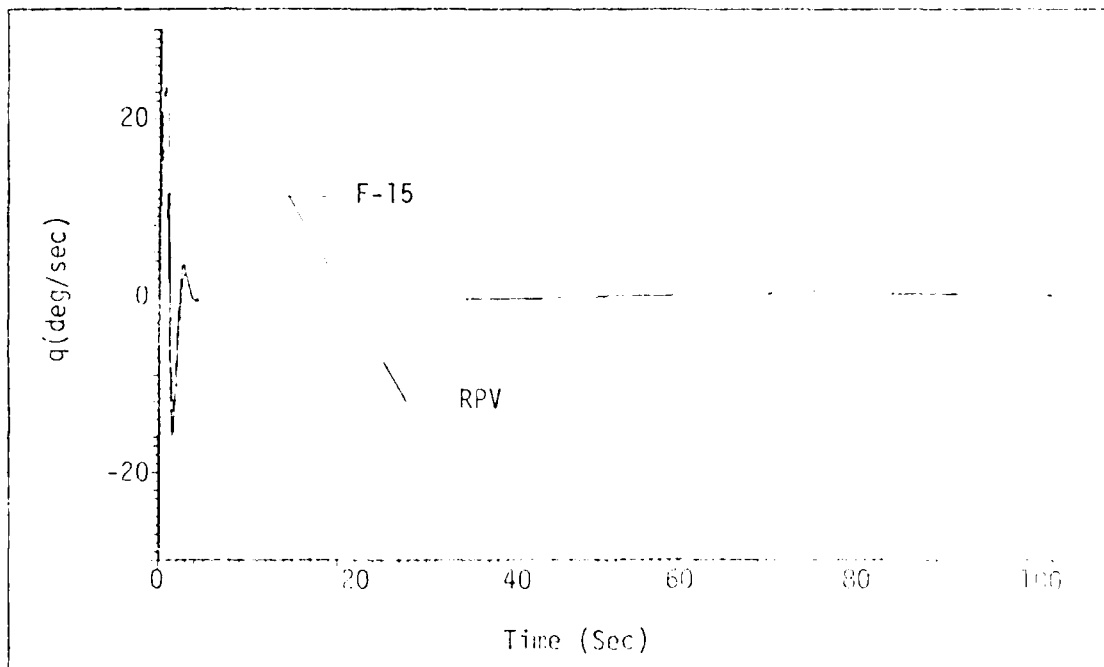


Figure 28. Comparison of the F-15 and the Model Matching RPV Pitch Rate due to a 1 sec Pulse Elevator Command of -5 deg

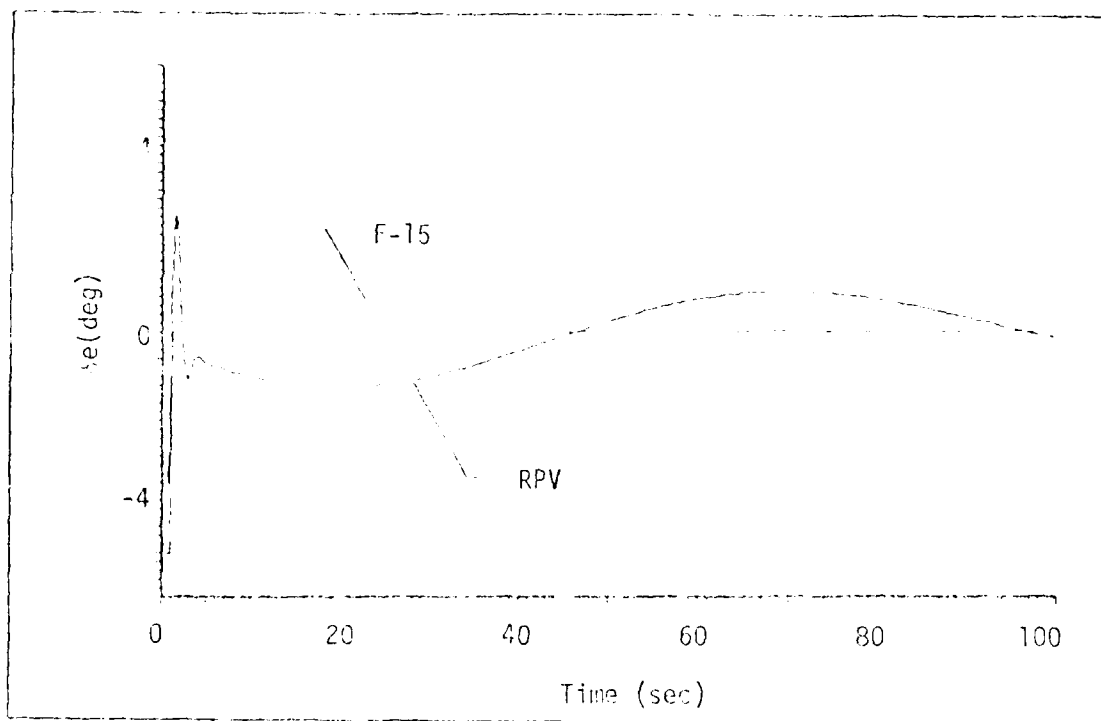


Figure 29. Comparison of the F-15 and the Model Matching RPV Elevator Deflection Angle due to a 1 sec Pulse Elevator Command of -5 deg

VI. Concluding Remarks

Conclusions

An analysis of the basic RPV provided the following conclusions:

1. Handling qualities were unsatisfied in the phugoid, dutch roll, and spiral modes.
2. The thrust vectoring unit had minimal effect on the longitudinal characteristics and no effect on the lateral-directional characteristics.
3. The short period damping ratio and natural frequency, phugoid damping ratio, and dutch roll natural frequency varied directly with the xcg location. All other characteristics remained essentially constant.

The following conclusions are based on the flight control system design:

1. Integral of pitch rate feedback to the elevator reduced phugoid oscillation.
2. Yaw rate feedback to the rudder increased the dutch roll damping ratio.
3. Yaw rate feedback to the ailerons stabilized the spiral mode.

The model matching application implied the following conclusions:

1. The Guillemin-Truxal design technique produced compensators that would duplicate only one state at a time. Also, these compensators were impractical to implement.
2. The Entire Eigenstructure Assignment technique was not well suited to single-input systems.

3. The Extension to Observer Theory technique accomplished the desired duplication; however, not to a high degree of accuracy.

Recommendations

Based on observations made throughout this study, the following recommendations are posed:

1. Digital Datcom is a very generalized algorithm so that many different aircraft configurations can utilize it for the generation of stability derivatives. However, for advanced research on this RPV, a more comprehensive algorithm (such as FLEXSTAB) might prove beneficial for the model construction.

2. The cost function minimized in the Extension of Observer Theory was one half the squared error. Alternate cost functions might provide better effectiveness in minimizing the coupling in the error equation.

3. The Extension of Observer Theory assumed full state feedback. Partial state feedback is a more realistic assumption which could be imposed on this design technique.

AD-A100 808 AIR FORCE INST OF TECH WRIGHT-PATTERSON AFB OH SCHOOL--ETC F/G 1/4
FLIGHT CONTROL SYSTEM ANALYSIS AND DESIGN FOR A REMOTELY PILOTE--ETC(U)
DEC 80 B L JONES
UNCLASSIFIED AFIT/6AE/AA/80D-12 NL

AIR FORCE INST OF TECH WRIGHT-PATTERSON AFB OH SCHOO--ETC F/G 1/4
FLIGHT CONTROL SYSTEM ANALYSIS AND DESIGN FOR A REMOTELY PILOTE--ETC(U)
DEC 80 B L JONES
AFIT/GAE/AA/80D-12 NL

NL

AD A
00009

AD A
- 00809

END
DATE
FILMED
7-81
DTIC

Bibliography

1. Abbott, I. H. and A. E. Von Doenhoff. Theory of Wing Sections. New York: Dover Publications, Inc., 1959.
2. Blakelock, J. H. Automatic Control of Aircraft and Missiles. New York: John Wiley and Sons, Inc., 1965.
3. CESA. Complete Eigenstructure Assignment. Air Force Institute of Technology Computer Program Library, Wright-Patterson AFB, Ohio, 43433, 1980.
4. Chalk, C. R., et al. Background Information and User Guide for MIL-F-8785B (ASG), "Military Specification - Flying Qualities of Piloted Airplanes". AFFDL-TR-69-72. Wright-Patterson AFB, Ohio, 45433, August 1969.
5. Chalk, C. R., et al. Background Information and User Guide for MIL-F-83300 - Military Specification - Flying Qualities of Piloted V/STOL Aircraft. AFFDL-TR-70-88. Wright-Patterson AFB, Ohio, 45433, March 1971.
6. D'Azzo, J. J. and C. H. Houpis. Linear Control System Analysis and Design: Conventional and Modern. New York: McGraw-Hill Book Co., 1975.
7. Hale, F. J. Instructional Text on Aerospace Vehicle Performance, MAE 261. Department of Mechanical and Aerospace Engineering, North Carolina State University, Raleigh, N.C., October 1976.
8. Hoak, D. E., et al. USAF Stability and Control DATCOM. Wright-Patterson AFB, Ohio, 45433, October 1960.
9. Houpis, C. H. and G. B. Lamont. Instructional Text on Digital Control Systems/Information Processing, EE 6.55. School of Engineering, Air Force Institute of Technology, Wright-Patterson AFB, Ohio, 45433, September 1979.
10. Houpis, C. H. Lecture Material distributed in EE 6.60, Feedback Systems Design. School of Engineering, Air Force Institute of Technology, Wright-Patterson AFB, Ohio, 45433, September 1979.
11. Likins, P. W. Elements of Engineering Mechanics. New York: McGraw-Hill Book Co., 1973.
12. McRuer, D., et al. Aircraft Dynamics and Automatic Control. Princeton, N.J.: Princeton University Press, 1973.
13. ODE. Ordinary Differential Equations. Control Data Corporation Computer Program Library, Wright-Patterson AFB, Ohio, 45433, 1980.
14. Prosser, C. F. and C. D. Wiler. RPV Flying Qualities Design Criteria. AFFDL-TR-76-125. Wright-Patterson AFB, Ohio, 45433, December 1976.

15. Roskam, J. Methods for Estimating Stability and Control Derivatives of Conventional Subsonic Airplanes. Lawrence, Kansas: Roskam Aviation and Engineering Corporation, 1973.
16. TOTAL. An Interactive Computer-Aided Design Program for Digital and Continuous Control System Analysis and Synthesis. Air Force Institute of Technology Computer Program Library, Wright-Patterson AFB, Ohio, 45433, 1980.
17. Townsend, J. L. and E. T. Raymond. Background Information and User Guide for MIL-F-9490D Flight Control Systems - Design, Installation and Test of Piloted Aircraft, General Specification for. AFFDL-TR-74-116. Wright-Patterson AFB, Ohio, 45433, January 1975.
18. Vukelich, S. R. and J. E. Williams. The USAF Stability and Control Digital Datcom. AFFDL-TR-79-3032. Wright-Patterson AFB, Ohio, 45433, April 1979.
19. Walton, J. D. A Feasibility Study of a Manual Bomb Release while in a Turn. MS Thesis, AFIT/GAE/AA/77D-17. Air Force Institute of Technology, Wright-Patterson AFB, Ohio, 45433, December 1977.

Appendix A

Hand Calculations

Several stability derivatives and all the control derivatives were not computed by Digital Datcom. In addition, the moments of inertia needed to be generated. Hence, the purpose of this appendix is to derive the above mentioned terms. All notation utilized in this appendix is defined in the references cited.

Stability Derivatives

Seven stability derivatives remained undetermined: C_{x_u} , $C_{x_{\dot{\alpha}}}$, $C_{x_{\alpha}}$, C_{x_q} , C_{z_u} , C_{m_u} , and C_{y_r} . The following relationships were utilized in their generation (Ref 2:19,112):

$$1. \quad C_{x_u} = -2C_D - U_0 \frac{\partial C_D}{\partial u}$$

The $U_0 \frac{\partial C_D}{\partial u}$ term is the compressibility effects and can be ignored.

Thus, for the TVU attached cases

$$\begin{aligned} C_{x_u} &= -2C_D \\ &= -2(0.05) \\ &= -0.10 \end{aligned}$$

and, for the TVU unattached cases

$$\begin{aligned} C_{x_u} &= -2(0.04) \\ &= -0.08 \end{aligned}$$

$$2. \quad C_{x_{\dot{\alpha}}} = 0$$

$$3. \quad C_{x_{\alpha}} = C_L - \frac{\partial C_D}{\partial \alpha}$$

Averaging the data produced

$$\frac{\partial C_D}{\partial \alpha} = 0.37 \quad (\text{TVU attached})$$

$$\frac{\partial C_D}{\partial \alpha} = 0.35 \quad (\text{TVU unattached})$$

Thus, for the TVU attached cases

$$\begin{aligned} C_{x_\alpha} &= 0.59 - 0.37 \\ &= 0.22 \end{aligned}$$

and, for the TVU unattached cases

$$\begin{aligned} C_{x_\alpha} &= 0.59 - 0.35 \\ &= 0.24 \end{aligned}$$

$$4. \quad C_{x_q} = 0$$

$$5. \quad C_{z_u} = -2C_L - U_0 \frac{\partial C_L}{\partial u}$$

The $U_0 \frac{\partial C_L}{\partial u}$ term also represents compressibility effects and was ignored.

Thus

$$\begin{aligned} C_{z_u} &= -2C_L \\ &= -2 (0.59) \\ &= -1.18 \end{aligned}$$

$$6. \quad C_{m_u} = 0$$

$$7. \quad C_{y_r} = 0$$

Control Derivatives

Control derivatives are nondimensional derivatives of force and moment coefficients with respect to the control surfaces. In all, nine

control derivatives were needed for the equations of motion: $C_{x_{\delta e}}$, $C_{z_{\delta e}}$, $C_{m_{\delta e}}$, $C_{y_{\delta a}}$, $C_{l_{\delta a}}$, $C_{n_{\delta a}}$, $C_{y_{\delta r}}$, $C_{l_{\delta r}}$, and $C_{n_{\delta r}}$. The following empirical relationships were used to compute these derivatives (Ref 15: Chapters 10, 11, and 12):

$$\begin{aligned}
 1. \quad C_{x_{\delta e}} &= 0 \\
 2. \quad C_{z_{\delta e}} &= -C_{L_{\delta f}} \frac{SH}{S} \\
 &= -(3.20) \frac{(6.38)}{30.98} \\
 &= -0.66 \\
 3. \quad C_{m_{\delta e}} &= -C_{L_{\delta e}} \frac{x_H}{c} \\
 &= -\frac{(0.66)(11.72 - x_{cg})}{2.271}
 \end{aligned}$$

Hence

$x_{cg}, \quad \% \text{ mac}$	$C_{m_{\delta e}}$
10	-2.04
25	-1.94
40	-1.84

$$\begin{aligned}
 4. \quad C_{y_{\delta a}} &= 0 \\
 5. \quad C_{l_{\delta a}} &= |\alpha_{\delta}| C_{l_{\sigma'}} \\
 &= (0.35)(0.38) \\
 &= 0.13 \\
 6. \quad C_{n_{\delta a}} &= KC_L C_{l_{\delta a}} \\
 &= (-0.20)(0.59)(0.13) \\
 &= -0.015
 \end{aligned}$$

$$\begin{aligned}
7. \quad C_{y_{\delta r}} &= C_{L_{\delta v}} \frac{(\alpha_{\delta}) C_L}{(\alpha_{\delta}) C_{L_0}} (\alpha_{\delta}) C_{L_0} K' K_b \frac{S_v}{S} \\
&= (5.42)(1.14)(-0.65)(1.00)(1.00) \frac{(6.97)}{30.98} \\
&= 0.90 \\
8. \quad C_{l_{\delta r}} &= C_{y_{\delta r}} \frac{Z_v \cos \alpha - l_v \sin \alpha}{b} \\
&= 0.90 \frac{1.01 \sin 0 - (11.07 - x_{cg}) \sin 0}{13.71} \\
&= 0.067 \\
9. \quad C_{n_{\delta r}} &= - C_{y_{\delta r}} \frac{l_v \cos \alpha + Z_v \sin \alpha}{b} \\
&= \frac{0.90}{13.71} [(11.07 - x_{cg}) \cos 0 + 1.01 \sin 0]
\end{aligned}$$

Hence

$x_{cg}, \% \text{ mac}$	$C_{n_{\delta r}}$
10	-0.42
25	-0.40
40	-0.38

Moments of Inertia

The method utilized in this computation consisted of separating the RPV into major components and calculating their moments of inertia. Two transformations and a summation determined the overall moments of inertia (Ref 8: Chapter 8). For accuracy purposes, this derivation was completed in the units lb-in.². Only the final results was converted to slug-ft².

Initially, a weight and balance study of the RPV's major components had to be completed, the results of which are in Table XVI. Thus, the Datcom method yields

Table XVI. Weight and Center of Gravity
Locations of the Major RPV Components

	W, lb.	x, in.	y, in.	z, in.
Body under wing	43.65	60.74	0	-6.65
Boom, left	8.70	90.00	30.00	7.00
Boom, right	8.70	90.00	-30.00	7.00
Engine	14.35	82.00	0	5.00
Fuel	30.00	39.00	0	2.00
Horizontal Tail	4.00	114.45	0	25.25
Instruments	10.00	25.50	0	3.00
Lead: Case 1	55.83	18.00	0	3.14
Case 2	45.99	18.00	0	3.04
Case 3	25.20	18.00	0	2.58
Case 4	32.28	18.00	0	3.67
Case 5	24.18	18.00	0	3.69
Case 6	7.07	18.00	0	3.91
Nose	5.00	16.00	0	0
TVU	20.00	106.30	0	5.00
Vertical Tail, left	5.80	138.00	30.00	17.85
Vertical Tail, right	5.80	138.00	-30.00	17.85
Wing	34.00	64.25	0	9.06

1. Wing

$$\begin{aligned}
 I &= \frac{\rho}{12} [-C_a^3 + C_b^3 + C_c^2 C_b + C_c C_b^2 + C_c^3] \\
 &= \frac{1.25}{12} [-(5.03)^3 + (29.03)^3 + (30.25)^2(29.03) \\
 &\quad + (30.25)(29.03)^2 + (30.25)^3] \\
 &= 10871.69 \text{ lb-in.}^2
 \end{aligned}$$

Thus

$$\begin{aligned}
 I_{0y} &= K_0 \left[I - \frac{(W_X X)^2}{W_W} \right] \\
 &= 0.70 \left[10871.69 - \frac{(545.41)^2}{34.00} \right] \\
 &= 1492.17 \text{ lb-in.}^2 \\
 I_{0x} &= \frac{W_W b_W^2}{24} K_1 \left[\frac{C_r + 3C_t}{C_r + C_t} \right] \\
 &= \frac{(34.00)(164.5)^2 (0.86)}{24} \left[\frac{30.25 + 3(24)}{24 + 30.25} \right] \\
 &= 62138.60 \text{ lb-in.}^2 \\
 I_{0x} &= I_{0y} + I_{0x} \\
 &= 1492.17 + 62138.60 \\
 &= 63630.77 \text{ lb-in.}^2
 \end{aligned}$$

2. Horizontal Tail

$$\begin{aligned}
 I &= \frac{\rho}{12} [-C_a^3 + C_b^3 + C_c^2 C_b + C_c C_b^2 + C_c^3] \\
 &= \frac{0.26}{12} [4(15.5)^3] \\
 &= 320.25 \text{ lb-in.}^2
 \end{aligned}$$

Thus

$$\begin{aligned}
 I_{0y} &= K_0 \left[I - \frac{(W_H X)^2}{W_H} \right] \\
 &= 0.77 \left[320.25 - \frac{(31)^2}{4} \right] \\
 &= 61.68 \text{ lb-in.}^2
 \end{aligned}$$

$$\begin{aligned}
 I_{0x} &= \frac{W_H b_H^2}{24} K_4 \left[\frac{C_r + 3C_t}{C_r + C_t} \right] \\
 &= \frac{(4)(60)^2(0.92)}{24} \left[\frac{15.5 + 3(15.5)}{15.5 + 15.5} \right] \\
 &= 1104.4 \text{ lb-in.}^2
 \end{aligned}$$

$$\begin{aligned}
 I_{0z} &= I_{0x} + I_{0y} \\
 &= 1104.00 + 61.68 \\
 &= 1165.68 \text{ lb-in.}^2
 \end{aligned}$$

3. Vertical Tail

$$\begin{aligned}
 I_{0x} &= \frac{W_v b_v^2}{18} K_5 \left[1 + \frac{2 C_{rv} C_{tv}}{(C_{rv} + C_{tv})^2} \right] \\
 &= \frac{(5.8)(26)^2(1.22)}{18} \left[1 + \frac{2(25.85)(15.6)}{(25.85 + 15.6)^2} \right] \\
 &= 390.49 \text{ lb-in.}^2
 \end{aligned}$$

$$\begin{aligned}
 I &= \frac{\rho}{12} (-C_a^3 + C_b^3 + C_c^2 C_b + C_c C_b^2 + C_c^3) \\
 &= \frac{0.280}{12} [-(19.606)^3 + (25.850)^3 + (35.206)^2 (25.850) \\
 &= 2541.91 \text{ lb-in.}^2
 \end{aligned}$$

Thus

$$\begin{aligned}
 I_{0z} &= K_0 \left[I - \frac{(W_v X)^2}{W_v} \right] \\
 &= 0.771 \left[2541.91 - \frac{(113.56)^2}{5.8} \right] \\
 &= 245.55 \text{ lb-in.}^2
 \end{aligned}$$

$$\begin{aligned}
 I_{0y} &= I_{0x} + I_{0z} \\
 &= 390.49 + 245.55 \\
 &= 636.04 \text{ lb-in.}^2
 \end{aligned}$$

4. Body

Initially, the body was separated into four different components which needed to be consolidated. This was done with the following results:

	Cases 1-3	Cases 4-6
Weight, lb	86.05	66.05
xcg, in.	74.65	65.06
ycg, in.	0	0
zcg, in.	-0.79	-2.54

Thus, for cases 1-3

$$\begin{aligned}
 I_{0y} &= \frac{W_f S_s K_2}{37.68} \left[\frac{3d}{2\ell_B} + \frac{\ell_B}{d} \right] \\
 &= \frac{(86.05)(7126.11)(0.88)}{37.68} \left[\frac{3(27.4)}{2(135)} + \frac{135}{27.4} \right] \\
 &= 74919.94 \text{ lb-in.}^2
 \end{aligned}$$

$$\begin{aligned}
 I_{0x} &= \frac{W_f K_3}{4} \left[\frac{S_s}{\pi \ell_B} \right]^2 \\
 &= \frac{(86.05)(1.04)}{4} \left[\frac{7126.11}{\pi (135)} \right]^2 \\
 &= 6316.29 \text{ lb-in.}^2
 \end{aligned}$$

$$\begin{aligned}
 I_{0z} &= I_{0y} \\
 &= 74919.94 \text{ lb-in.}^2
 \end{aligned}$$

For cases 4-6

$$\begin{aligned}
 I_{0y} &= \frac{(66.05)(4160.45)(0.42)}{37.68} \left[\frac{3(14.47)}{2(81)} + \frac{81}{14.47} \right] \\
 &= 17964.73 \text{ lb-in.}^2
 \end{aligned}$$

$$\begin{aligned}
 I_{0x} &= \frac{(66.05)(0.78)}{4} \left[\frac{4160.45}{\pi (81)} \right]^2 \\
 &= 3442.85 \text{ lb-in.}^2
 \end{aligned}$$

$$\begin{aligned}
 I_{0z} &= I_{0y} \\
 &= 17964.73 \text{ lb-in.}^2
 \end{aligned}$$

5. Engine

$$\begin{aligned} I_{0y} &= 0.061 \left[\frac{3}{4} W_p d_e^2 + W_e x_e^2 + (W_p - W_e) x_p^2 \right] \\ &= 0.061 \left[\frac{3}{4} (14.35)(26)^2 + (14.35)(8)^2 \right] \\ &= 499.82 \text{ lb-in.}^2 \end{aligned}$$

$$\begin{aligned} I_{0x} &= 0.083 W_p d_e^2 \\ &= 0.083 (14.35)(26)^2 \\ &= 805.15 \text{ lb-in.}^2 \end{aligned}$$

$$\begin{aligned} I_{0z} &= I_{0y} \\ &= 499.82 \text{ lb-in.}^2 \end{aligned}$$

6. Fuel

Assuming a 24 x 12 x 4 in. tank

$$\begin{aligned} I_{0y} &= \frac{W_f}{12} (x_x^2 + x_z^2) \\ &= \frac{30}{12} (12^2 + 4^2) \\ &= 400 \text{ lb-in.}^2 \end{aligned}$$

$$\begin{aligned} I_{0x} &= \frac{W_f}{12} (x_y^2 + x_z^2) \\ &= \frac{30}{12} (24^2 + 12^2) \\ &= 1800 \text{ lb-in.}^2 \end{aligned}$$

7. Instruments

Assuming a 3 x 4 x 6 in. pack

$$\begin{aligned} I_{0y} &= \frac{W_i}{12} (x_x^2 + x_z^2) \\ I_{0y} &= \frac{10}{12} [(3)^2 + (6)^2] \\ &= 37.50 \text{ lb-in.}^2 \end{aligned}$$

$$\begin{aligned}
 I_{0x} &= \frac{Wl}{12} [x_y^2 + x_z^2] \\
 &= \frac{10}{12} [(4)^2 + (6)^2] \\
 &= 43.33 \text{ lb-in.}^2
 \end{aligned}$$

$$\begin{aligned}
 I_{0z} &= \frac{Wl}{12} [x_x^2 + x_y^2] \\
 &= \frac{10}{12} [(3)^2 + (4)^2] \\
 &= 20.83 \text{ lb-in.}^2
 \end{aligned}$$

8. Lead

Assuming a cubic shape, the volume of lead needed and the length of a side was

<u>Case</u>	<u>W, lb.</u>	<u>Vol, in.³</u>	<u>ℓ, in.</u>
1	55.83	136.17	5.14
2	45.99	112.17	4.82
3	25.20	61.46	3.95
4	32.28	78.73	4.28
5	24.18	58.98	3.89
6	7.07	17.24	2.58

Since a cubic shape was assumed, all the moments of inertia will be the same.

$$I_0 = \frac{Wl}{6} \ell^2$$

Hence

<u>Case</u>	<u>I₀, lb-in.²</u>
1	245.83
2	178.08
3	65.53
4	98.55
5	60.98
6	7.84

Before the summation of individual moments of inertia could be done, each moment of inertia needed to be transformed into the RPV's axis system. The first transformation was to a set of parallel axes located at the RPV's nose. Hence

$$I_x = \Sigma[W(y^2 + z^2) + I_{0x}]$$

$$I_y = \Sigma[W(x^2 + z^2) + I_{0y}]$$

$$I_z = \Sigma[W(x^2 + y^2) + I_{0z}]$$

$$I_{xz} = \Sigma[Wxz + I_{0xz}]$$

The second transformation was to the aircraft's center of gravity via

$$I_{0x}|_{cg} = I_x - W(\bar{y}^2 + \bar{z}^2)$$

$$I_{0y}|_{cg} = I_y - W(\bar{x}^2 + \bar{z}^2)$$

$$I_{0z}|_{cg} = I_z - W(\bar{x}^2 + \bar{y}^2)$$

$$I_{0xz}|_{cg} = I_{xz} - W\bar{x}\bar{z}$$

Substituting the appropriate values from Tables XVI and XVII into the above two transformations provided the RPV's moments of inertia utilized in this study (Table XVIII).

Table XVII. Moments of Inertia of the
RPV's Major Components

	I_{0x} , lb in. ²	I_{0y} , lb in. ²	I_{0z} , lb in. ²	I_{0xz} , lb in. ²
Engine	805.15	499.82	499.82	0
Fuel	400.00	1480.00	1800.00	0
Horizontal Tail	1104.00	61.68	1165.68	0
Instruments	43.33	37.50	20.83	0
Vertical Tail, left	390.49	636.04	245.55	0
Vertical Tail, right	390.49	636.04	245.55	0
Wing	62138.60	1492.17	63630.77	0
Body: Case 1-3	6316.29	74919.40	74919.40	0
Case 4-6	3442.85	17964.73	17964.73	0
Lead: Case 1	245.83	245.83	245.83	0
Case 2	178.08	178.08	178.08	0
Case 3	65.53	65.53	65.53	0
Case 4	98.55	98.55	98.55	0
Case 5	60.98	60.98	60.98	0
Case 6	7.84	7.84	7.84	0

Table XVIII. RPV Moments of Inertia

	$I_{0x} _{cg}$, slug-ft ²	$I_{0y} _{cg}$, slug-ft ²	$I_{0z} _{cg}$, slug-ft ²	$I_{0xz} _{cg}$, slug-ft ²
Case 1	19.26	65.24	79.52	4.38
Case 2	19.24	46.99	61.26	3.93
Case 3	19.22	38.20	52.47	3.93
Case 4	18.82	37.95	52.04	4.80
Case 5	18.78	22.94	37.03	4.43
Case 6	18.76	15.71	29.81	4.43

Appendix B

Aircraft Equations of Motion

The aircraft equations of motion are a set of nonlinear, coupled force and moment equations defined in inertial space. The purpose of this appendix is to derive these equations in their complete form and to simplify them into a more useful form.

Definitions

Initially, two fundamental definitions needed to be made, inertial velocity and inertial angular velocity. These two quantities were defined in body fixed coordinates as

$$\begin{aligned}\underline{V} &= U \hat{X}_b + V \hat{Y}_b + W \hat{Z}_b \\ \underline{\omega}^{bi} &= P \hat{X}_b + Q \hat{Y}_b + R \hat{Z}_b\end{aligned}\tag{34}$$

Force Equations

The inertial acceleration was found by differentiating Eq (34).

$$\begin{aligned}\underline{A} &= \frac{d}{dt} (\underline{V}) \\ &= \frac{b}{d} \frac{d}{dt} (\underline{V}) + \underline{\omega}^{bi} \times \underline{V} \\ &= (\dot{U} + QW - RV) \hat{X}_b + (\dot{V} + RU - PW) \hat{Y}_b + (\dot{W} + PV - QU) \hat{Z}_b\end{aligned}$$

Applying Newton's second law in component form yielded the three force equations.

$$\begin{aligned}\Sigma F_x &= m (\dot{U} + QW - RV) \\ \Sigma F_y &= m (\dot{V} + RU - PW) \\ \Sigma F_z &= m (\dot{W} + PV - QU)\end{aligned}$$

(35)

Moment Equations

The vector moment equation was given by (Ref 11:286, 418).

$$\begin{aligned}\underline{\Sigma M} &= \frac{d}{dt} (\underline{H}) \\ &= \frac{b}{dt} (\underline{H}) + \underline{\omega}^{bi} \times \underline{H}\end{aligned}\quad (36)$$

where

$$\underline{H} = [\hat{X}_b \ \hat{Y}_b \ \hat{Z}_b] \begin{bmatrix} I_x & 0 & -I_{xz} \\ 0 & I_y & 0 \\ -I_{xz} & 0 & I_z \end{bmatrix} \begin{bmatrix} P \\ Q \\ R \end{bmatrix} \quad (37)$$

Expanding Eq (37), substituting into Eq (36), and simplifying

$$\begin{aligned}\underline{\Sigma M} &= [\dot{P}I_x + (-\dot{R}-PQ)I_{xz} + QR(I_z - I_y)]\hat{X}_b \\ &\quad + [PR(I_x - I_z) + (P^2-R^2)I_{xz} + \dot{Q}I_y]\hat{Y}_b \\ &\quad + [PQ(I_y - I_x) + (QR-\dot{P})I_{xz} + \dot{R}I_z]\hat{Z}_b\end{aligned}$$

Recall

$$\underline{\Sigma M} = L \hat{X}_b + M \hat{Y}_b + N \hat{Z}_b$$

Thus, the three moment equations were

$$\begin{aligned}\Sigma L &= \dot{P}I_x + (-\dot{R} - PQ)I_{xz} + QR(I_z - I_y) \\ \Sigma M &= PR(I_x - I_z) + (P^2 - R^2)I_{xz} + \dot{Q}I_y \\ \Sigma N &= PQ(I_y - I_x) + (QR - \dot{P})I_{xz} + \dot{R}I_z\end{aligned}\quad (38)$$

Assumptions

Equations (35) and (38) are the aircraft equations of motion in their complete form. Several assumptions were made in their derivation and are listed below:

- The mass of the aircraft remains constant.
- The aircraft is a rigid body.
- The earth is an inertial reference frame.
- The \hat{X}_b and \hat{Z}_b axes form a plane of symmetry.

Decoupling the Equations of Motion

Due to the coupling terms, the complete form of the aircraft equations of motion was very difficult to use. By assuming perturbations about straight and level flight, these equations decoupled into a longitudinal and lateral-directional set of equations.

The longitudinal equations had only one control input, a deflection of which would not cause any P, R, or V. Hence, Eqs (35) and (38) simplified to

$$\begin{aligned}\Sigma F_X &= m (\dot{U} + QW) \\ \Sigma F_Z &= m (\dot{W} - QU) \\ \Sigma M &= \dot{Q} I_y\end{aligned}\tag{39}$$

Similarly, the lateral-directional equations had two control inputs, deflections of either would not cause any Q. Hence, Eqs (35) and (38) simplified to

$$\begin{aligned}\Sigma F_y &= m (\dot{V} + RU - PW) \\ \Sigma L &= \dot{P} I_x - \dot{R} I_{xz} \\ \Sigma N &= \dot{P} I_{xz} + \dot{R} I_z\end{aligned}\tag{40}$$

Longitudinal Equations

Simplification of Eq (39) was obtained by assuming stability axes and small perturbations about straight and level flight. These assumptions constituted a linearization about an arbitrary equilibrium point. Thus

$$\begin{aligned}U &= U_0 + u \\ \dot{U} &= \dot{u} \\ Q &= q \\ \dot{Q} &= \dot{q} \\ W &= w \\ \dot{W} &= \dot{w}\end{aligned}$$

Substituting into Eq (39) and ignoring second order terms produced the linearized perturbation equations

$$\begin{aligned} \Sigma F_x &= m\dot{u} \\ \Sigma F_z &= m(\dot{w} - q U_0) \\ \Sigma M &= \dot{q} I_y \end{aligned} \quad (41)$$

The longitudinal forces and moments were of three types: aerodynamic, gravitational, and thrust forces. Assuming a constant altitude, the aerodynamic forces consisted of lift and drag which were a function of U , α , $\dot{\alpha}$, q , and δ_e . The gravitational forces were a function of θ . Hence, assuming that the thrust line was along X_b and through the center of gravity, the longitudinal forces and moments could be expressed in functional form as

$$\begin{aligned} \Sigma F_x &= F_x (U, \alpha, \dot{\alpha}, \theta, q, \delta_e, \delta_T) \\ \Sigma F_z &= F_z (U, \alpha, \dot{\alpha}, \theta, q, \delta_e) \\ \Sigma M &= M (U, \alpha, \dot{\alpha}, q, \delta_e) \end{aligned} \quad (42)$$

Expanding the x-force equation of Eq (42) in a first order Taylor series expansion

$$\begin{aligned} \Sigma F_x &= \frac{\partial F_x}{\partial U} u + \frac{\partial F_x}{\partial \alpha} \alpha + \frac{\partial F_x}{\partial \dot{\alpha}} \dot{\alpha} \\ &+ \frac{\partial F_x}{\partial \theta} \theta + \frac{\partial F_x}{\partial q} q + \frac{\partial F_x}{\partial \delta_e} \delta_e + \frac{\partial F_x}{\partial \delta_T} \delta_T \end{aligned} \quad (43)$$

But $\frac{\partial F_x}{\partial \delta_T} \delta_T = 0$ because thrust (i.e. throttle setting) was constant.

Also

$$F_x \Big|_{\text{gravity}} = -mg \sin \theta$$

Thus

$$\begin{aligned} \frac{\partial F_x}{\partial \theta} &= -mg \cos \theta \\ &\approx -mg \end{aligned}$$

Substituting the above and Eq (43) into Eq (41)

$$\begin{aligned} m\dot{u} = & \frac{\partial F_X}{\partial u} u + \frac{\partial F_X}{\partial \alpha} \alpha + \frac{\partial F_X}{\partial \dot{\alpha}} \dot{\alpha} - mg\theta \\ & + \frac{\partial F_X}{\partial q} q + \frac{\partial F_X}{\partial \delta e} \delta e \end{aligned} \quad (44)$$

Substituting $u \equiv \frac{U}{U_0}$ and the longitudinal stability derivatives (Table XIX) into Eq (44)

$$\begin{aligned} \frac{mU_0}{S\bar{q}} \dot{u} - C_{Xu} u - \frac{\bar{c}}{2U_0} C_{X\dot{\alpha}} \dot{\alpha} - C_{X\alpha} \alpha \\ - \frac{\bar{c}}{2U_0} C_{Xq} q + \frac{mg}{S\bar{q}} \theta = C_{X\delta e} \delta e \end{aligned} \quad (45)$$

This same procedure was used for the z-force and pitching moment equation. Note the substitution of $W \approx U_0\alpha$ was made in the z-force equation. Hence the remainder of Eq (41) became

$$\begin{aligned} -C_{Zu} u + \left[\frac{mU_0}{S\bar{q}} + \frac{\bar{c}}{2U_0} C_{L\dot{\alpha}} \right] \dot{\alpha} + C_{L\alpha} \alpha \\ + \left[\frac{\bar{c}}{2U_0} C_{Lq} - \frac{mU_0}{S\bar{q}} \right] q = C_{Z\delta e} \delta e \end{aligned} \quad (46)$$

$$\begin{aligned} -C_{mu} u - \frac{\bar{c}}{2U_0} C_{m\dot{\alpha}} \dot{\alpha} - C_{m\alpha} \alpha + \frac{I_y}{S\bar{q}c} \dot{q} \\ - \frac{\bar{c}}{2U_0} C_{mq} q = C_{m\delta e} \delta e \end{aligned} \quad (47)$$

Equations (45) - (47) needed to be rearranged into a more useful form, i.e., a state equation. Define

$$C1 = \frac{mU_0}{S\bar{q}} + \frac{\bar{c}}{2U_0} C_{L\dot{\alpha}}$$

Table XIX. Definitions of the Longitudinal Stability Derivatives

$C_{x_u} = \frac{U_0}{S\bar{q}} \frac{\partial F_x}{\partial u}$	$C_{L_q} = \frac{-2U_0}{S\bar{q}c} \frac{\partial F_x}{\partial q}$
$C_{x_\alpha} = \frac{1}{S\bar{q}} \frac{\partial F_x}{\partial \alpha}$	$C_{z_{\delta e}} = \frac{1}{S\bar{q}} \frac{\partial F_z}{\partial \delta e}$
$C_{x_{\dot{\alpha}}} = \frac{2U_0}{S\bar{q}c} \frac{\partial F_x}{\partial \dot{\alpha}}$	$C_{m_u} = \frac{U_0}{S\bar{q}c} \frac{\partial M}{\partial u}$
$C_{x_q} = \frac{2U_0}{S\bar{q}c} \frac{\partial F_x}{\partial q}$	$C_{m_\alpha} = \frac{1}{S\bar{q}c} \frac{\partial M}{\partial \alpha}$
$C_{x_{\delta e}} = \frac{1}{S\bar{q}} \frac{\partial F_x}{\partial \delta e}$	$C_{m_{\dot{\alpha}}} = \frac{2U_0}{S\bar{q}c^2} \frac{\partial M}{\partial \dot{\alpha}}$
$C_{z_u} = \frac{U_0}{S\bar{q}} \frac{\partial F_z}{\partial u}$	$C_{m_q} = \frac{2U_0}{S\bar{q}c^2} \frac{\partial M}{\partial q}$
$C_{L_\alpha} = \frac{-1}{S\bar{q}} \frac{\partial F_z}{\partial \alpha}$	$C_{m_{\delta e}} = \frac{1}{S\bar{q}c} \frac{\partial M}{\partial \delta e}$
$C_{L_{\dot{\alpha}}} = \frac{-2U_0}{S\bar{q}c} \frac{\partial F_z}{\partial \dot{\alpha}}$	

Solving Eq (46) for $\dot{\alpha}$

$$\dot{\alpha} = \frac{C_{zu}}{C_l} \dot{u} - \frac{C_{L\alpha}}{C_l} \alpha + \frac{1}{C_l} \left[\frac{mU_0}{S\bar{q}} - \frac{\bar{c}}{2U_0} C_{Lq} \right] q + \frac{C_{z\delta e}}{C_l} \delta e \quad (48)$$

Substituting Eq (48) into Eq (45) and solving for \dot{u}

$$\begin{aligned} \dot{u} = & \left[\frac{S\bar{q}}{mU_0} C_{xu} + \frac{S\bar{q}\bar{c}}{2mU_0^2} \frac{C_{x\dot{\alpha}} C_{zu}}{C_l} \right] \dot{u} \\ & + \left[\frac{S\bar{q}}{mU_0} C_{x\alpha} + \frac{S\bar{q}\bar{c}}{2mU_0^2} \frac{C_{x\dot{\alpha}} C_{L\alpha}}{C_l} \right] \alpha \\ & + \left[-\frac{g}{U_0} \right] \theta \\ & + \left[\frac{S\bar{q}\bar{c}}{2mU_0^2} \frac{C_{x\dot{\alpha}}}{C_l} \frac{mU_0}{S\bar{q}} - \frac{\bar{c} C_{Lq}}{2U_0} + \frac{S\bar{q}\bar{c}}{2mU_0^2} C_{xq} \right] q \\ & + \left[\frac{S\bar{q}\bar{c}}{2mU_0^2} \frac{C_{x\dot{\alpha}} C_{z\delta e}}{C_l} + \frac{S\bar{q}}{mU_0} C_{x\delta e} \right] \delta e \end{aligned} \quad (49)$$

Substituting Eq (48) into Eq (47) and solving for \dot{q}

$$\begin{aligned} \dot{q} = & \left[\frac{S\bar{q}\bar{c}}{I_y} C_{mu} + \frac{S\bar{q}\bar{c}^2}{2U_0 I_y} \frac{C_{m\dot{\alpha}} C_{zu}}{C_l} \right] \dot{u} \\ & + \left[\frac{S\bar{q}\bar{c}}{I_y} C_{m\alpha} - \frac{S\bar{q}\bar{c}^2}{2U_0 I_y} \frac{C_{m\dot{\alpha}} C_{L\alpha}}{C_l} \right] \alpha \\ & + \left[\frac{S\bar{q}\bar{c}^2}{2U_0 I_y} \frac{C_{m\dot{\alpha}}}{C_l} \left[\frac{mU_0}{S\bar{q}} - \frac{\bar{c}}{2U_0} C_{Lq} \right] + \frac{S\bar{q}\bar{c}^2}{2U_0 I_y} C_{mq} \right] q \\ & + \left[\frac{S\bar{q}\bar{c}}{I_y} C_{m\delta e} + \frac{S\bar{q}\bar{c}^2}{2U_0 I_y} \frac{C_{m\dot{\alpha}} C_{z\delta e}}{C_l} \right] \delta e \end{aligned} \quad (50)$$

Choosing

$$x_1 = u$$

$$x_2 = \alpha$$

$$x_3 = \theta$$

$$x_4 = q$$

Eqs (48) - (50) formed the desired state equation as

$$\dot{\underline{x}} = \underline{A} \underline{x} + \underline{B} \delta e_{cmd} \quad (51)$$

where

$$C1 = \frac{mU_0}{S\bar{q}} + \frac{\bar{c}}{2U_0} C_{L\alpha}$$

$$A_{11} = \frac{S\bar{q}}{mU_0} C_{Xu} + \frac{S\bar{q}\bar{c}}{2mU_0^2} \frac{C_{X\alpha}C_{zu}}{C1}$$

$$A_{12} = \frac{S\bar{q}}{mU_0} C_{X\alpha} - \frac{S\bar{q}\bar{c}}{2mU_0^2} \frac{C_{X\alpha}C_{L\alpha}}{C1}$$

$$A_{13} = \frac{-g}{U_0}$$

$$A_{14} = \frac{S\bar{q}\bar{c}}{2mU_0} \left[\frac{C_{X\alpha}}{C1} \left[\frac{mU_0}{S\bar{q}} - \frac{\bar{c}}{2U_0} C_{Lq} \right] + C_{Xq} \right]$$

$$A_{21} = \frac{C_{zu}}{C1}$$

$$A_{22} = \frac{-C_{L\alpha}}{C1}$$

$$A_{23} = 0$$

$$A_{24} = \frac{1}{C1} \left[\frac{mU_0}{S\bar{q}} - \frac{\bar{c}}{2U_0} C_{Lq} \right]$$

$$A_{31} = 0$$

$$A_{32} = 0$$

$$A_{33} = 0$$

$$A_{34} = 1$$

$$A_{41} = \frac{S\bar{q}\bar{c}}{I_y} C_{mu} + \frac{S\bar{q}\bar{c}^2}{2U_0I_y} \frac{C_{M\alpha}C_{zu}}{C1}$$

$$A_{42} = \frac{S_{\bar{q}\bar{c}}}{I_y} C_{m_{\alpha}} - \frac{S_{\bar{q}\bar{c}}^2}{2U_0 I_y} \frac{C_{m_{\dot{\alpha}}} C_{L_{\alpha}}}{C_l}$$

$$A_{43} = 0$$

$$A_{44} = \frac{S_{\bar{q}\bar{c}}^2}{2U_0 I_y} \left[\frac{C_{m_{\dot{\alpha}}}}{C_l} \left[\frac{mU_0}{S_{\bar{q}}} - \frac{\tau C_{L_q}}{2U_0} \right] + C_{m_q} \right]$$

$$B_{11} = \frac{S_{\bar{q}}}{mU_0} C_{x_{\delta e}} + \frac{S_{\bar{q}\bar{c}}}{2mU_0^2} \frac{C_{x_{\dot{\alpha}}} C_{z_{\delta e}}}{C_l}$$

$$B_{21} = \frac{C_{z_{\delta e}}}{C_l}$$

$$B_{31} = 0$$

$$B_{41} = \frac{S_{\bar{q}\bar{c}}}{I_y} C_{m_{\delta e}} + \frac{S_{\bar{q}\bar{c}}^2}{2U_0 I_y} \frac{C_{m_{\dot{\alpha}}} C_{z_{\delta e}}}{C_l}$$

Lateral-Directional Equations

As in the longitudinal equations, a linearization about an arbitrary equilibrium point was completed. Thus

$$U = U_0 + u$$

$$V = v$$

$$\dot{V} = \dot{v}$$

$$W = w$$

$$P = p$$

$$\dot{P} = \dot{p}$$

$$R = r$$

$$\dot{R} = \dot{r}$$

Substituting into Eq (40) and ignoring second order terms produced the linearized perturbation equations

$$\begin{aligned} \Sigma F_y &= m(\dot{V} + U_0 r) \\ \Sigma L &= \dot{p} I_x - \dot{r} I_{xz} \\ \Sigma N &= -\dot{p} I_{xz} - \dot{r} I_z \end{aligned}$$

(52)

The lateral-directional forces and moments consisted only of aerodynamic and gravitational forces. As before, the aerodynamic forces were lift and drag; however, in this case they were a function of β , r , p , δa , and δr . The gravitational forces were a function of only ϕ . Hence, in functional form

$$\begin{aligned}\Sigma F_y &= F_y(\beta, r, p, \delta a, \delta r, \phi) \\ \Sigma L &= L(\beta, r, p, \delta a, \delta r) \\ \Sigma N &= N(\beta, r, p, \delta a, \delta r)\end{aligned}\tag{53}$$

Expanding the y-force equation of Eq (53) in a first order Taylor series expansion

$$\begin{aligned}\Sigma F_y &= \frac{\partial F_y}{\partial \beta} \beta + \frac{\partial F_y}{\partial r} r + \frac{\partial F_y}{\partial p} p + \frac{\partial F_y}{\partial \delta a} \delta a \\ &+ \frac{\partial F_y}{\partial \delta r} \delta r + \frac{\partial F_y}{\partial \phi} \phi\end{aligned}\tag{54}$$

Recall

$$F_y|_{\text{gravity}} = mg \sin \phi$$

Therefore

$$\begin{aligned}\frac{\partial F_y}{\partial \phi} &= mg \cos \phi \\ &\approx mg\end{aligned}$$

Also

$$\begin{aligned}v &\approx U_0 \\ \dot{v} &\approx U_0 \dot{\beta}\end{aligned}$$

Substituting the above and Eq (54) into Eq (52)

$$\begin{aligned}mU_0 (\dot{\beta} + r) &= \frac{\partial F_y}{\partial \beta} \beta + \frac{\partial F_y}{\partial r} r + \frac{\partial F_y}{\partial p} p \\ &+ \frac{\partial F_y}{\partial \delta a} \delta a + \frac{\partial F_y}{\partial \delta r} \delta r + mg \phi\end{aligned}\tag{55}$$

Substituting the lateral-directional stability derivatives (Table XX) into Eq (55)

$$\begin{aligned} -C_{y\beta} \beta + \frac{mU_0}{Sq} \dot{\beta} + \left[\frac{mU_0}{Sq} - \frac{b}{2U_0} C_{yr} \right] r - \frac{mg}{Sq} \phi \\ - \frac{b}{2U_0} C_{yp} p = C_{y\delta a} \delta a + C_{y\delta r} \delta r \end{aligned} \quad (56)$$

This same procedure was used for the rolling and yawing moment equations with the following results

$$\begin{aligned} -C_{l\beta} \beta - \frac{b}{2U_0} C_{lr} r - \frac{I_{xz}}{Sq b} \dot{r} - \frac{b}{2U_0} C_{lp} p + \frac{I_x}{Sq b} \dot{p} \\ = C_{l\delta a} \delta a + C_{l\delta r} \delta r \end{aligned} \quad (57)$$

$$\begin{aligned} -C_{n\beta} \beta - \frac{b}{2U_0} C_{nr} r + \frac{I_z}{Sq b} \dot{r} - \frac{b}{2U_0} C_{np} p - \frac{I_{xz}}{Sq b} \dot{p} \\ = C_{n\delta a} \delta a + C_{n\delta r} \delta r \end{aligned} \quad (58)$$

As before, Eqs (56) - (58) needed to be put in state equation form. Solving Eq (56) for $\dot{\beta}$

$$\begin{aligned} \dot{\beta} = \frac{Sq}{mU_0} C_{y\beta} \beta + \left[\frac{Sq b}{2mU_0^2} C_{yr} - 1 \right] r + \frac{g}{U_0} \phi \\ + \frac{Sq b}{2mU_0^2} C_{yp} p + \frac{Sq}{mU_0} C_{y\delta a} \delta a + \frac{Sq}{mU_0} C_{y\delta r} \delta r \end{aligned} \quad (59)$$

Solving Eq (57) for \dot{p}

$$\begin{aligned} \dot{p} = \frac{Sq b}{I_x} C_{l\beta} \beta + \frac{Sq b^2}{2U_0 I_x} C_{lr} r + \frac{I_{xz}}{I_x} \dot{r} \\ + \frac{Sq b^2}{2U_0 I_x} C_{lp} p + \frac{Sq b}{I_x} C_{l\delta a} \delta a + \frac{Sq b}{I_x} C_{l\delta r} \delta r \end{aligned} \quad (60)$$

Substituting Eq (60) into Eq (58) and solving for \dot{r}

Table XX. Definitions of the Lateral-Directional Stability Derivatives

$C_{Y\beta} = \frac{1}{S\bar{q}} \frac{\partial F_y}{\partial \beta}$	$C_{L\delta a} = \frac{1}{S\bar{q}b} \frac{\partial L}{\partial \delta a}$
$C_{Yr} = \frac{2U_0}{S\bar{q}b} \frac{\partial F_y}{\partial r}$	$C_{L\delta r} = \frac{1}{S\bar{q}b} \frac{\partial L}{\partial \delta r}$
$C_{Yp} = \frac{2U_0}{S\bar{q}b} \frac{\partial F_y}{\partial p}$	$C_{n\beta} = \frac{1}{S\bar{q}b} \frac{\partial N}{\partial \beta}$
$C_{Y\delta a} = \frac{1}{S\bar{q}} \frac{\partial F_y}{\partial \delta a}$	$C_{nr} = \frac{2U_0}{S\bar{q}b^2} \frac{\partial N}{\partial r}$
$C_{Y\delta r} = \frac{1}{S\bar{q}} \frac{\partial F_y}{\partial \delta r}$	$C_{np} = \frac{2U_0}{S\bar{q}b^2} \frac{\partial N}{\partial p}$
$C_{L\beta} = \frac{1}{S\bar{q}b} \frac{\partial L}{\partial \beta}$	$C_{n\delta a} = \frac{1}{S\bar{q}b} \frac{\partial N}{\partial \delta a}$
$C_{Lr} = \frac{2U_0}{S\bar{q}b^2} \frac{\partial L}{\partial r}$	$C_{n\delta r} = \frac{1}{S\bar{q}b} \frac{\partial N}{\partial \delta r}$
$C_{Lp} = \frac{2U_0}{S\bar{q}b^2} \frac{\partial L}{\partial p}$	

$$\begin{aligned}
\dot{r} = & \frac{1}{C^2} \left[\frac{Sqb}{I_z} C_{n\beta} + \frac{I_{xz}}{I_z} \frac{Sqb}{I_x} C_{l\beta} \right] \beta \\
& + \frac{1}{C^2} \left[\frac{Sqb^2}{2U_0 I_z} C_{nr} + \frac{I_{xz}}{I_z} \frac{Sqb^2}{2U_0 I_x} C_{lr} \right] r \\
& + \frac{1}{C^2} \left[\frac{Sqb}{2U_0 I_z} C_{np} + \frac{I_{xz}}{I_z} \frac{Sqb^2}{2U_0 I_x} C_{lp} \right] p \\
& + \frac{1}{C^2} \left[\frac{Sqb}{I_z} C_{n\delta a} + \frac{I_{xz}}{I_z} \frac{Sqb}{I_x} C_{l\delta a} \right] \delta a \\
& + \frac{1}{C^2} \left[\frac{Sqb}{I_z} C_{n\delta r} + \frac{I_{xz}}{I_z} \frac{Sqb}{I_x} C_{l\delta r} \right] \delta r
\end{aligned} \tag{61}$$

where

$$C^2 = 1 - \frac{I_{xz}^2}{I_x I_z}$$

Substituting Eq (61) into Eq (60) and solving for \dot{p}

$$\begin{aligned}
\dot{p} = & \left[\frac{Sqb}{C^2} \frac{I_{xz}}{I_x I_z} C_{n\beta} + \frac{Sqb}{I_x} C_{l\beta} \left[1 + \frac{I_{xz}^2}{C^2 I_x I_z} \right] \right] \beta \\
& + \left[\frac{Sqb^2}{2U_0 C^2} \frac{I_{xz}}{I_x I_z} C_{nr} + \frac{Sqb^2}{2U_0 I_x} C_{lr} \left[1 + \frac{I_{xz}^2}{C^2 I_x I_z} \right] \right] r \\
& + \left[\frac{Sqb^2}{2U_0 C^2} \frac{I_{xz}}{I_x I_z} C_{np} + \frac{Sqb^2}{2U_0 I_x} C_{lp} \left[1 + \frac{I_{xz}^2}{C^2 I_x I_z} \right] \right] p \\
& + \left[\frac{Sqb}{C^2} \frac{I_{xz}}{I_x I_z} C_{n\delta a} + \frac{Sqb}{I_x} C_{l\delta a} \left[1 + \frac{I_{xz}^2}{C^2 I_x I_z} \right] \right] \delta a \\
& + \left[\frac{Sqb}{C^2} \frac{I_{xz}}{I_x I_z} C_{n\delta r} + \frac{Sqb}{I_x} C_{l\delta r} \left[1 + \frac{I_{xz}^2}{C^2 I_x I_z} \right] \right] \delta r
\end{aligned} \tag{62}$$

Choosing

$$x_1 = \beta$$

$$x_2 = r$$

$$x_3 = \phi$$

$$x_4 = p$$

Eqs (59), (61), and (62) formed the desired state equation as

$$\dot{\underline{x}} = \underline{A}\underline{x} + \underline{B} \begin{bmatrix} \delta a \text{ cmd} \\ \delta e \text{ cmd} \end{bmatrix} \quad (63)$$

where

$$C_2 = 1 - \frac{I_{xz}^2}{I_x I_z}$$

$$A_{11} = \frac{S\bar{q}}{m U_0} C_{y\beta}$$

$$A_{12} = \frac{S\bar{q}b}{2mU_0^2} C_{yr} - 1$$

$$A_{13} = \frac{g}{U_0}$$

$$A_{14} = \frac{S\bar{q}b}{2mU_0^2} C_{yp}$$

$$A_{21} = \frac{1}{C_2} \left[\frac{S\bar{q}b}{I_z} C_{n\beta} + \frac{I_{xz}}{I_z} \frac{S\bar{q}b}{I_x} C_{\ell\beta} \right]$$

$$A_{22} = \frac{1}{C_2} \left[\frac{S\bar{q}b^2}{2U_0 I_z} C_{nr} + \frac{I_{xz}}{I_z} \frac{S\bar{q}b^2}{2U_0 I_x} C_{\ell r} \right]$$

$$A_{23} = 0$$

$$A_{24} = \frac{1}{C_2} \left[\frac{S\bar{q}b^2}{2U_0 I_z} C_{np} + \frac{I_{xz}}{I_z} \frac{S\bar{q}b^2}{2U_0 I_x} C_{\ell p} \right]$$

$$A_{31} = 0$$

$$A_{32} = 0$$

$$A_{33} = 0$$

$$A_{34} = 1$$

$$A_{41} = \frac{S\bar{q}b}{C^2} \frac{I_{xz}}{I_x I_z} C_{n\beta} + \frac{S\bar{q}b}{I_x} C_{\ell\beta} \left[1 + \frac{I_{xz}^2}{C^2 I_x I_z} \right]$$

$$A_{42} = \frac{S\bar{q}b^2}{2U_0 C^2} \frac{I_{xz}}{I_x I_z} C_{nr} + \frac{S\bar{q}b^2}{2U_0 I_x} C_{\ell r} \left[1 + \frac{I_{xz}^2}{C^2 I_x I_z} \right]$$

$$A_{43} = 0$$

$$A_{44} = \frac{S\bar{q}b^2}{2U_0 C^2} \frac{I_{xz}}{I_x I_z} C_{np} + \frac{S\bar{q}b^2}{2U_0 I_x} C_{\ell p} \left[1 + \frac{I_{xz}^2}{C^2 I_x I_z} \right]$$

$$B_{11} = \frac{S\bar{q}}{mU_0} C_{y\delta a}$$

$$B_{12} = \frac{S\bar{q}}{mU_0} C_{y\delta r}$$

$$B_{21} = \frac{1}{C^2} \left[\frac{S\bar{q}b}{I_z} C_{n\delta a} + \frac{I_{xz}}{I_z} \frac{S\bar{q}b}{I_x} C_{\ell\delta a} \right]$$

$$B_{22} = \frac{1}{C^2} \left[\frac{S\bar{q}b}{I_z} C_{n\delta r} + \frac{I_{xz}}{I_z} \frac{S\bar{q}b}{I_x} C_{\ell\delta r} \right]$$

$$B_{31} = 0$$

$$B_{32} = 0$$

$$B_{41} = \frac{S\bar{q}b}{C^2} \frac{I_{xz}}{I_x I_z} C_{n\delta a} + \frac{S\bar{q}b}{I_x} C_{\ell\delta a} \left[1 + \frac{I_{xz}^2}{C^2 I_x I_z} \right]$$

$$B_{42} = \frac{S\bar{q}b}{C^2} \frac{I_{xz}}{I_x I_z} C_{n\delta r} + \frac{S\bar{q}b}{I_x} C_{\ell\delta r} \left[1 + \frac{I_{xz}^2}{C^2 I_x I_z} \right]$$

Summary

The complete form of the force and moment equations can be found in Eqs (35) and (38). The decoupled linearized perturbation equations can be found in Eqs (41) and (52). Lastly, the longitudinal and lateral-directional state equations can be found in Eqs (51) and (63).

Appendix C

Time Responses

Representative time responses were generated for the basic RPV, the augmented RPV, and the nonlinear simulation and are contained in this appendix. Each figure contains a series of three time responses, one for each of the systems mentioned above. This arrangement facilitates easy comparison between the different systems. The longitudinal time responses are displayed in Figs 30 - 35. The lateral time responses are given in Figs 36 - 44. Lastly, the directional time responses are contained in Figs 45 - 53.

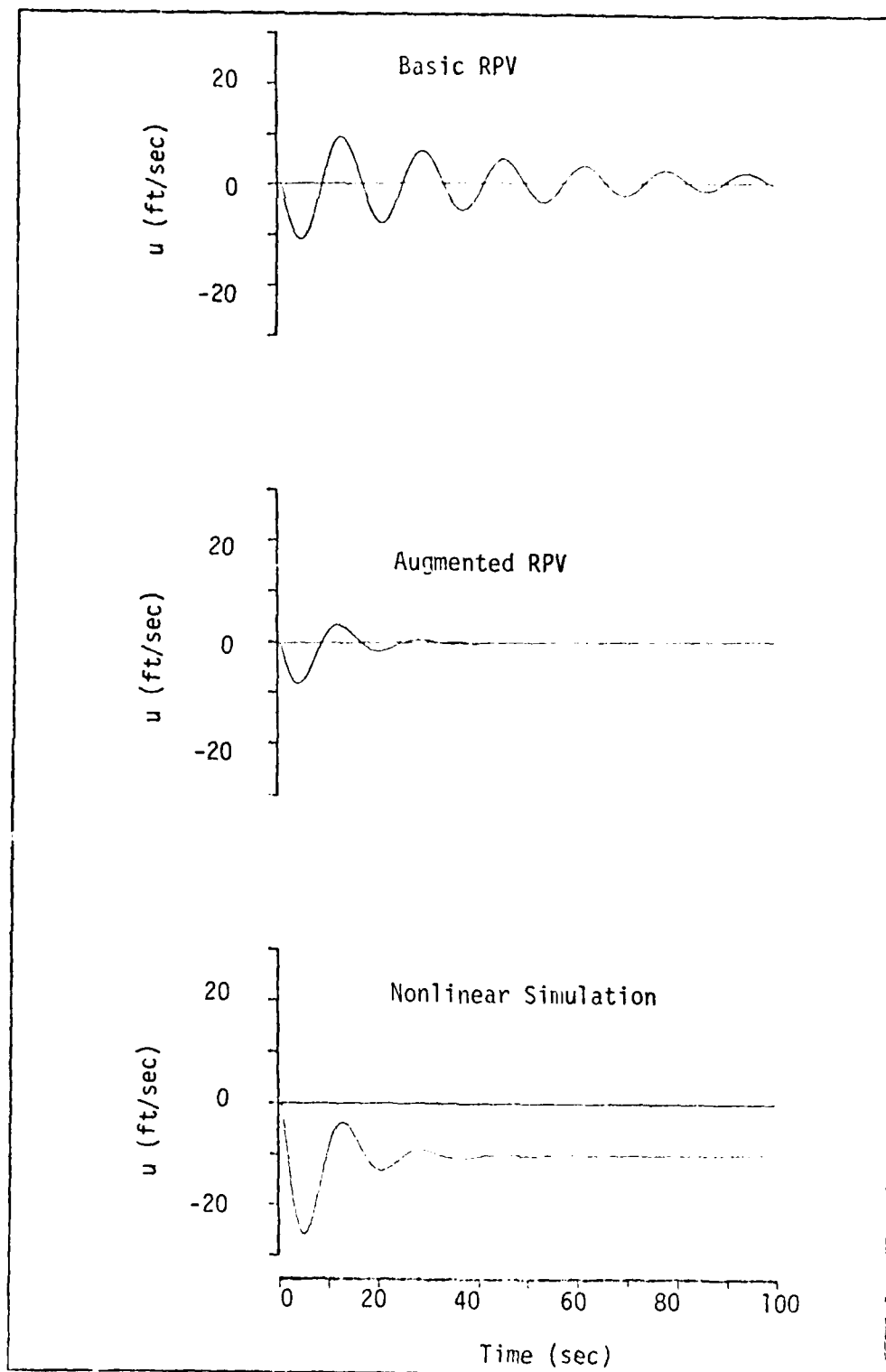


Figure 30. RPV Forward Velocity due to a 1 sec Pulse Elevator Command of -5 deg

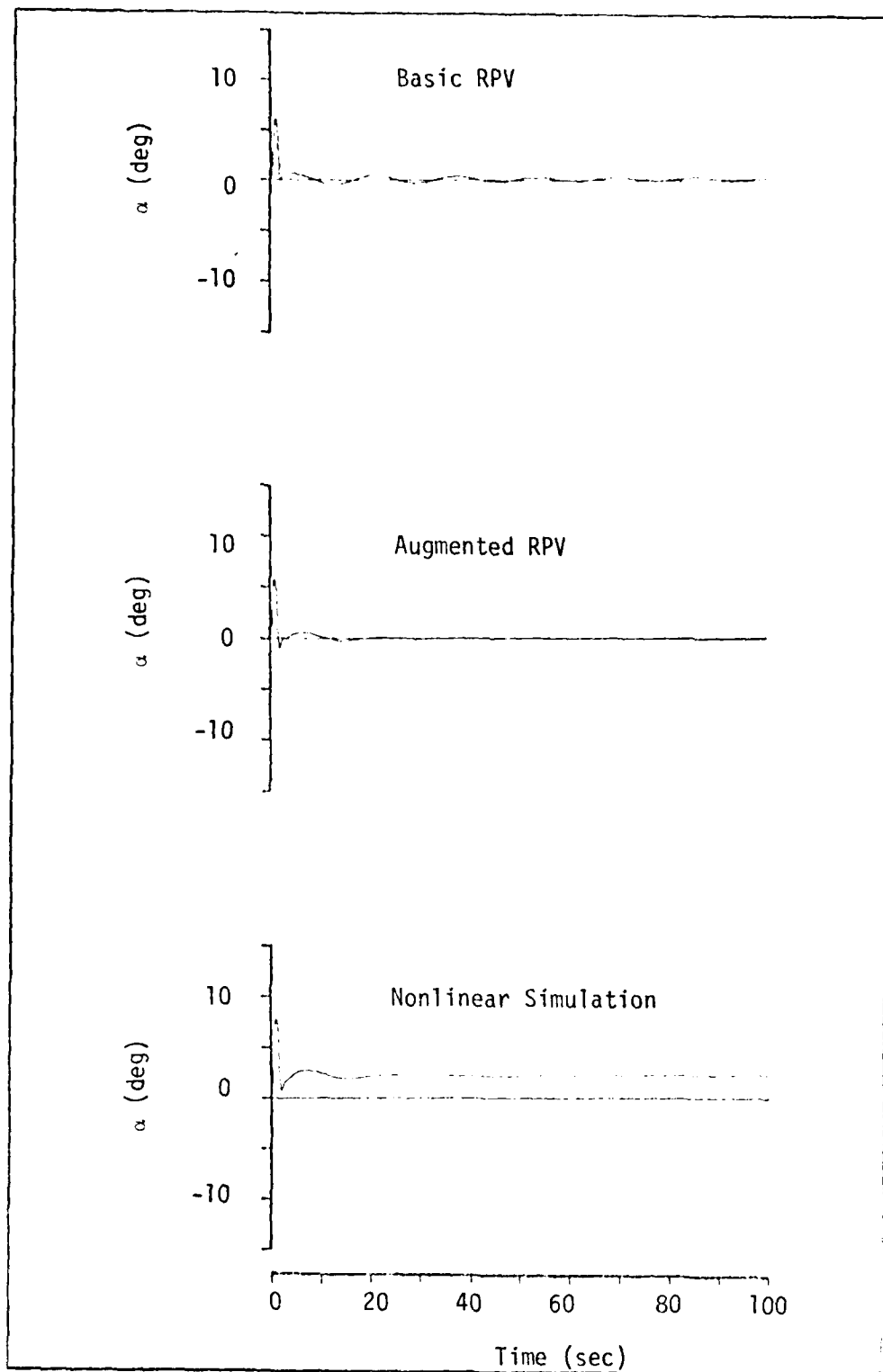


Figure 31. RPV Angle of Attack due to a 1 sec Pulse Elevator Command of -5 deg

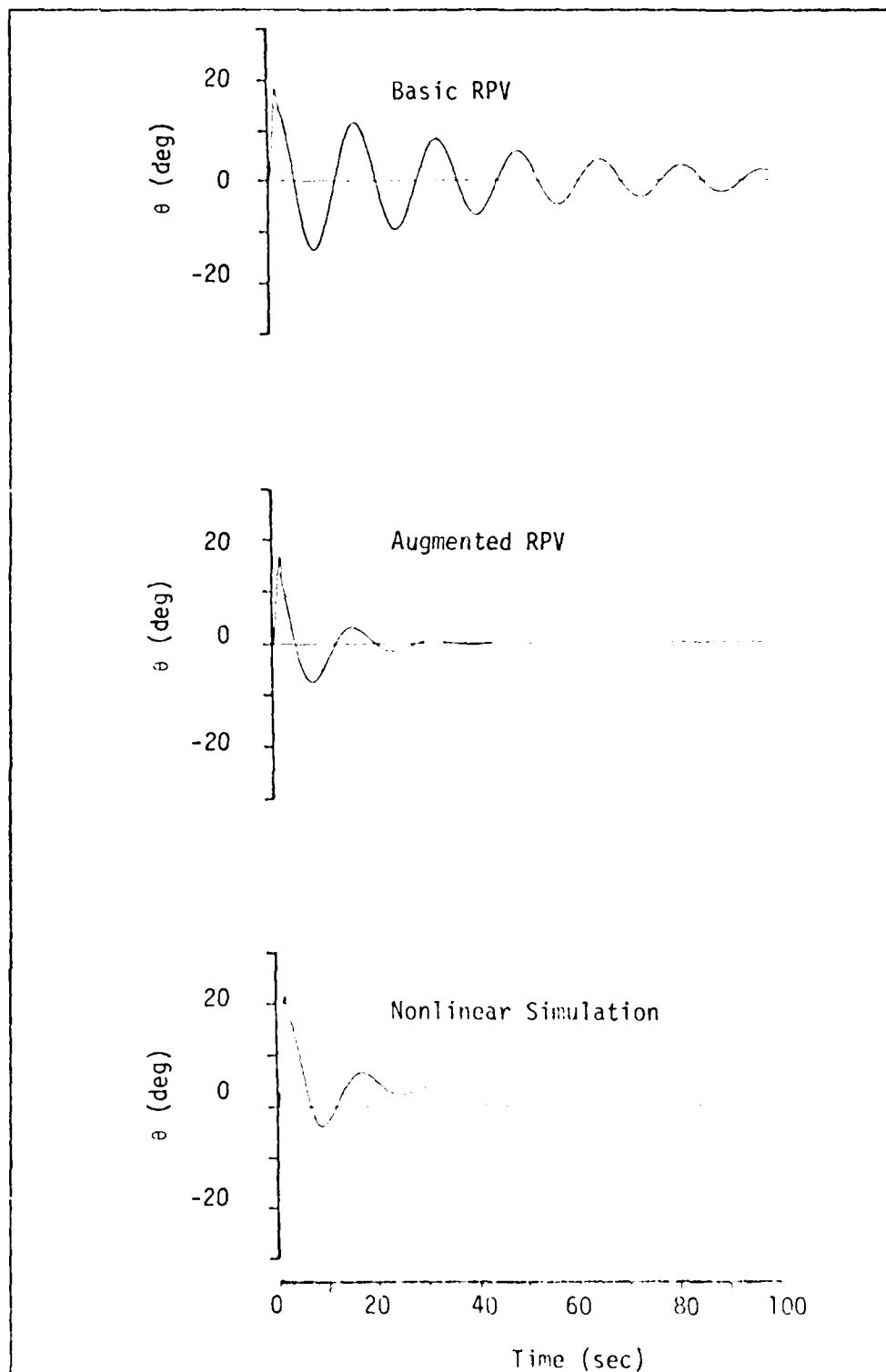


Figure 32. RPV Pitch Angle due to a 1 sec Pulse Elevator Command of -5 deg

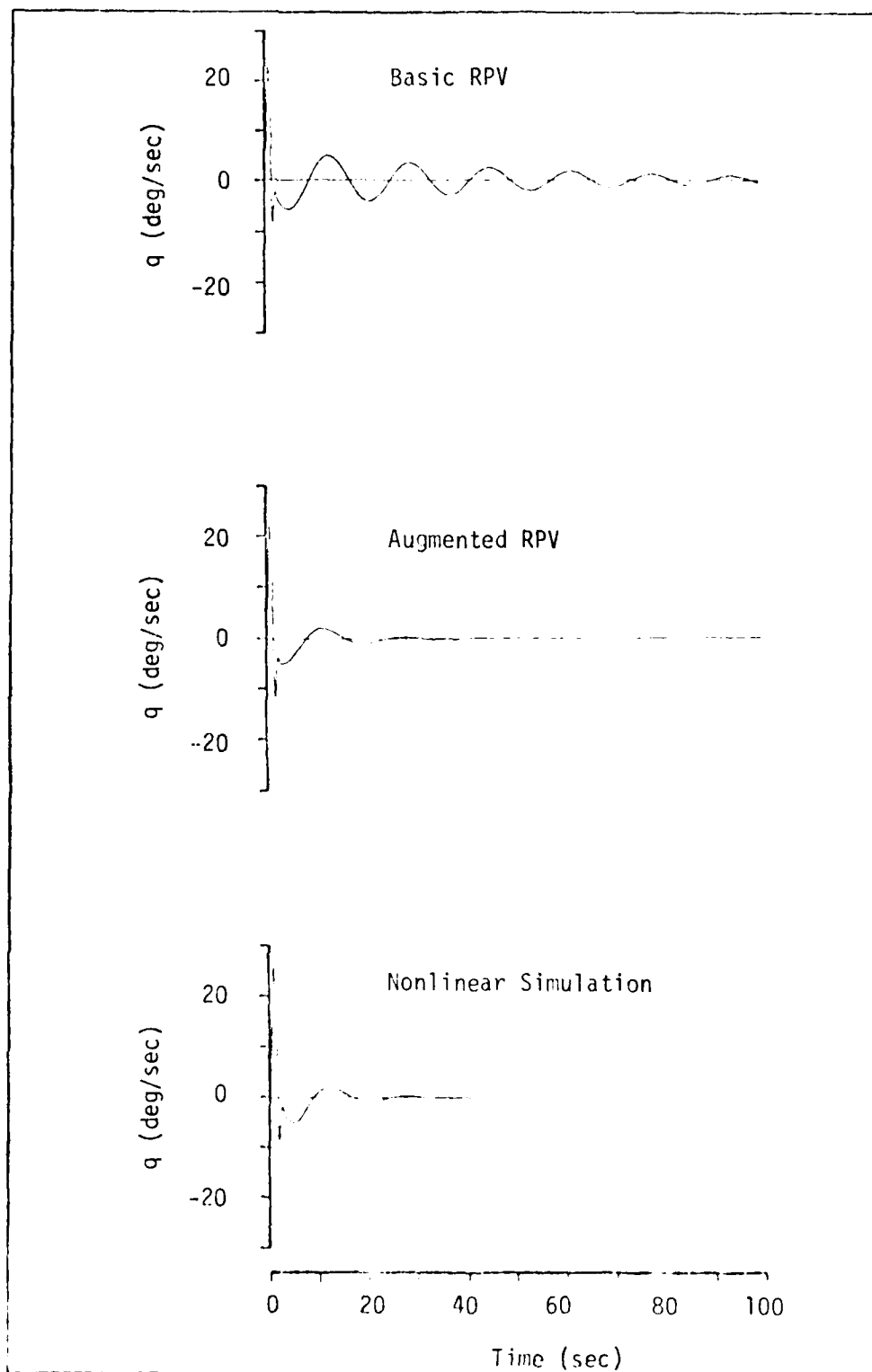


Figure 33. RPV Pitch Rate due to a 1 sec Pulse Elevator Command of -5 deg

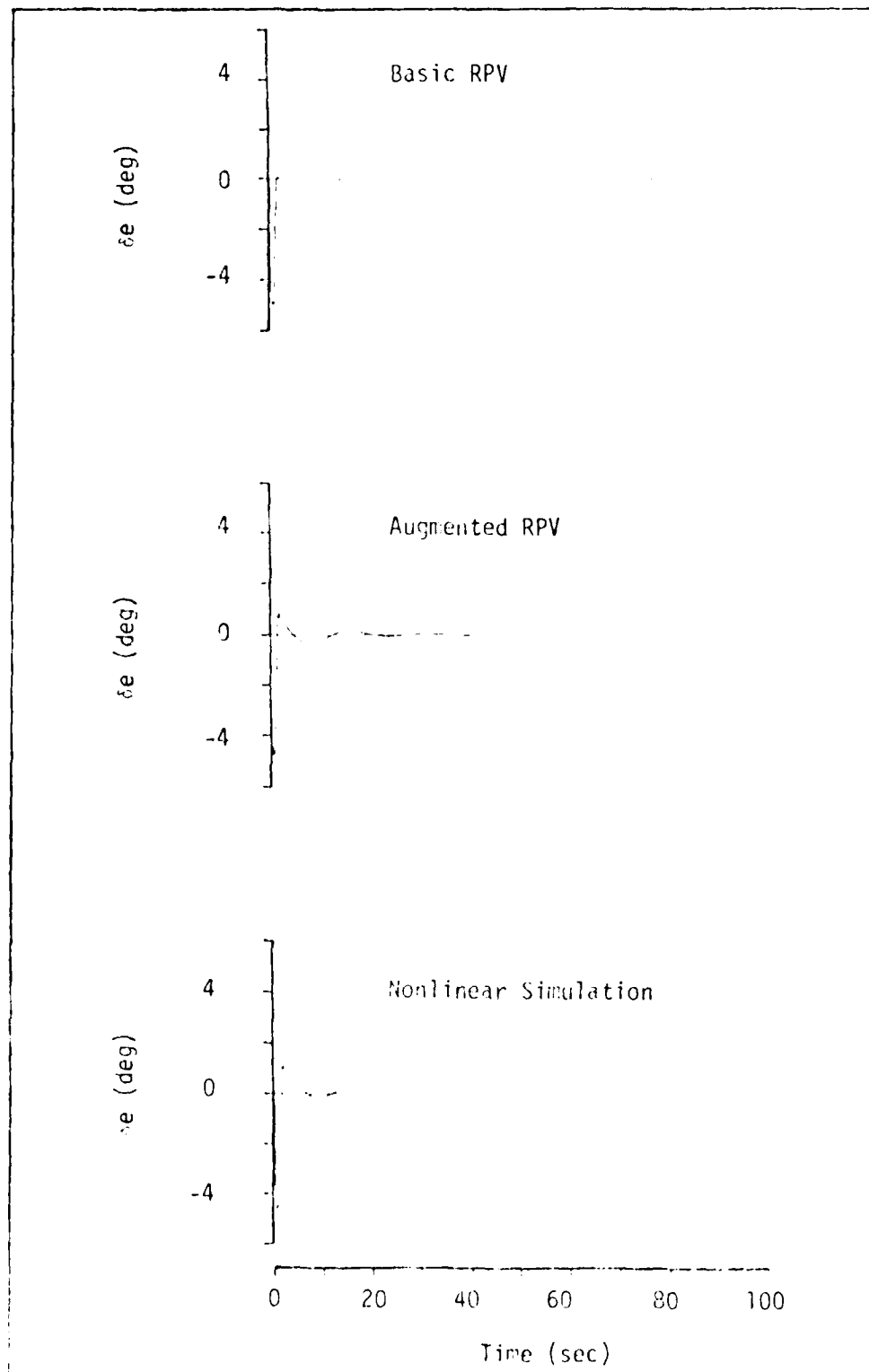


Figure 34. RPV Elevator Deflection Angle due to a 1 sec Pulse Elevator Command of -5 deg

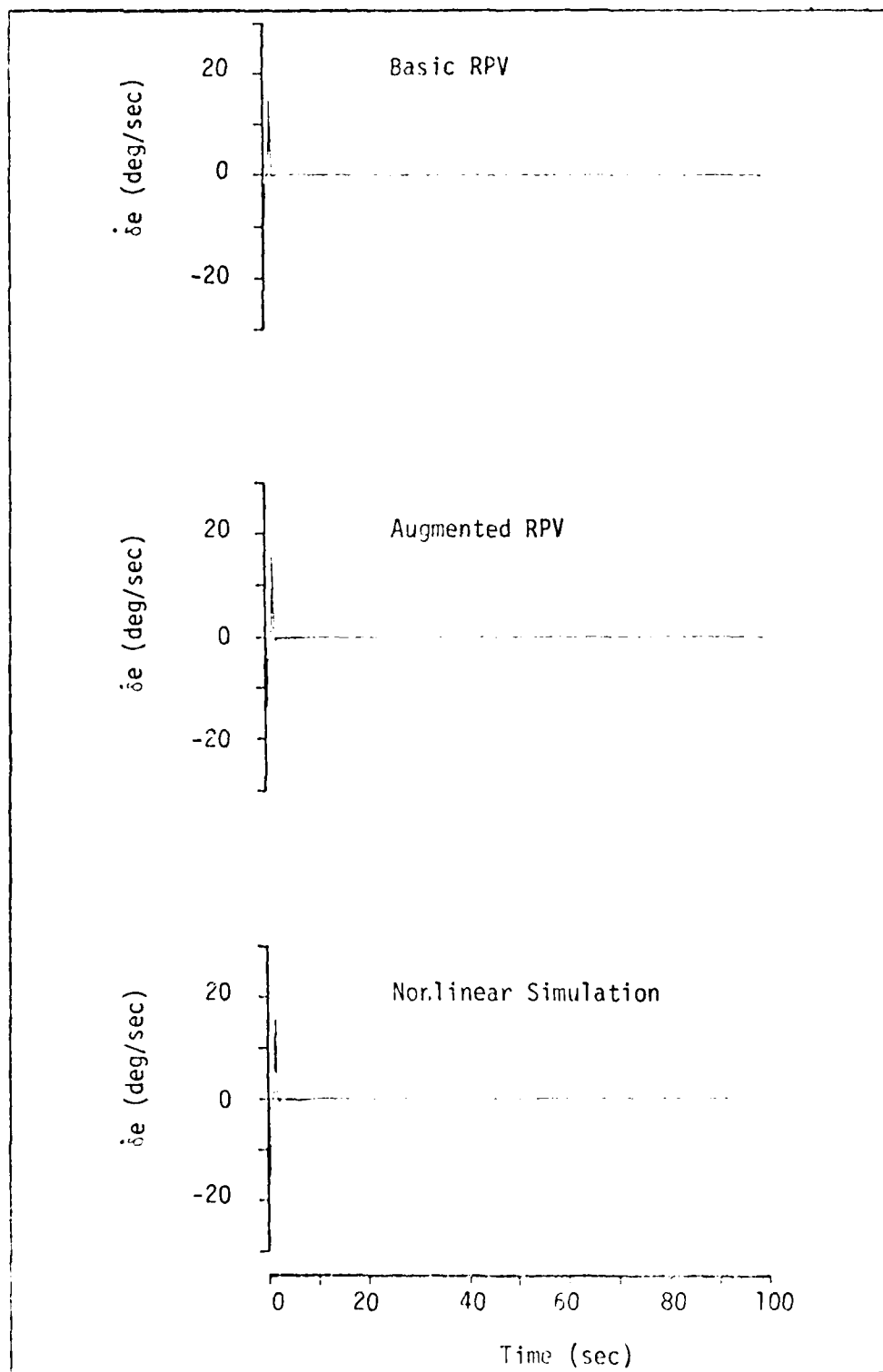


Figure 35. RPV Elevator Deflection Rate due to a 1 sec Pulse Elevator Command of -5 deg

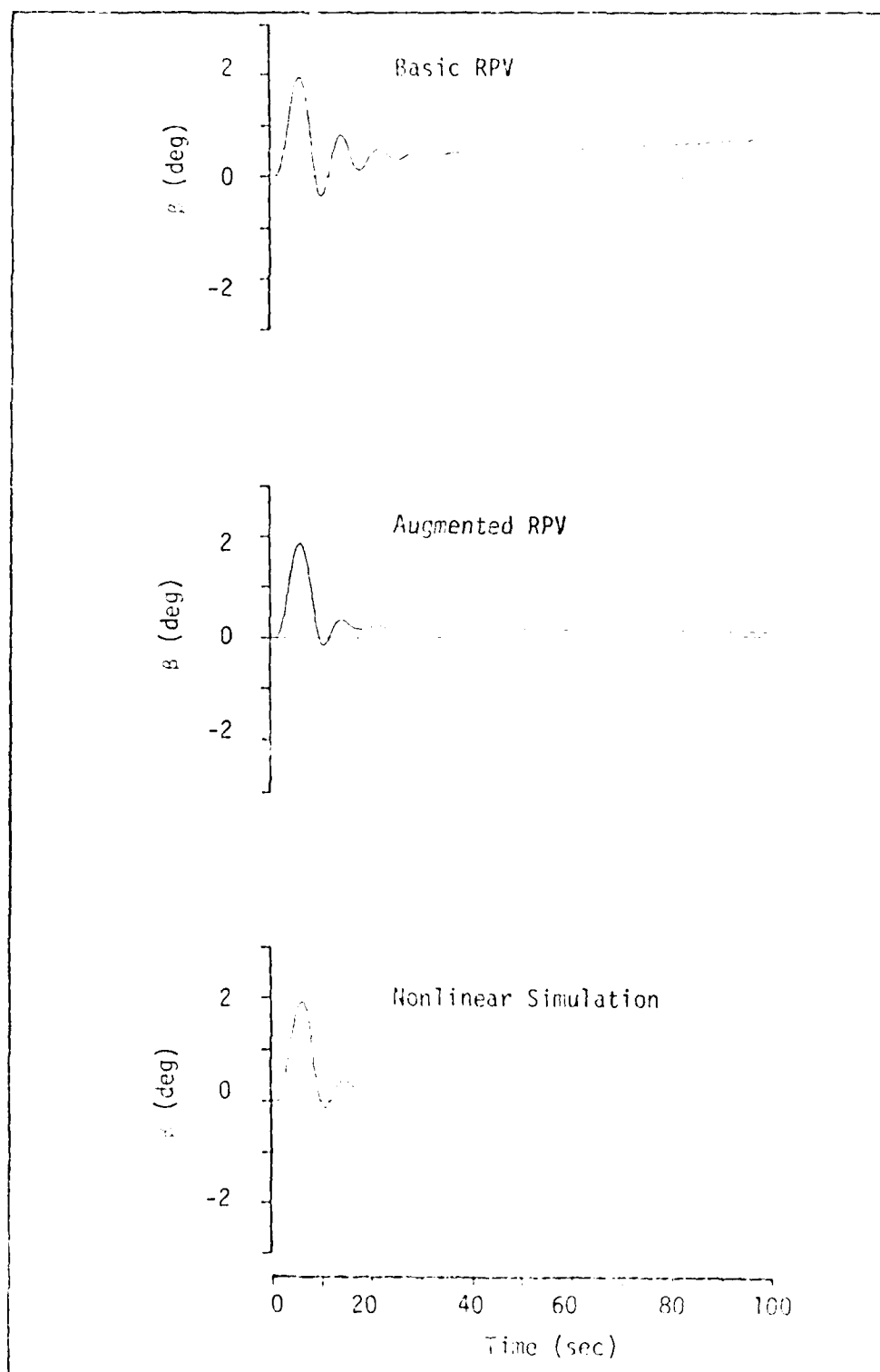


Figure 36. RPV Sideslip Angle due to a 1 sec Pulse Aileron Command of 5 deg

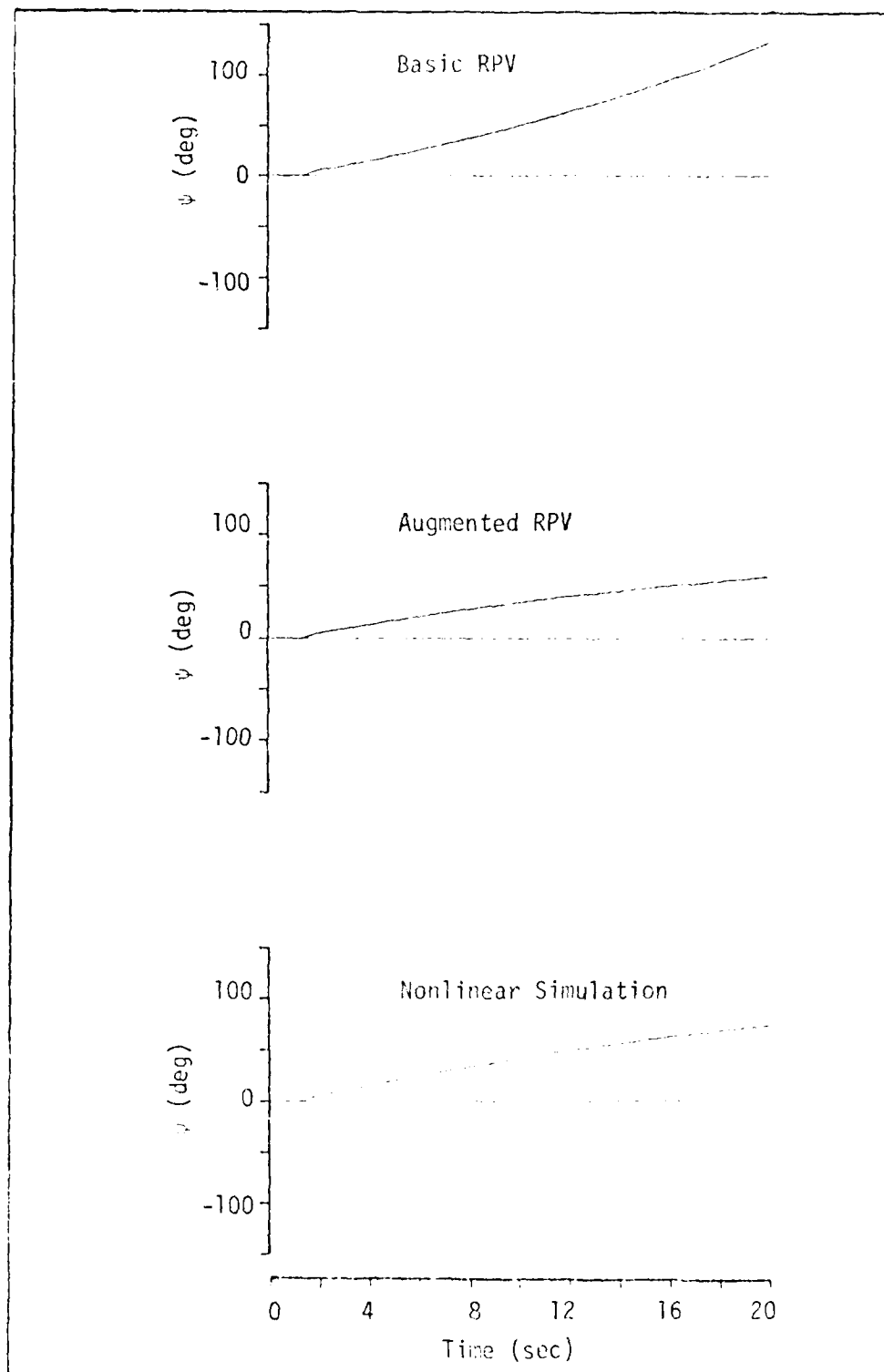


Figure 37. RPV Yaw Angle due to a 1 sec Pulse Aileron Command of 5 deg

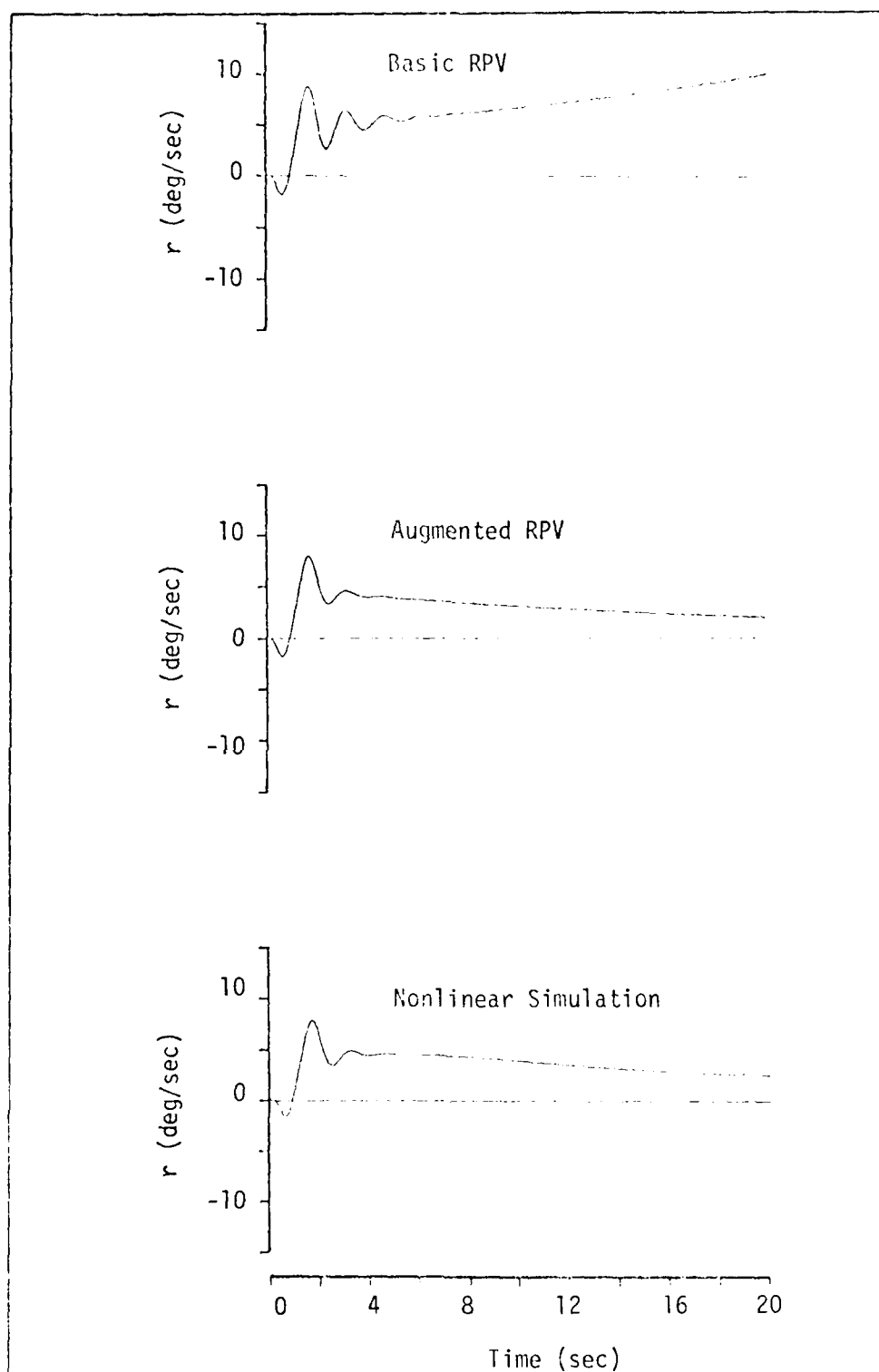


Figure 38. RPV Yaw Rate due to a 1 sec Pulse Aileron Command of 5 deg

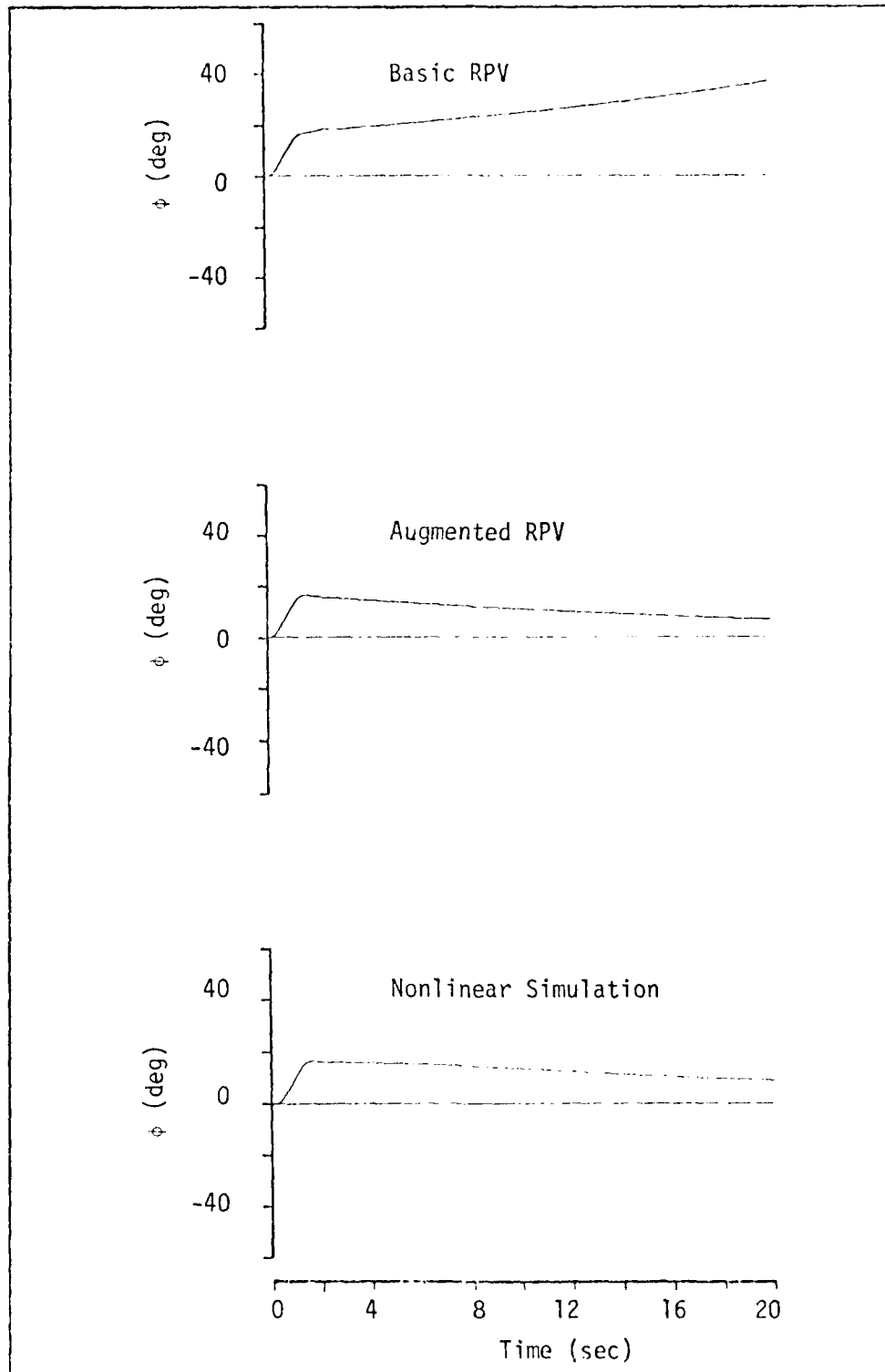


Figure 39. RPV Bank Angle due to a 1 sec Pulse Aileron Command of 5 deg

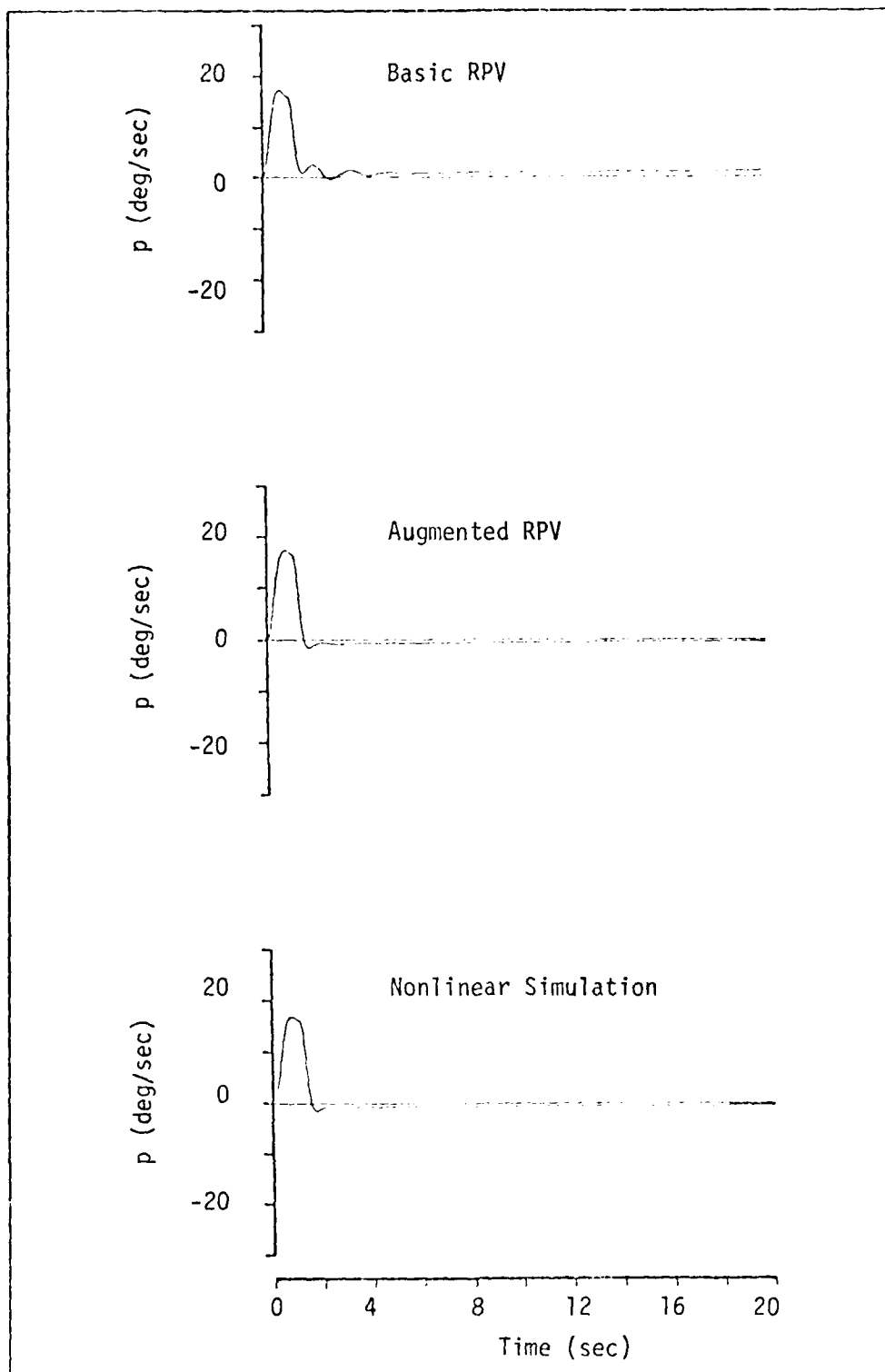


Figure 40. RPV Roll Rate due to a 1 sec Pulse Aileron Command of 5 deg

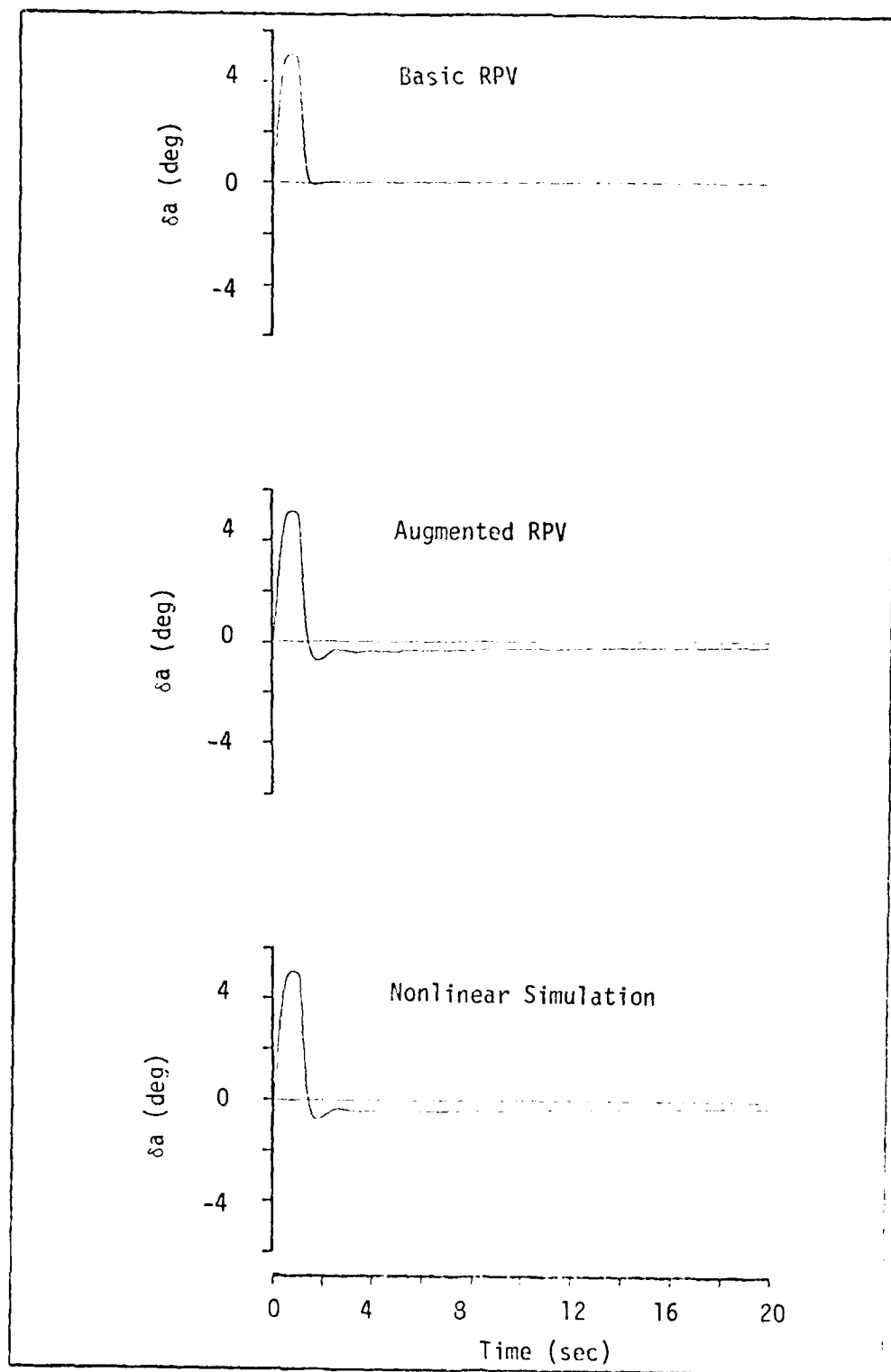


Figure 41. RPV Aileron Deflection Angle due to a 1 sec Pulse Aileron Command of 5 deg

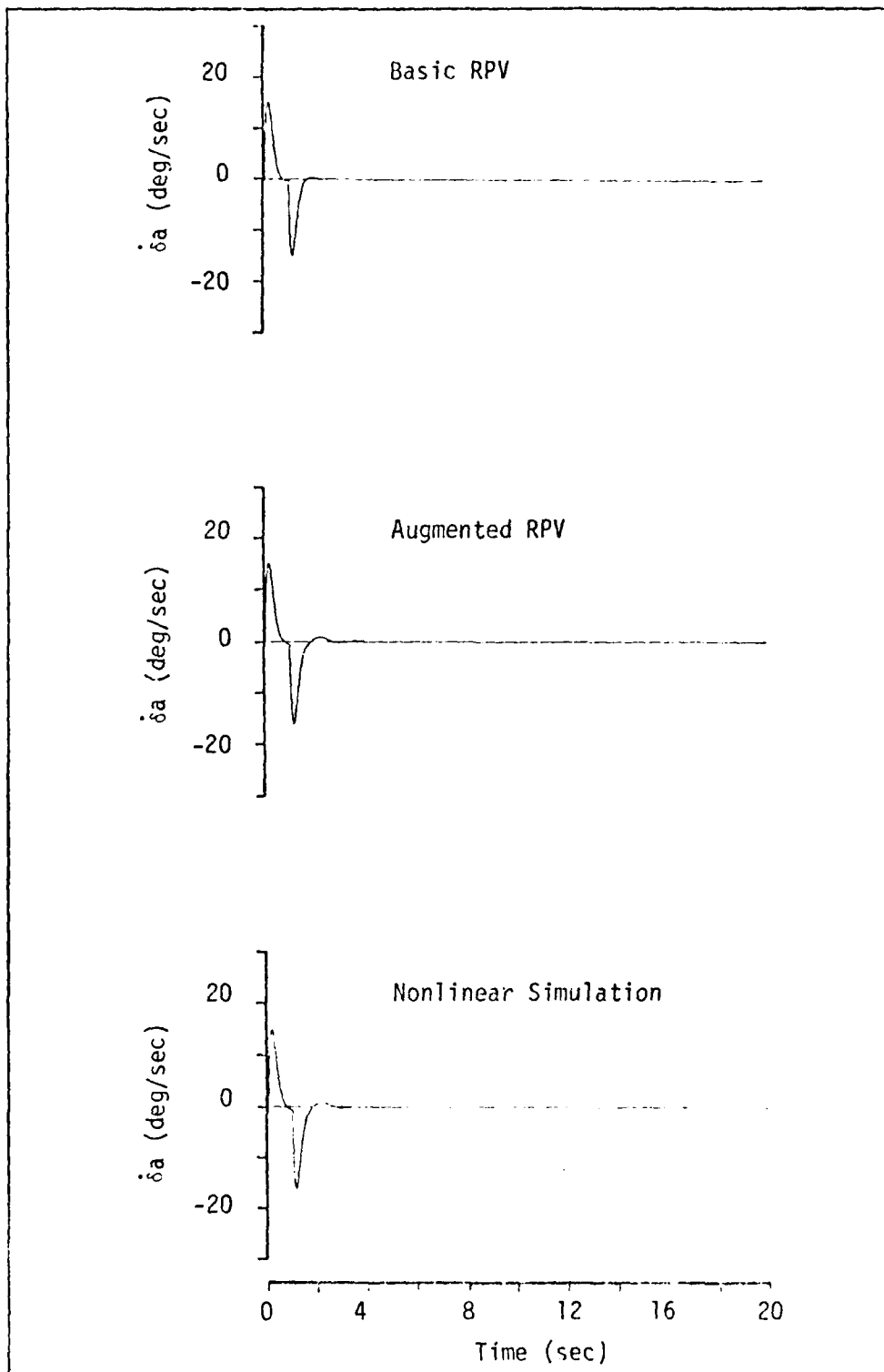


Figure 42. RPV Aileron Deflection Rate due to a 1 sec Pulse Aileron Command of 5 deg

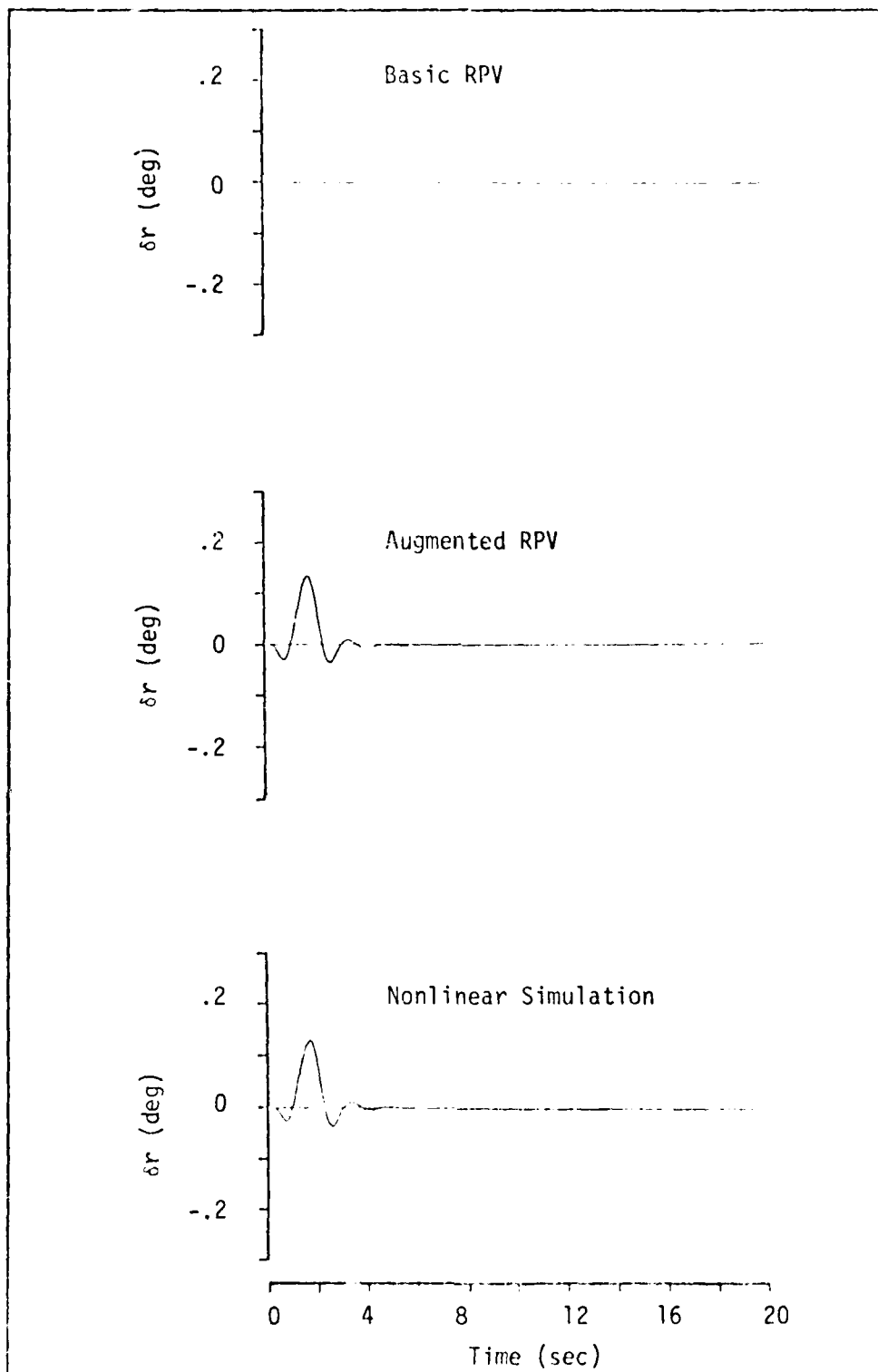


Figure 43. RPV Rudder Deflection Angle due to a 1 sec Pulse Aileron Command of 5 deg

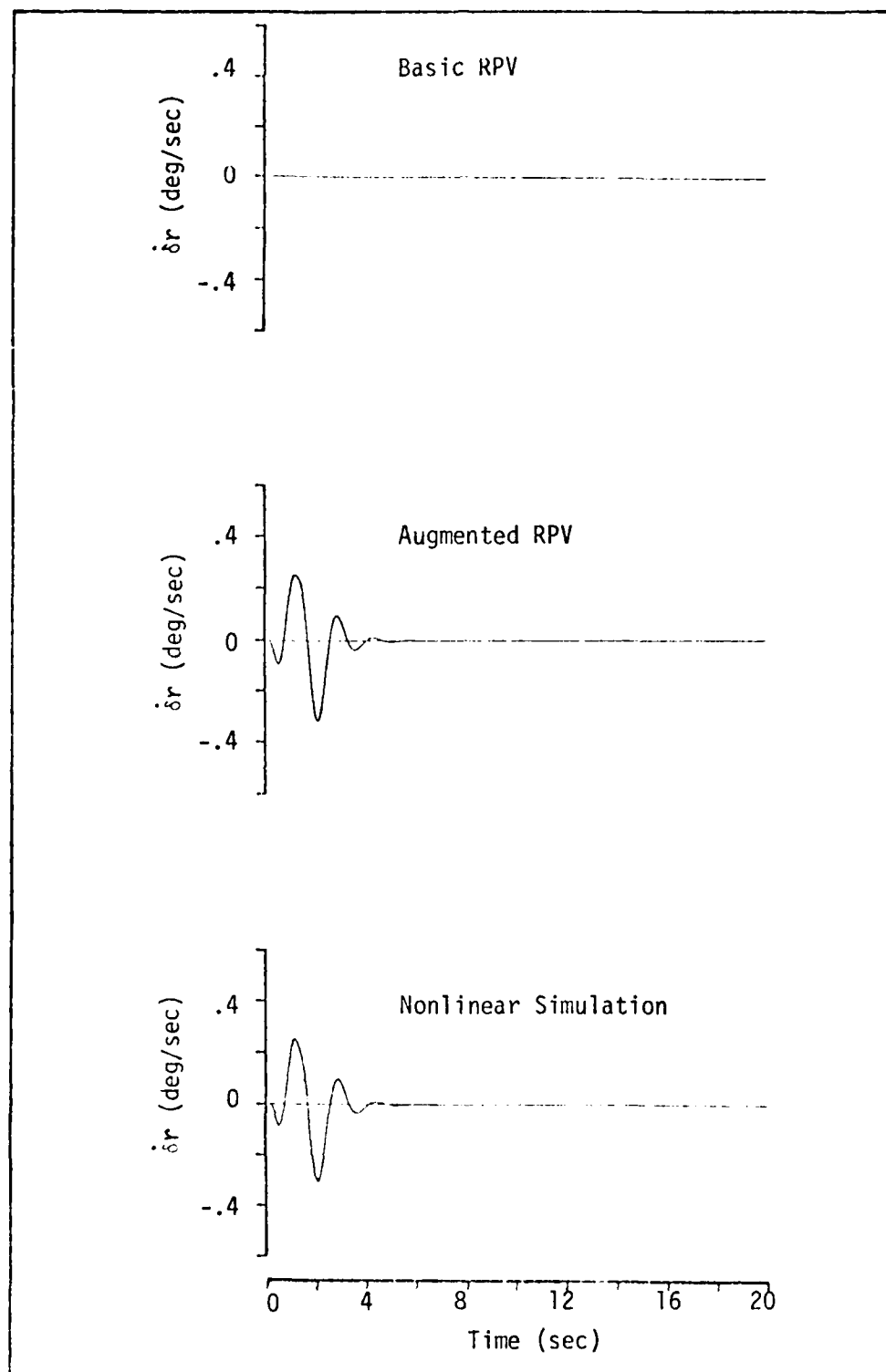


Figure 44. RPV Rudder Deflection Rate due to a 1 sec Pulse Aileron Command of 5 deg

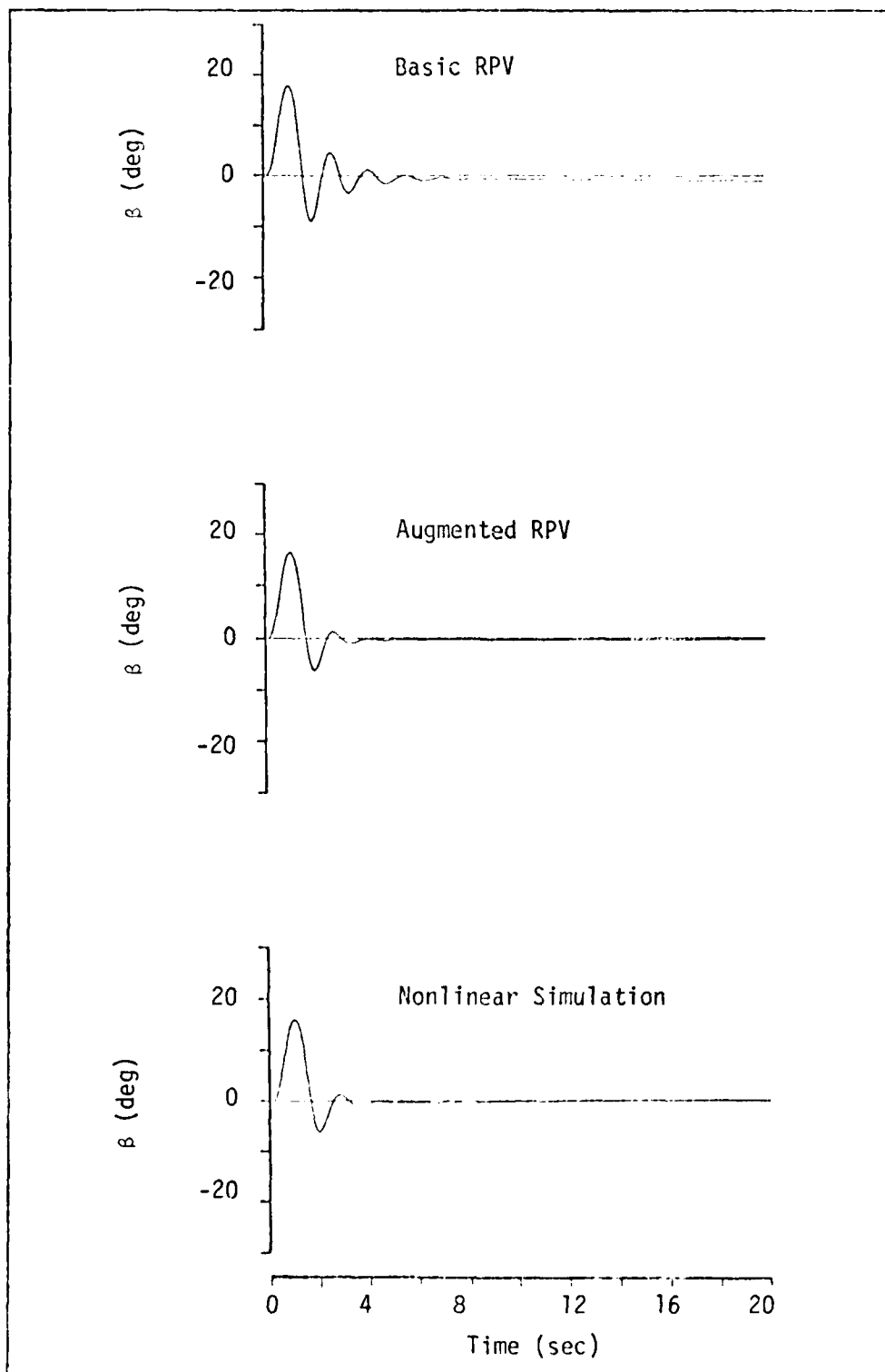


Figure 45. RPV Sideslip Angle due to a 1 sec Pulse Rudder Command of 5 deg

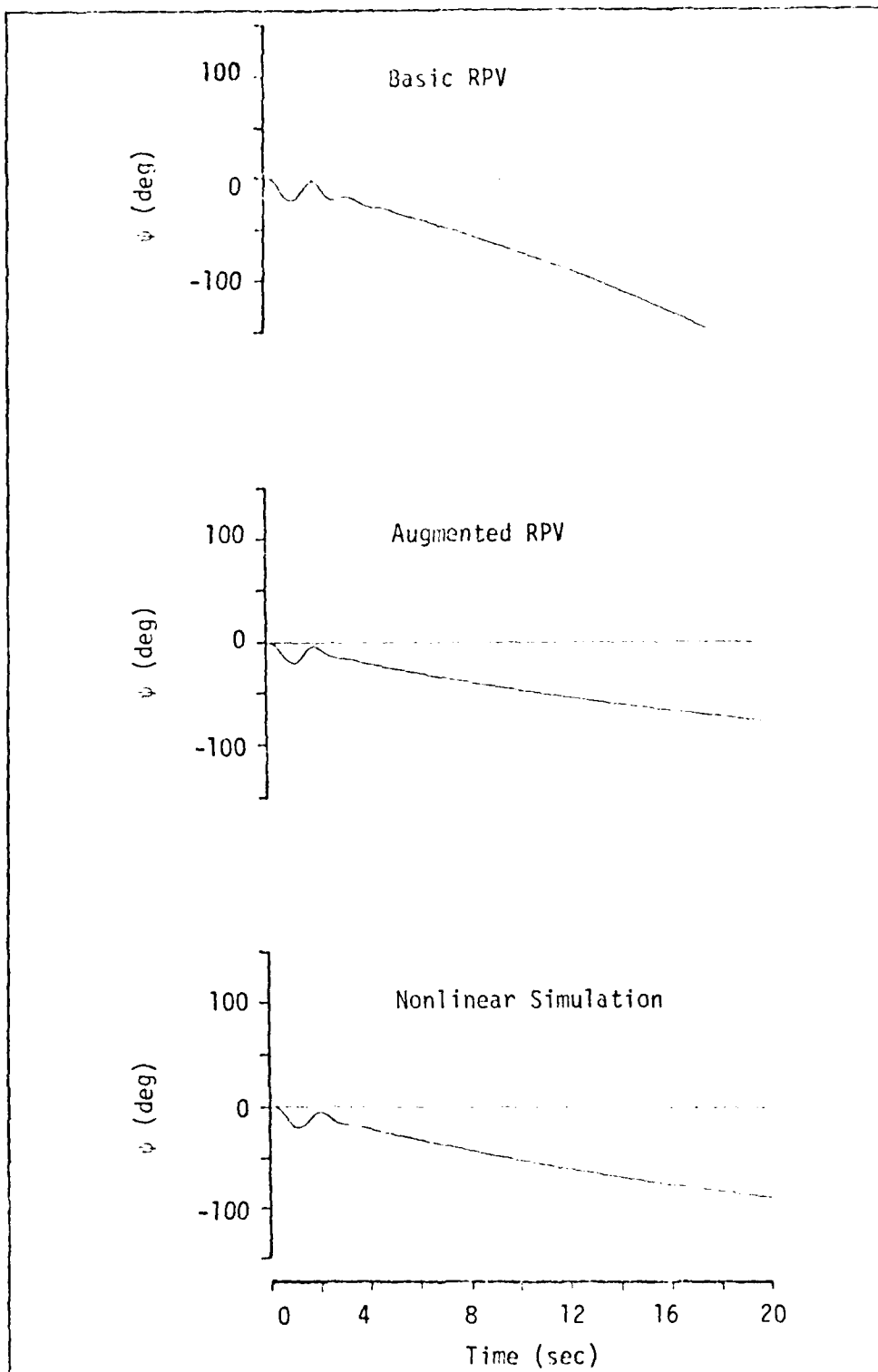


Figure 46. RPV Yaw Angle due to a 1 sec Pulse Rudder Command of 5 deg

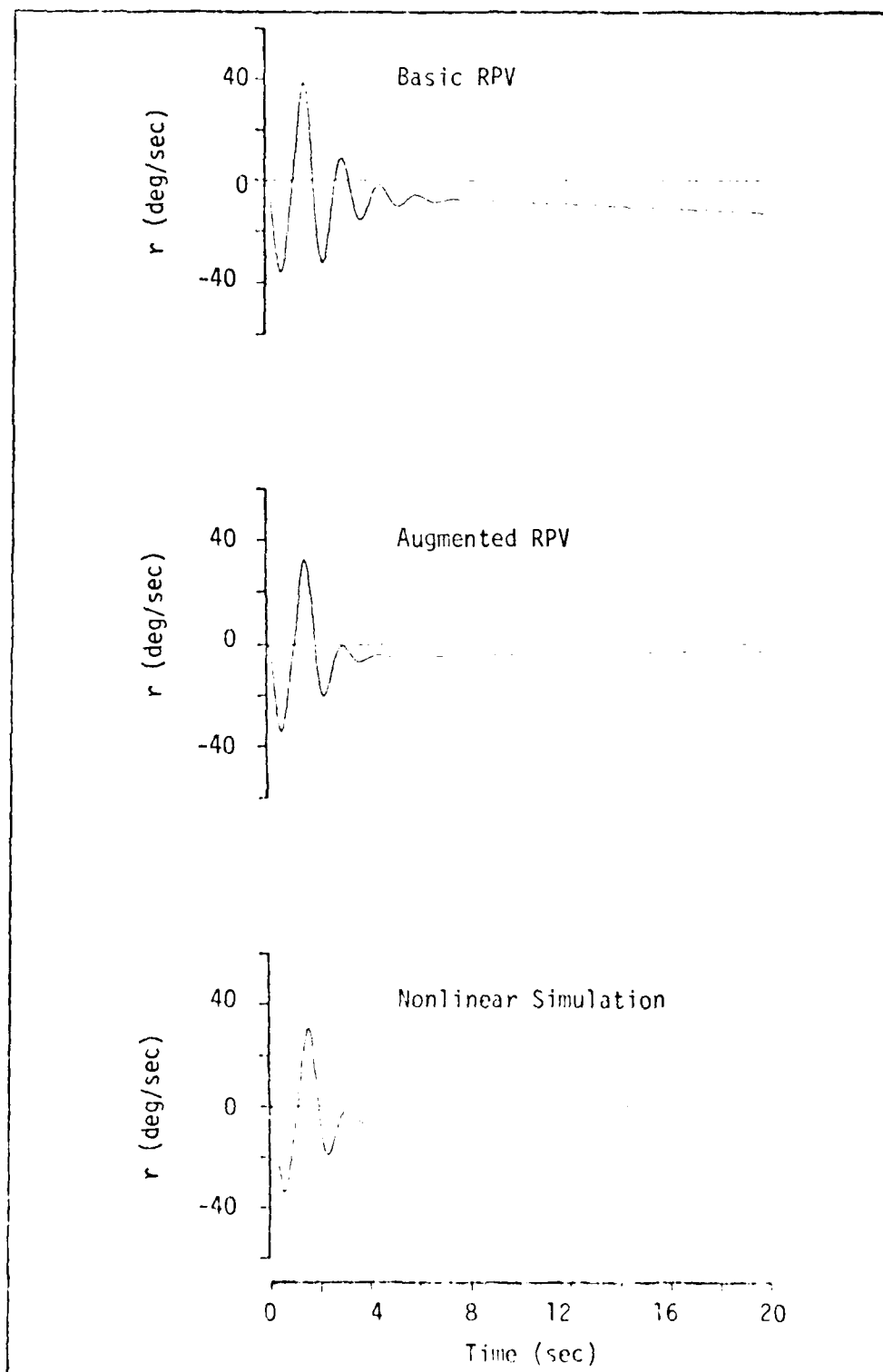


Figure 47. RPV Yaw Rate due to a 1 sec Pulse Rudder Command of 5 deg

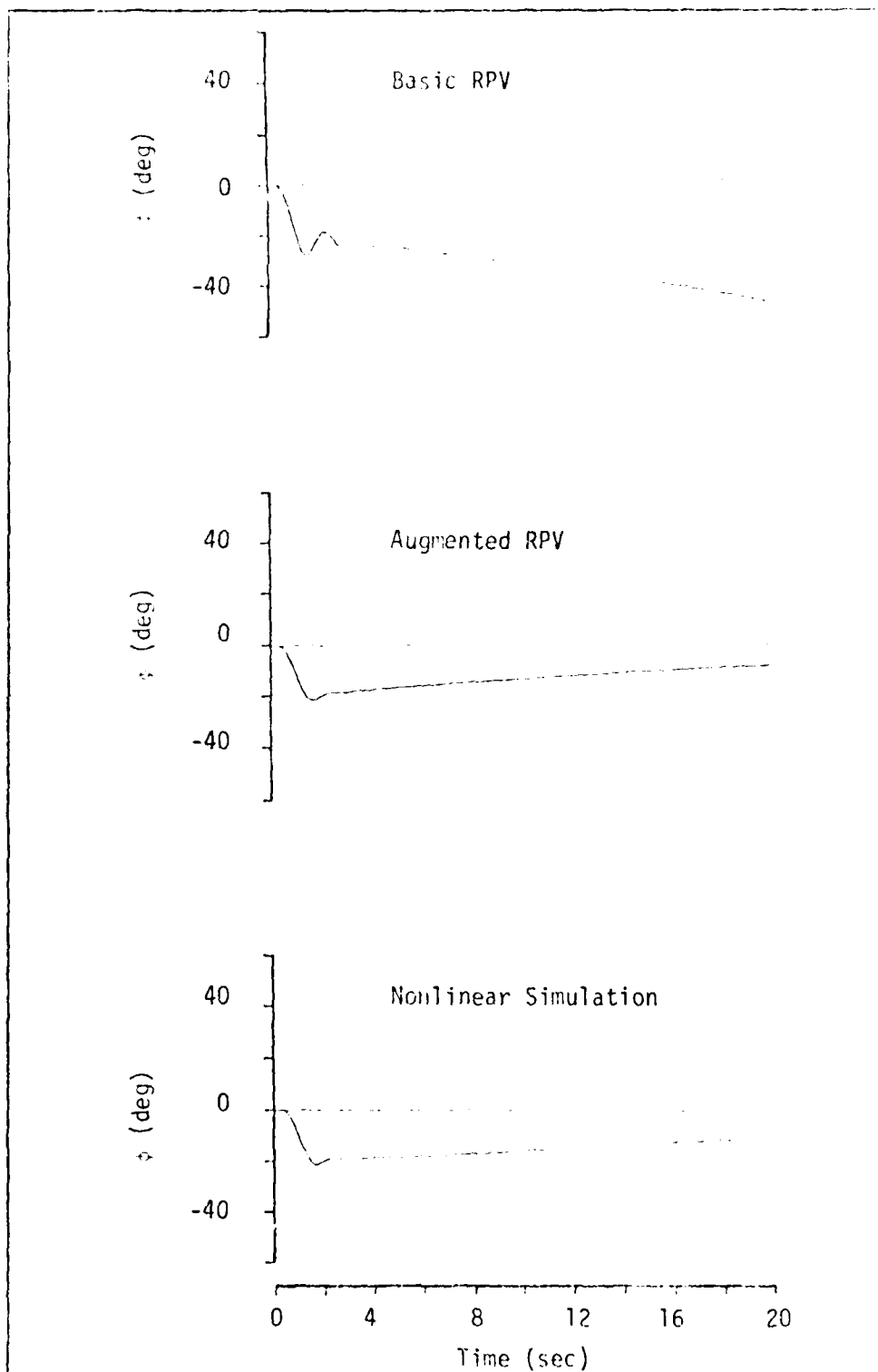


Figure 48. RPV Bank Angle due to a 1 sec Pulse Rudder Command of 5 deg

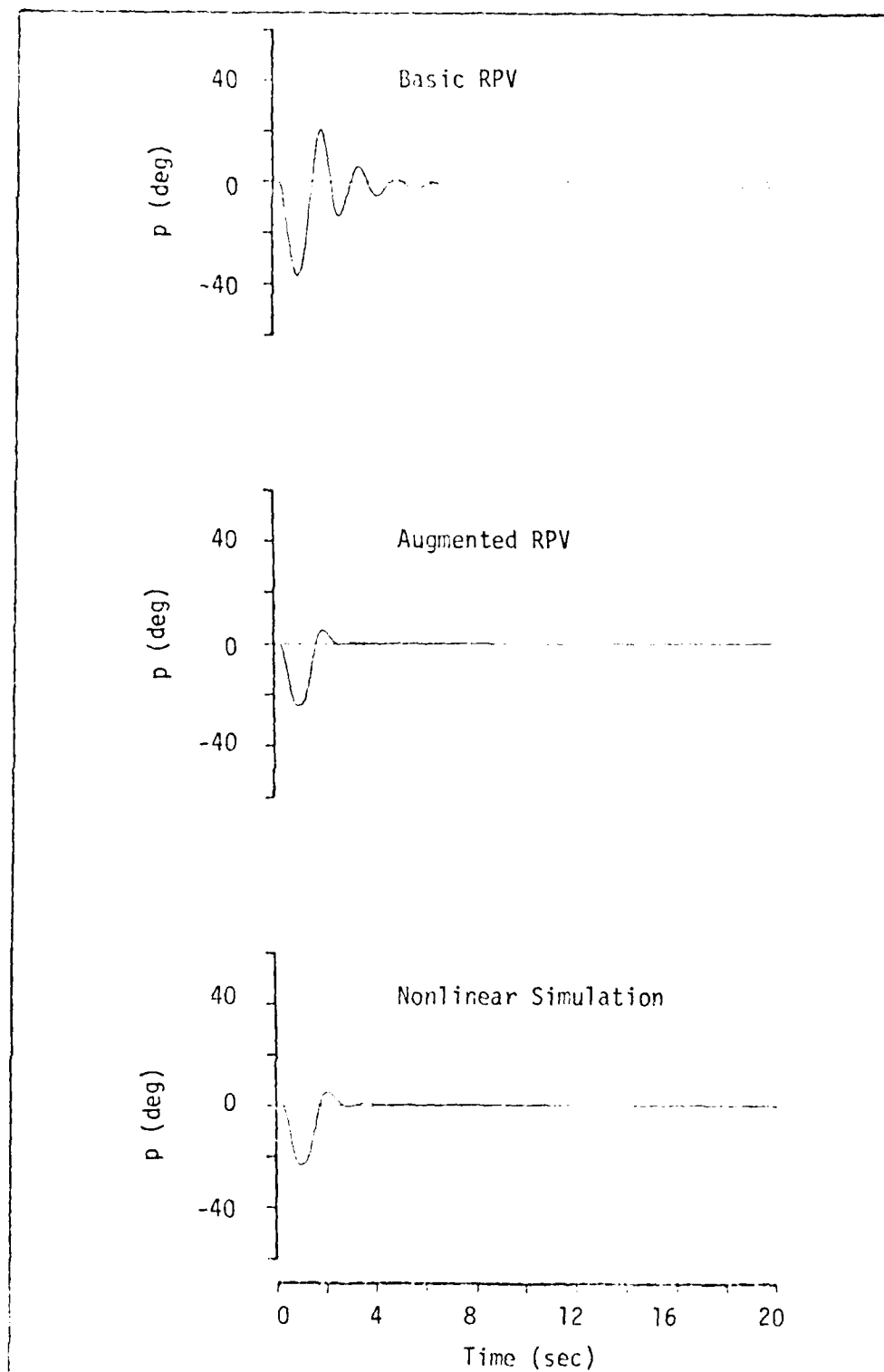


Figure 49. RPV Roll Rate due to a 1 sec Pulse Rudder Command of 5 deg

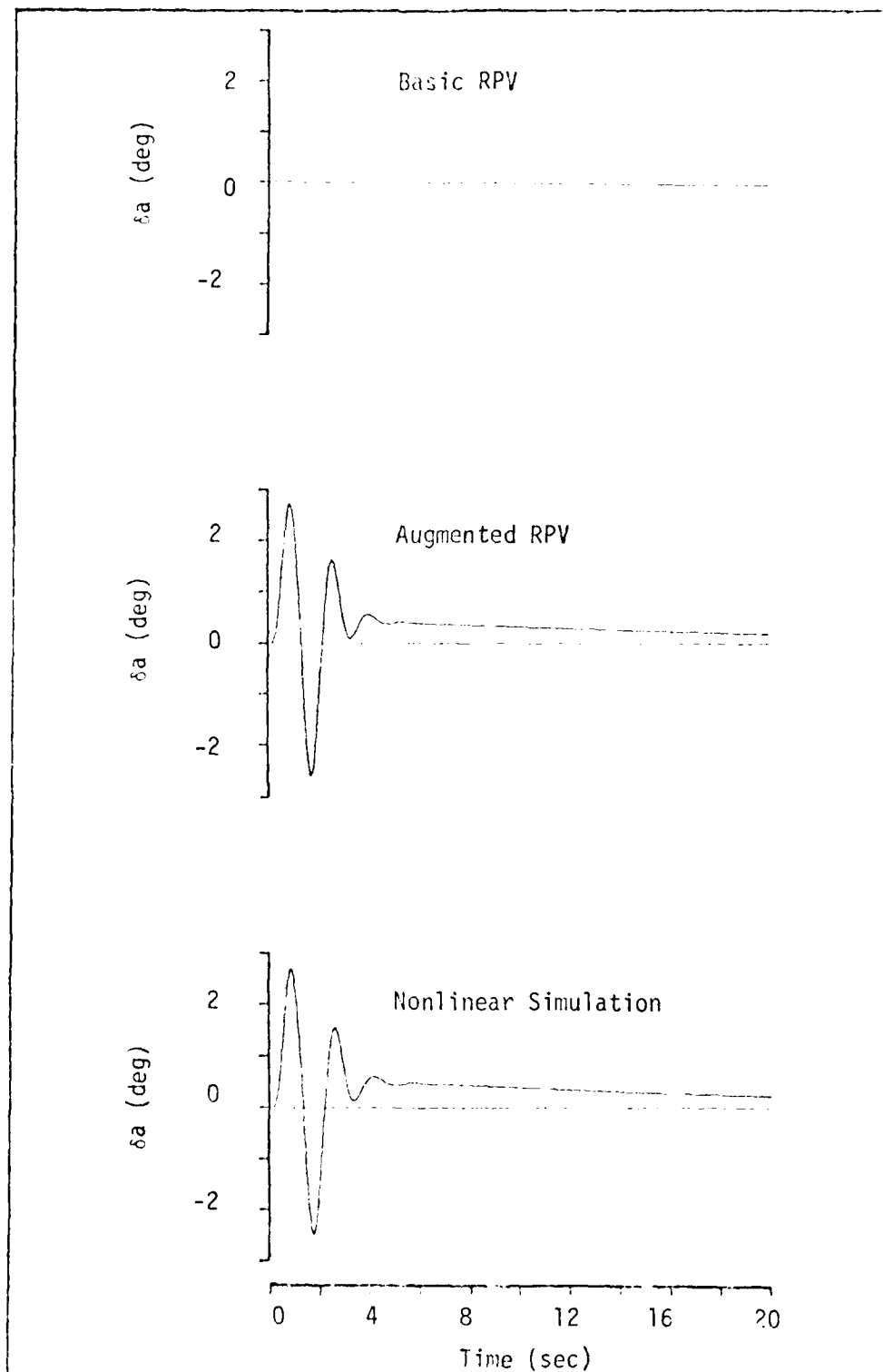


Figure 50. RPV Aileron Deflection Angle due to a 1 sec Pulse Rudder Command of 5 deg

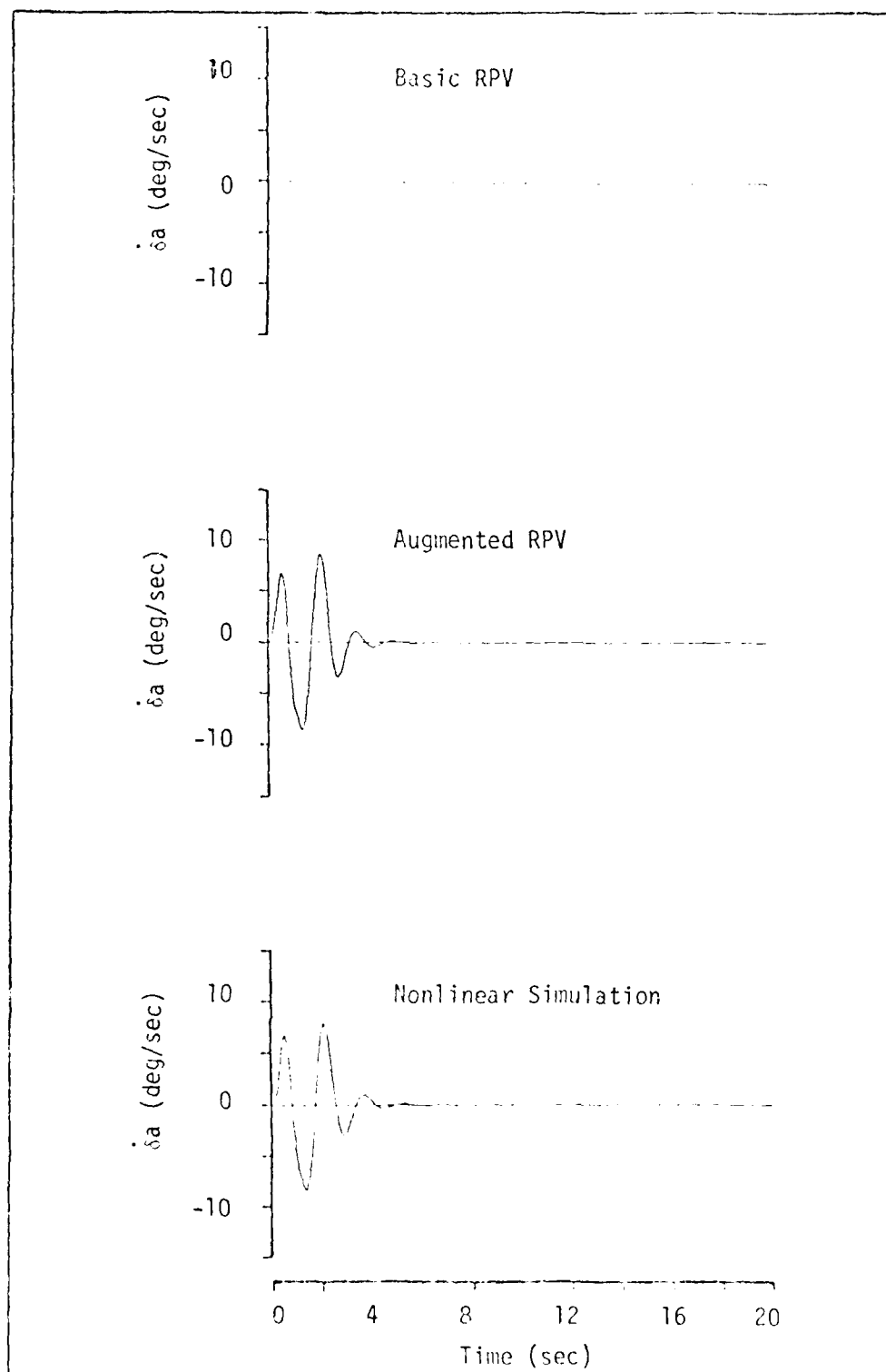


Figure 51. RPV Aileron Deflection Rate due to a 1 sec Pulse Rudder Command of 5 deg

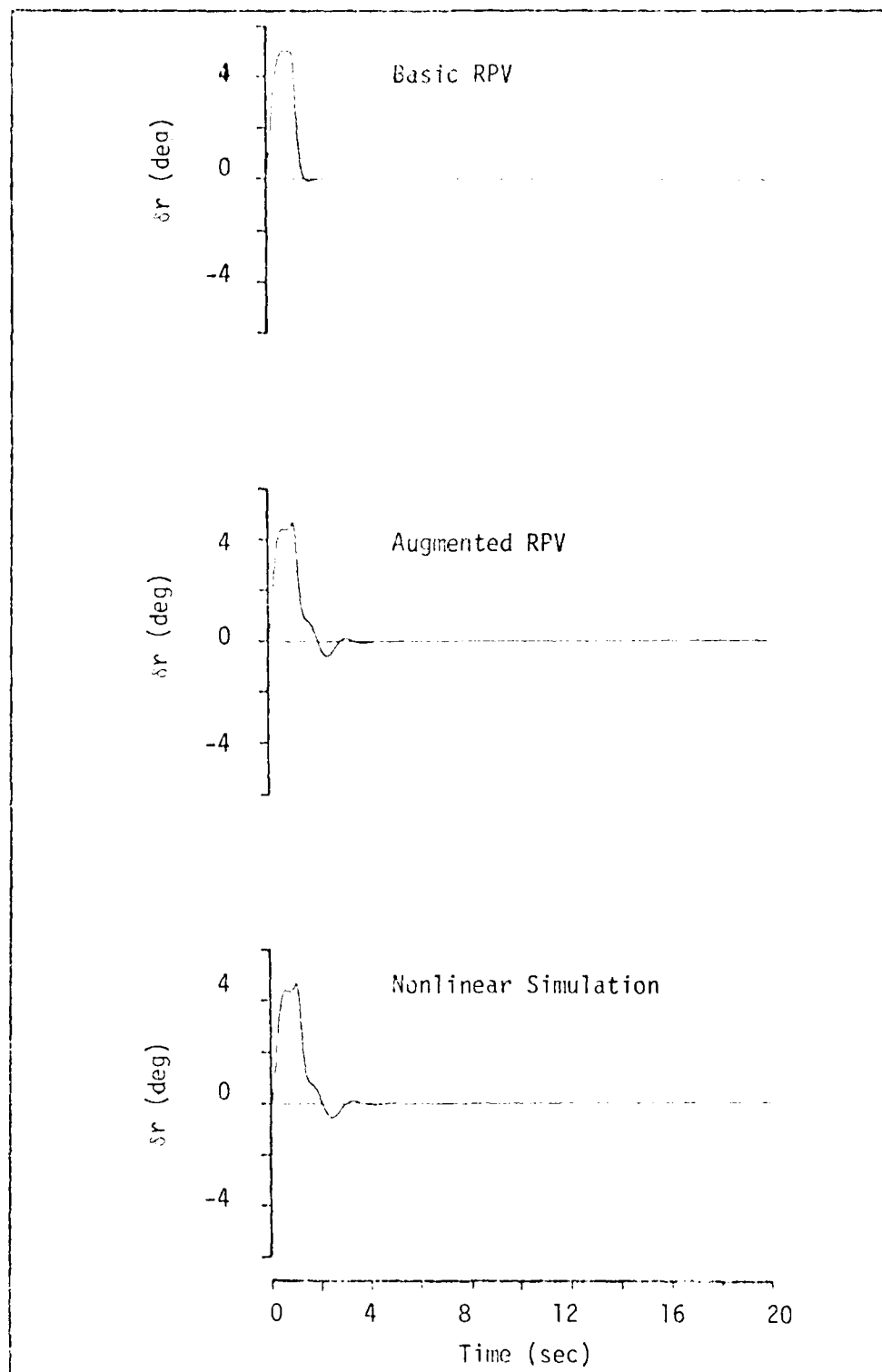


Figure 52. RPV Rudder Deflection Angle due to a 1 sec Pulse Rudder Command of 5 deg

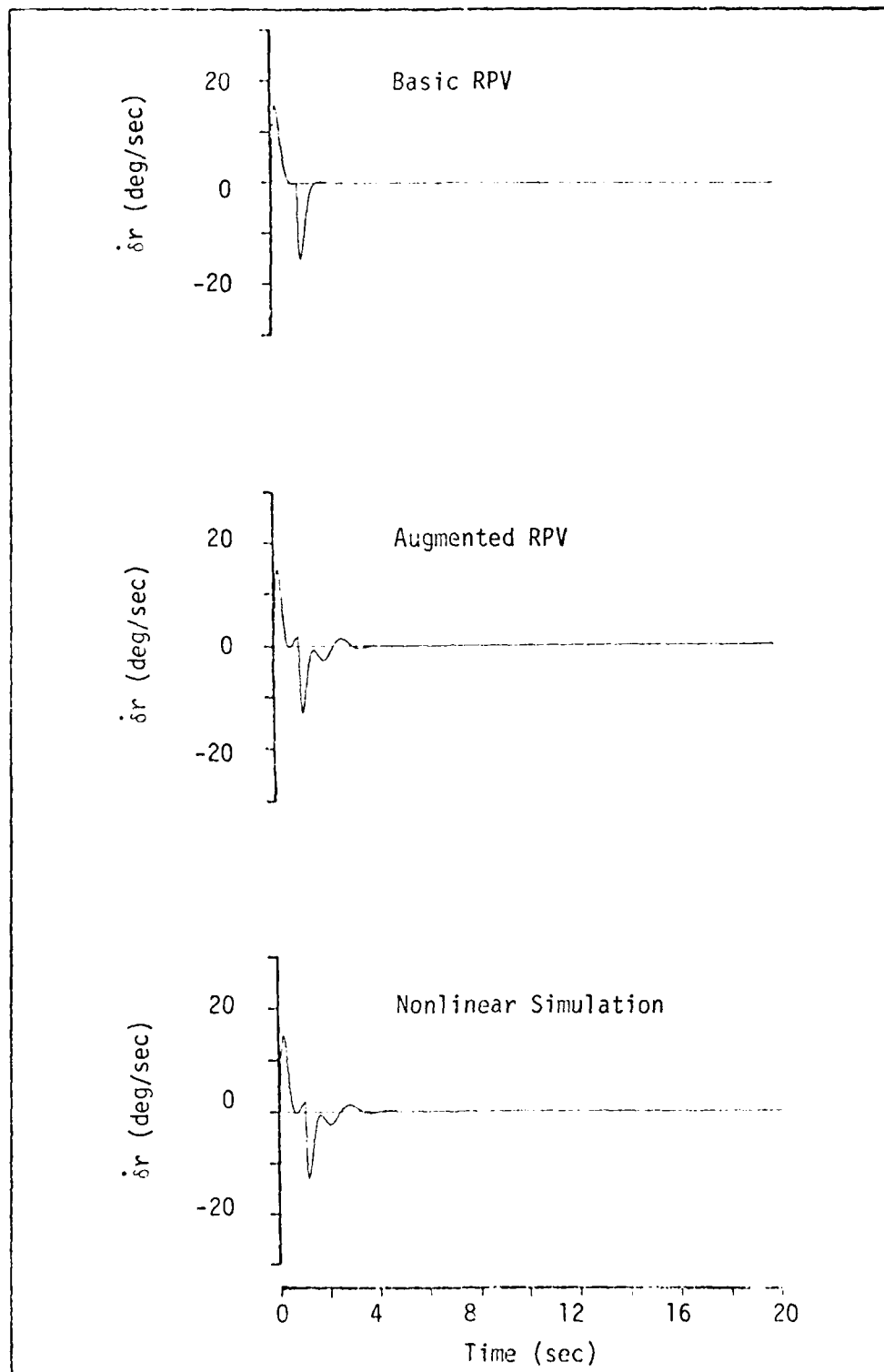


Figure 53. RPV Rudder Deflection Rate due to a 1 sec Pulse Rudder Command of 5 deg

Vita

Brian Leigh Jones was born on 4 October 1957 in Charlotte, North Carolina, to Mary and Owen Jones. In June 1975, he completed his high school education in North Wilkesboro, North Carolina at Wilkes Central High School. That fall, he entered North Carolina State University where, in May 1979, he received a B.S.A.E. degree and a commission as a Second Lieutenant in the United States Air Force. Three weeks later, Lt Jones entered the Graduate Aeronautical Engineering program of the Air Force Institute of Technology.

Permanent address: 5431 Mitchell Drive
Dayton, Ohio 45431

This thesis was typed by Mrs Anna L. Lloyd.

Unclassified

REPORT DOCUMENTATION PAGE	
AFIT/GAE/AA/80D-12 <i>AD-A100 818</i>	
4. TITLE (and Subtitle) Flight Control System Analysis and Design for a Remotely Piloted Vehicle with Thrust Vectoring Unit	5. TYPE OF REPORT & PERIOD COVERED MS Thesis
7. AUTHOR Brian L. Jones 2d Lt, USAF	6. PERFORMING ORG. REPORT NUMBER
9. PERFORMING ORGANIZATION NAME AND ADDRESS Air Force Institute of Technology Wright-Patterson AFB, Ohio 45433	8. CONTRACT OR GRANT NUMBER 24030270
11. CONTROLLING OFFICE NAME AND ADDRESS Control Systems Development Branch (AFWAL/F1GL) Flight Dynamics Laboratory Air Force Wright Aeronautical Laboratories	10. PROGRAM ELEMENT, PROJECT, TASK, AND AFRL G O WORK UNIT NUMBER December 1980 151
14. MONITORING AGENCY NAME & ADDRESS (if different from Controlling Office)	12. REPORT DATE 13. NUMBER OF PAGES 15. SECURITY CLASS. of this report Unclassified 15a. DECLASS. & DOWNGRADING SCHEDULE
16. DISTRIBUTION STATEMENT for this Report Approved for public release; distribution unlimited.	
17. DISTRIBUTION STATEMENT (of the abstract entered in Block 20, if different from Report)	
18. SUPPLEMENTARY NOTES Approved for public release; IAM APR 190-17 <i>Fredric C. Lynch</i> FREDRIC C. LYNCH, Major, USAF Director of Public Affairs 30 DEC 1980 16 JUN 1991	
19. KEY WORDS (on reverse side if necessary and identify by block number) Remotely Piloted Vehicle (RPV) Thrust Vectoring Flight control system analysis Flight control system design Model matching	
20. ABSTRACT (continue on reverse side if necessary and identify by block number) This study investigated the stability and control of a remotely piloted vehicle (RPV) with a thrust vectoring unit attached. All geometric and aerodynamic data was generated and used to analyze the RPV. Specific handling qualities were developed and compared with the RPV characteristics. This comparison indicated that the RPV was too oscillatory in both the phugoid and dutch roll modes. Also, the RPV displayed a divergent spiral mode. A flight control system was synthesized to eliminate these traits. Evaluation of this flight control system was conducted through the use of three different sensitivity studies and a nonlinear	

Unclassified

SECURITY CLASSIFICATION OF THIS PAGE (When Data Entered)

simulation. In addition, a model matching application was examined for this RPV. Model matching entails using design procedures to synthesize an expanded flight control system so that the RPV has dynamic characteristics similar to the F-15.

Unclassified

SECURITY CLASSIFICATION OF

**DAT
FILM**

7-1